Method development using ICP-MS and LA-ICP-MS and their application in environmental and material science

Dissertation
zur Erlangung des Grades
„Doktor der Naturwissenschaften“
(Dr. rer. nat.)

Fachbereich Chemie, Pharmazie und Geowissenschaften
der Johannes Gutenberg-Universität Mainz

Izmer Andrei
geboren in Berezino, Weissrussland

Mainz 2006

Index

1. Introduction

1.1. Motivation

Developments of new technologies in material science, space research, clinical medicine or energy production strongly requests analytical methods for measuring the chemical composition of applied materials to meet the constantly arising demands on improved quality and safety. Recently, the European spallation source (ESS) project has been started which aims the design and construction of a next generation facility for research with neutrons. The neutron beams produced in such spallation source can be used for fundamental and applied research in physics, chemistry, biotechnology, engineering and material science.

In particular, the ESS project requires further improvement of analytical techniques for monitoring of particular radionuclides as well as for the analysis of chemical composition of special construction materials. Numerous spallation products are present in the irradiated material, whereas their composition and induced activity depends on the applied target material. For example, when irradiating a tantalum target with high-energy protons a significant amounts of lanthanides with different abundances in the μg g^{-1} to low ng g^{-1} concentration range are produced[1]. Information about nuclide abundances and their concentrations is necessary for accessing the dose levels and for assuring irradiation safety when handling these types of samples. Although, well established radioanalytical techniques have been successfully applied for general radiation safety purposes, those methods encountered difficulties when monitoring volatile isotopes, such as iodine. Other potential problems are related to the ^{90}Sr determination due to the fact that beta-radiometry is limited in sensitivity for direct determination of this isotope or it requires long analysis time (up to two weeks). As a result, the response time to provide the information of a possible contamination is significant delayed and cannot fulfill today's safety requirements.

Another challenging task for analytical chemist in the frame of ESS project is the quality control of the chemical composition of special construction materials used in the target, reflectors, moderator and beam entrance window. The composition of these materials is subject to a permanent change due to activation with protons and neutrons, which results in deterioration of their physical and mechanical properties.

Therefore the aim of this work was focused on inductively coupled plasma mass spectrometry based method developments for the analysis of radionuclides (such as ^{129}I, ^{90}Sr and lanthanides) and direct solid analysis of new materials to provide analytical support and maintenance for the ESS project. In addition, the methods developed within this work were validated and analytical figures of merit were determined to evaluate the suitability for routine applications.

Amongst the variety of analytical techniques for element and isotope analysis, ICP-MS is one of the most suitable for the tasks listed above. The suitability of ICP-MS for determination of long-lived radionuclides is mainly attributed to its high sensitivity and good precision for isotope analysis, its flexibility to be coupled to chromatography or electrophoresis equipments and its capability to acquire transient signals in multielement mode when measuring low concentrations within different matrices. In addition, ICP-MS can also be coupled to Laser Ablation or electrothermal vaporization devices which enables direct solid analysis, including bulk and micro analysis of a wide variety of elements. Today, a variety of ICP-MS types and a wide spectrum of concomitant equipment exist enabling element, species and isotope measurements at concentrations previously inaccessible, which opens new capabilities for further development of different branches of science and technology, where the problems of chemical composition, material purity or safety play crucial role.

Technological and environmental monitoring of radionuclides and material science are among "regular customers" of the analysts, and therefore the ESS project perpetually required further development and improvement of appropriate analytical techniques, serving an important motivation for this work.

In 2003 the decision to build the ESS was further delayed by several years and the started activities towards the ESS stopped. Therefore it needs to be mentioned that the initial focus of the PhD work originally strated in the ESS project was changed with respect to develop and to apply the elaborated analytical techniques to environmental applications and material science within the research programs of the Forschungszentrum Jülich.

The determination of concentrations and enrichments of ^{90}Sr, ^{129}I, ^{236}U and Pu at ultratrace levels is of particular interest for radiation safety purposes at running nuclear installations, for environmental monitoring of fallout and for nuclear forensics. This is due to the fact, that tolerance and safety levels of many radionuclides are decreasing. Therefore, sensitive microanalytical techniques are required to determine for instance low-level chronic doses, and local doses created on biological tissue ("hot spots")[2-4]. Thus, one specific task was focused on the monitoring of uranium concentration on leaf surfaces. This work was due to the concern

about uranium emission in fly dust originating from a conventional coal-fired power station, which amounts yearly to approximately 2.6 kg for a 600 MW power station[5].

The aim of the first part of the work focuses on the development of ICP-MS methods for ultrasensitive ^{129}I, ^{90}Sr and lanthanide determination in environmental samples such as water and soil. Furthermore, LA-ICP-MS was applied in order to investigate the capabilities in precision and accuracy of direct micro local uranium isotope ratio measurement at ultratrace concentrations on the surface of biological samples. This work includes the development of a cooled ablation cell, which was designed and investigated for biological applications.

In a second part, the potential of LA-ICP-MS in material science was evaluated. In many technical applications, metallic, alloyed or ceramic construction materials are subject to corrosion, in particular oxidation, high temperatures corrosion, which results in a deterioration of physical and mechanical, properties. To reduce the corrosion effects on materials the surface is covered with temperature-resistant protective coatings with a thickness of several hundred µm. The most commonly systems used for high-temperature Ni-based alloys are coatings of the type MCrAlY (M = Ni or Co). The base materials are characterized by relatively low chromium contents, and the substantial addition of titanium, tantalum, tungsten, etc., results in poor oxidation resistance of the materials[6]. Development and application of coating systems which guarantee reliable component protection during long-term service is a crucial requirement for these types of materials in industrial gas turbines. Inter-diffusion between coating and substrate (base material) after oxidation in air at a temperature of 980 ˚C for several thousand hours reduces the life-time of the coating and causes the formation of new, frequently occurring brittle phases at the coating/substrate interface. Several other effects could also result in an alteration of the mechanical properties and/or oxidation performance. Therefore, the determination of the lateral element distribution and diffusion profiles between coating and substrate materials were of major interest. Various materials were studied in dependence on oxidation time in air at a temperature of 980 ˚C.

1.2. Summary of results

1.2.1. Environmental research

^{129}I, ^{90}Sr, uranium and transuranium elements are among the most environmentally important radionuclides. The natural ^{129}I inventory in the atmosphere, hydrosphere and biosphere has been estimated to be about 263 kg[7]. However, the release of ^{129}I from reprocessing plants and the behavior of ^{129}I in the environment has not been explored in detail. In this work, a method for direct, rapid and highly-sensitive determination of low $^{129}I/^{127}I$ isotope ratios in artificial and environmental samples (water, soils) without sample preparation was developed, which applies an ICP-MS instrument equipped with a hexapole collision cell (ICP-CC-QMS). The application of a hexapole collision cell with oxygen and helium as collision gas effectively reduces $^{129}Xe^{+}$ ions and hence improves limits of detection (LOD), accuracy and precision in determination of ^{129}I. The background ion intensity caused by $^{129}Xe^{+}$ ions was reduced to the level of detector specific noise (Daly type detector used in analog mode). By hot extraction of iodine from environmental samples (soils or sediments), its accumulation in a cooling finger and a following on-line introduction of analyte via the gas phase into ICP-CC-QMS was developed. LOD for ^{129}I were significantly improved to concentrations as low as 0.4 pg g^{-1}. For the first time $^{129}I/^{127}I$ isotope ratios as low as 10^{-7} were measured in contaminated sediments, in SRM 4357 (Ocean Sediment Environment Radioactivity Standard) and in contaminated soil samples by using ICP-MS. $^{129}I/^{127}I$ isotope ratio measurements in real environmental samples lead to good precision when applying the developed method.

Significant amounts of ^{90}Sr were produced and dispersed worldwide during atmospheric nuclear weapons tests of the 1950s and 1960s and the accident at the Chernobyl nuclear power plant in 1986. The determination of radioactive ^{90}Sr is of special interest because of its environmental impact on human health via soil-plant-mammals element transfer mechanisms[8]. Therefore, the detection capability of ^{90}Sr using an ICP-CC-QMS was studied in order to improve the LOD for water sample analyses. First, the forward power of ICP ion source was optimised to achieve separation of Sr from potential isobaric interferences. It was found that the operation of the ICP using cool plasma conditions increases the Sr/Zr intensity ratio by a factor of 5. Furthermore, oxygen was added to the nebulizer gas (argon) at various gas flow rates in order to improve cool plasma conditions for Sr measurement[9]. Applying the optimized operating conditions, the

calculated LOD for ^{90}Sr was as a low as 2 ng L^{-1}. Although the application of ICP-CC-QMS in combination with cool plasma conditions reduced the influence of isobaric interferences on m/z=90, the peak tailing of $^{88}Sr^{+}$ and in particular the Daly detector noise were evaluated to be the critical factors for the determination of ultra-low concentration of ^{90}Sr, as required in environmental monitoring of this radionuclide.

Irradiated target material contains numerous spallation products including lanthanide nuclides. Because nuclide abundances of the lanthanides in such samples differ from natural abundance, commonly known isobaric and polyatomic interference corrections are not applicable. This work was focused on the determination of lanthanide isotopes in aqueous samples. Therefore, a capillary electrophoresis based online method coupled to a quadrupole ICP-MS was developed. Here it needs to be mentioned that the technique was aimed to be developed for irradiated EES targets. Due to the earlier mentioned reasons, only lanthanides with natural isotopic composition were used for the method development and testing. The CE-ICP-MS interface was equipped with a self-aspirating electrolyte make-up solution for electrical ground connection and as a control of nebulizer uptake. Fast CE separation (< 15 min) of all lanthanide elements was achieved. The small sample amounts of ≈35 nL were evaluated to be beneficial for reducing the contamination of the ICP-MS, which is even more important for the analysis of radioactive samples. This chemical separation procedure resolves all ions of lanthanides from polyatomic interferences (mainly isobaric interferences generated from oxides of low-mass lanthanide nuclides). The elimination of polyatomic and isobaric ICP-MS interferences only accomplishable using the chromatographic approach due to the fact that ICP-SF-MS is not capable to resolve isobaric interferences. Furthermore, the use of the chromatographic separation allowed to maintain high sensitivity necessary for the determination of the isotopic composition of lanthanides with unnatural isotope abundances.

Contamination of plant leaves is caused by emission originating from nuclear installations and coal-fired plants. Therefore, determinations of the uranium concentration together with the isotopic composition on leaf surfaces are of potential interest for radiation safety and nuclear forensics. In this work an analytical method applying LA-ICP-MS was developed, which can be applied for the determination of uranium isotope ratios on a surface of leaves or for biological samples in general. To maintain the sample in its original form, a cooling system within the ablation chamber was built using two Peltier elements in serial connection under the aluminium

target holder. In order to simulate contamination by atmospheric precipitates and to study the figures of merit of the method, small droplets (20 μL, U concentration 200 ng mL^{-1}) of certified isotope reference standards NIST U350, NIST U930, uranium isotopic standard CCLU-500 and natural uranium were deposited on the biological surface (flower leaf). The leaves were analyzed by LA-ICP-MS and it was found that the cooled ablation chamber contributed significantly to an improved precision and accuracy of isotope ratio measurements in comparison to a non-cooled ablation chamber. An explanation of the observed improvement could be related to an more controlled and reduced water vapour content in the ablated aerosol, which leads to less disturbed ICP excitation conditions. In addition, the change in the adsorption properties influence the laser energy deposited into the sample. Therefore, more material per laser pulse is removed and transported to the plasma, which also improves precision and accuracy. Furthermore, the uranium determination by on-line LA-ICP-IDMS on the surface of biological sample was tested by measuring spiked samples. Thus, the sum of the certified (bulk concentration of uranium in a biological sample) and doped quantity of U in the NIST-SRM 1515 (apple leaves) sample amounted to concentrations of 0.006 μg g^{-1} and 10 ± 0.5 μg g^{-1}, respectively. The values were in good agreement with the by LA-ICP-IDMS determined concentrations of 11.19 ± 1.11 μg g^{-1}.

1.2.2. Material science

To study the elemental diffusion at the interface of NiCrAlY-based coatings on high-temperature alloys, LA-ICP-MS was applied as micro and local analysis technique. Various capabilities of LA-ICP-MS using ‘‘line scan’’ and ‘‘single point’’ mode at laser energies of 2 and 4 mJ and different focus positions were investigated and compared. In general, using the ‘‘line scan’’ mode the RSDs varied for both laser energies between 8 and 20%. A further loss of ion intensities was observed when using a defocused laser beam in combination with ‘‘single point’’ ablation mode, which was mainly attributed to a significant decrease in laser power density during the ablation.
A certified alloy reference material (BAM-328-1) with a matrix composition similar to that of the samples of interest was employed to determine the relative sensitivity coefficients (RSCs) of various elements, which were later applied to quantify the sample composition. In addition to the laser parameter, the dependence of RSCs on the carrier gas flow rate and RF power of the ICP were investigated and optimized. It was found that rf-power and carrier gas flow rates had only a

minor influence on RSCs of the elements measured within this study. RSC values varied within the range of 0.2 to 2, which implies that a semi-quantitative analysis of elements without reference material is possible, whenever an error factor in this range is acceptable. In addition however, other calibration procedures involving external calibration and solution-based calibration were applied and investigated. Analysis of CRM BAM-327-2 using external calibration yields generally better accuracy in comparison to the RSC based quantification method. However, this calibration technique is more time-consuming and the possibility of quantification is limited to the certified elements within the alloy standards.

Based on the optimized quantification procedure, LA-ICP-MS was used to study the lateral element distribution on NiCrAlY-based alloy and coatings after oxidation in air (300, 1000, 5000, 15 000 hours) at a temperature of 980 ℃. Interestingly, the spatial resolution of the technique was sufficient to determine an increasing loss of aluminium due to diffusion from the coating into the high-temperature base alloy. In this study, the diffusion of several substrate alloying elements (e.g., Co, Ta, Mo, W) into the coating after annealing was found. Therefore it is most likely that these diffusion processes contribute to the alteration of the mechanical properties (high-temperature stability) and/or oxidation performance.

2. Measurements techniques

2.1. Radionuclide analysis in environmental samples

2.1.1. Overview of most important techniques for radionuclides analysis

There is a range of well-established radioanalytical and mass spectrometric techniques, which can be used for the trace, ultra-trace and isotope analysis of long-lived radionuclides in different types of samples.

The principle of radioanalytical techniques is based on the direct measurement of the activity of selected radionuclides. Based on the type of emission, the methods can be divided into α-, β and γ-spectrometry. At present, these analytical techniques are effectively used for the analysis of short and middle lived radionuclides[10-14]. However, the characterization of radionuclides with very long half-life the radioanalytical analysis becomes less sensitive, more labor- and time-consuming and careful chemical separation and enrichment of the analytes of interest is required. The major disadvantage of radioanalytical techniques is caused by the long counting time required for determination of long-lived radionuclides, which can take from few days up to several weeks, depending on the sensitivity required[15]. In addition, because of the similarity of the emission energy, certain radionuclides (e.g. for ^{239}Pu and ^{240}Pu) can not be resolved.

Mass spectrometric techniques have several advantages compared to radioanalytical techniques for the analysis of long-lived radionuclides. These include a shorter analysis time, the possibility to distinguish radionulcides with similar alpha-emission energies, an improvement in analytical precision and reducing sample volumes.

For the determination of radionuclides in different sample matrices thermal ionisation mass spectrometry (TIMS)[16, 17], accelerator mass spectrometry (AMS)[18], resonance ionisation mass spectrometry (RIMS)[19] have been routinely used in many analytical laboratories. For example, radiochemical neutron activation analysis (RNAA) and AMS[20, 21] have been well established for the determination of ^{129}I. Depth profiles of ^{129}I and ^{129}I/^{127}I ratios in a sediment core determined by AMS provided information on the transfer of these isotopes from nuclear fuel reprocessing plants to marine sediments[22]. An abundance sensitivity (and following minimal detectable isotopic ratio for ^{129}I/^{127}I) of about 10^{-10} has been achieved using RNAA[21]. High abundance sensitivity for ^{129}I/^{127}I ratio to as low as 10^{-12} has been reported using AMS[21].

However, both of these techniques are based on complicated instrumentation and the analysis is to expensive for routine analyses. An advanced review on different analytical techniques for ^{129}I determination was published by Schmidt et al[23].

Radiochemical analysis techniques are typically used for the determination of ^{90}Sr and show LOD as low as 0.02 pg L^{-1} after sample preconcentration[24]. Paul et al. [25] determined in water solution LOD's of about 2-4 10^7 atoms of ^{90}Sr, but the costs and centralized locations of AMS facilities restrict its use to specialized applications. In general, the determination of ^{90}Sr requires complicated isolation procedures in order to eliminate interferences from other radioactive species (e.g. radioactive isotopes of lead, polonium, plutonium, neptunium and potassium[26]). Furthermore, the liquid scintillation technique for ^{90}Sr is based on the detection of ^{90}Y which is a daughter product of ^{90}Sr due to significantly higher energy of beta-irradiation of ^{90}Y and therefore, significantly better detection efficiency. However, this method requires radioactive equilibrium between ^{90}Sr and ^{90}Y and thus analysis increases significantly (1- 2 weeks).

RIMS has been successfully applied on environmental samples at ultratrace concentrations with detection limits of ~3 x 10^6 atoms ^{90}Sr per sample (~2 mBq) and an isotopic selectivity of $\geq 10^{10}$[27, 28]. Nunnemann et al.[19] determined Pu isotope ratios in environmental samples in order to distinguish between Pu from nuclear power plants and from global nuclear fallout (nuclear weapons tests or from Chernobyl nuclear fallout). Recently, Trautmann[29] and Wendt[30] described the progress of RIMS for the determination of extremely small isotope ratios for a variety of applications.

2.1.2. Capability of ICP-MS and LA-ICP-MS for analysis of radionuclides

Since the last few years ICP-MS has become an established analytical technique for the determination of long-lived radionuclides. This method provides high sensitivity, low background resulting in low LOD's, good precision and accuracy for isotope and isotope ratio measurements and relatively simple sample preparation procedures[31-34]. In order to illustrate the growing application of ICP-MS for the determination of long-lived radionuclides, the number of publication using this technique are compared to those using radioanalytical methods[35].

The major problem using ICP-MS for determining long-lived radionuclides in environmental samples is the appearance of isobaric interferences with stable isotopes of other elements or

molecular ions. Until few years, quadrupole mass analyzers have been used as standard ion separation tools in ICP-MS because of their linear dynamic range, robustness and relatively low costs. However, quadrupole-based ICP-MS provide a resolution power of 300, which is insufficient to deal with the interference problems mentioned above.

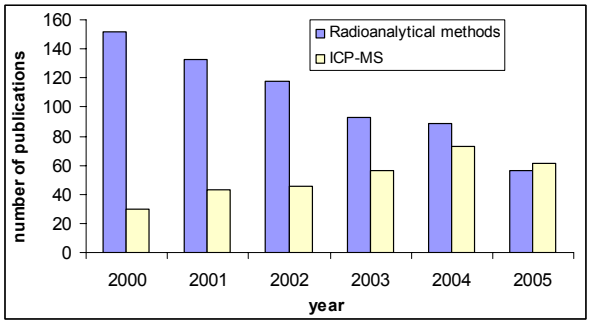

Fig. 2.1.1. Comparison of the numbers of publications reporting about the determination of long-lived radionuclides by ICP-MS and radioanalytical method (2000-2005).

Advanced ICP-MS techniques provide useful features to solve these inherent interference problems. In many cases, molecular interferences can be resolved from the isotope of interest using double-focusing sector field ICP-MS by using higher mass resolution (>3000). Their increasing availability is now allowing to determine rapidly long-lived radionuclides in environmental samples[36-38]. The measurement of Pu in environmental matrices such as sediment and mosses have gain a lot of interest. For example, Agarande et al.[39] found that ICP-MS measurements on moss samples and a certified soil sample agreed well with measurements of $^{240+239}$Pu by the much slower alpha spectrometry technique. The measurements of isotopic ratios of ^{240}Pu / ^{239}Pu and ^{236}U/^{238}U by mass spectrometry[40] have been used as an indicator of an anthropogenic input from irradiated U or for source apportionment studies. Whenever sufficiently elevated concentrations have been present, ICP-MS was able to generate such informations rapidly. ICP-SFMS at medium mass resolution has also been used to assess the ^{236}U/^{238}U ratios in sediments and soils at a realtive abundance of 2×10^{-7}. However, the major limiting factors for the determination of ^{236}U are (a) interference from $^{235}UH^{+}$ and (b) tailing from the ^{238}U peak, i.e., abundance sensitivity.

In contrast to the other ICP-MS instrumentation, the application of reaction/collision cell technology in ICP-MS offers in particular to reduce the contributions from interfering isobaric

ions, which is one of the major advantages of this recently introduced technology. Therefore, ICP-MS with collisional/reaction chemistry has been successfully applied to measure the radioisotopes ^{90}Sr, ^{135}Cs, ^{137}Cs, ^{210}Pb and ^{226}Ra[41]. By optimising the collision cell parameters an improvement in sensitivity for all these radioisotopes has been achieved by a factor of 100, 33, 22, 500 and 50 for ^{90}Sr, ^{135}Cs, ^{137}Cs, ^{210}Pb and ^{226}Ra, respectively. The authors demonstrated that measurement of ^{135}Cs and ^{90}Sr required different collision cell parameters when measuring in the presence or absence of Ba and Zr, which is based on the isobaric interference from the nonradioactive ^{135}Ba and ^{90}Zr isotopes.

Special sample introduction and coupling techniques such as HPLC and CE have been demonstrated to be suitable to avoid interference problems by on-line separating the analytes from interfering ions. A CE coupled to ICP-MS was used by Kuczewski et al.[42] to study the redox speciation of Pu and Np in solution. Separation of Np^{IV}, U^{VI}, La^{III} and Th^{IV} in aqueous acetic acid solution (1 mol L^{-1}) was accomplished within 15 min and LODs of 50 ng mL^{-1} have been reported. Similarly, separation of various Pu and Np oxidation states in a variety of aqueous matrices has also been demonstrated[42].

Measurement of isotope ratios on transient signals by MC-ICP-MS has been described by Günther-Leopold et al.[43] and Krupp et al.[44] (GC-MC-ICP-MS). MC-ICP-MS permits precise isotope ratio measurements for a wide range of elements combined with low limits of detection due to its high sensitivity. The technique is usually applied to continuously introduced samples, but in[43] it was applied for isotope ratio determinations on transient signals generated by a HPLC coupled to an MC-ICP-MS instrument. The results demonstrated that the major contribution to the precision and accuracy in the measured isotope ratios relates to effects within the ICP-MS rather than to fractionation effects on the HPLC column. Preliminary studies on short transient signals of gaseous samples (i.e., dry plasma conditions) showed a reverse fractionation effect compared to flow injection and HPLC generated transient signals (i.e., wet plasma conditions).

Laser ablation ICP-MS was used by Seltzer[45] to detect depleted uranium (DU) in soils. Pressed pellet samples have been analyzed by laser ablation and the $^{235}U/^{238}U$ ratios were measured in order to distinguish between DU and naturally occurring U. Measured ratios were in agreement with those measured by gamma spectrometry. Therefore, the author highlighted the significant reduction in sample preparation. However, problems were caused by the heterogeneity of the sample, which lead to sporadic introduction of analyte into the plasma.

The direct analysis of Pu in soils and sediments using LA-ICP-MS, as reported by Boulyga et al. [46], offered low LOD and fast analysis times suitable for routine analysis. A laser ablation

system (LINA-Spark[47, 48]), modified to produce high ablation rates, was coupled to an ICP-SFMS instrument. Interferences from polyatomic ions (UH^+ and PbO_2^+) and peak tailing from $^{238}U^+$ were reduced by using dry plasma conditions and medium mass resolution (R=4000). This yielded LOD of ~3 x 10^{-13} g g^{-1} (700 μBq g^{-1} ^{239}Pu) for Pu isotopes in soil samples containing U in the low μg g^{-1} range. Quantification has been based on the isotope dilution technique, where a spike has being added to the sample, followed by drying and pressing of the sample into a pellet. The LA-ICP-IDMS quantification has been in good agreement with digestion based alpha-spectrometry or ICP-MS determined concentrations. A CRM has been also analyzed (NIST 4357) and agreement with the certified value of ^{239}Pu + ^{240}Pu (10.4 ± 0.2 mBq g^{-1}) has been demonstrated (9.8 ± 3 mBq g^{-1}). The uncertainty of the LA-ICP-IDMS determinations has been significantly larger than those assigned to the reference value. Therefore, the limitations of the method for the analysis of inhomogeneous samples have been discussed, e.g., the presence of ‘‘hot’’ particles[46].

Furthermore, LA-ICP-MS has been used to detect U on plant leaf surfaces near a radiological settling pond in South Carolina, USA[49]. Residual U has been detected within surface irregularities after the leaves had been washed.

To illustrate the current capabilities of different techniques, the detection limits for the determination of long-lived radionuclides measured by different ICP-MS techniques and LA-ICP-MS were compared and are summarized in Table 2.2.1. It should be mentioned however, although LA-ICP-MS is being increasingly used for ultratrace and isotopic analysis of long-lived radionuclides, the precision and accuracy of this method has usually not been competitive to the conventional solution nebulization ICP-MS employing sample digestion[50].

Table 2.2.1. LOD of different ICP-MS techniques for determination of long-lived radionuclides[50]

Analytical method	Detection limit
ICP-MS (ng l^{-1})	
Quadrupole ICP-MS	0.01-0.6
ICP-SFMS (m/Δm = 300)	0.00004-0.005
ICP-QMS with collision cell	0.003-0.01
ICP-TOFMS	0.1-1
MC-ICP-MS (sector field)	0.0001-0.0002
LA-ICP-MS **(μg g^{-1})**	0.010-0.00001

2.2. Surface analysis in material science

2.2.1. Overview of most important techniques for surface analysis

Amongst a wide variety of analytical techniques for surface analysis, secondary ion mass spectrometry (SIMS) and sputtered neutral mass spectrometry (SNMS)[51, 52] have been extensively used for the determination of lateral element distribution on cross section surfaces in order to investigate diffusion effects at the interface in layered systems. However, a major problem for obtaining quantitative results using SIMS is related to the matrix-dependence of the ion yield, which makes SIMS intensity profiles difficult to quantify without matrix matched calibration standards[53]. SNMS overcomes some inherent limitations of SIMS by detecting sputtered and post-ionized neutrals.

Diffusion of Bi, Sr or Ta from an strontium bismuth tantalite (SBT) layer into a thin layer of silica have been stimulated by annealing at 800 °C for time periods in the range of 1–24 h[54]. The diffusion profiles of the analytes have been determined using SIMS and, in an attempt to elucidate the diffusion mechanism, the results have been compared to profiles derived from theoretical calculations. Although SIMS cannot determine the analytes binding state and environment, it can be used in conjunction with theoretical calculations to obtain indirect information. Therefore it was possible to conclude that that Bi and Sr reacted with vacancies in the silica. The diffusion coefficients for Bi and Sr at 800 °C have been determined to be 10^{-14} and 10^{-15} cm^2 s^{-1}, respectively.

Furthermore, the diffusion of ^{18}O in polycrystalline (Hg,Re)Ba_2-Ca_2Cu_3Ox ceramic superconductors at 450 ºC has also been measured using SIMS by Tsukui and co-workers[55].

SIMS measurements helped to identify a metal–ceramic diffusion interlayer[56]. An electrochemical assisted process under cathodic polarization has been used to coat titanium surfaces with hydroxyapatite[56]. The effects of current density, polarization time and on different Ca/P ratios (1, 1.33 and 1.67) have been studied. ICP-OES has been used to measure the Ca/P ratios of the actual coatings and a Ca/P ratio of about 2 has been determined which indicates an excess of Ca stored in the layer.

The determination of ^{44}Ca, ^{88}Y and ^{96}Zr self-diffusion in single crystalline calcia and yttria doped zirconia over a temperature range of 960–1700 ºC has been performed by SIMS[57]. It was found that Zr bulk diffusion is slower than Ca and Y bulk diffusion and that the rate of diffusion is

related to the cationic radius. For the Y stabilized zirconia, the bulk diffusivity for both Y and Zr is maximal when the Y content was 10–11%. For the Ca stabilized zirconia, The obtained results for the Ca stabilized zirconia show that diffusion of both Ca and Zr is independent of Ca content. The role of diffusion phenomena in the processing of ceramics and the use of SIMS for the evaluation of diffusion coefficients has been discussed in detail by Haneda[58].

Both TOF-SIMS and SIMS have been used to investigate diffusion or layering within polymers. X-ray and neutron reflectivity have been applied in conjunctions with SIMS to determine the extent of probe segregation to an interface in ultra-thin polymer films as a function of thermal cycles[59]. However, the results indicate the absence of segregation[59].

Many semiconductor devices are encapsulated in epoxy moulding compounds[60]. Often, these compounds contain halide ions (either Br as flame retardant or Cl from epichlorohydrin used in the epoxidation) which are able to break down the protective oxide layer on the surface of aluminium metallized components in the presence of water and therefore, accelerate corrosion. Since the rate of corrosion will depend on the rate of ion diffusion, Lantz and Pecht used TOF-SIMS to measure ion diffusion in the epoxy moulding compounds[60]. It has been found that the rate of diffusion depends on the type of moulding compound, on the pH and on the ion concentration.

The Cu diffusion barrier properties of layered silicate/fluorinated polyimide nanocomposites have been studied by Jiang and Wei using transmission electron microscopy (TEM) and SIMS[61]. They found that Cu is effectively retarded from penetrating into the polyimide layers by the layered silicates, and hence the diffusion coefficients of the layered nanocomposites are lower than that of pure polyimide.

Diffusion coefficients of Ag in yttrium barium copper oxide (YBCO) films have been measured over the temperature range 700–850 ºC using energy dispersive X-ray fluorescence (EDXRF)[62]. The Ag atoms have been excited by an annular 50 mCi americium-241 radioisotope source emitting 59.543 keV photons. The authors derived a mathematical algorithm that describes the Ag diffusion across the grains and over the grain boundaries.

Furthermore, Cravetchi et al.[63] applied laser induced breakdown spectroscopy (LIBS) for microanalysis of aluminium alloys to determine minor element precipitates (Mg–Cu and Mn–Cu– Fe) on the surface plane of alloys. Single shot UV laser pulses <μJ have been used to map the surface composition. It has been shown that the two different techniques provide similar information. Authors reported that compositional distribution maps of inclusion elements such as Al, Ca, Mg, Mn and Ti in stainless steel can be generated by an automated line imaging of LIBS

through a "*microline laser*" operating at 532 nm[64]. The emitted light from the micro-plasma was collected onto a charge coupled device (CCD) detector to generate the spatially resolved data. Tomographic maps have been generated using 50 μm spatial resolution between craters by the automated LIBS system. The same approach has been applied by Loebe et al.[65] for the analysis of the element distribution in the area where tool steel was soldered. In this study, a 266 nm diode pumped Nd:YAG laser has been used in combination with echelle optics to generated 2-D information. With this set up it has been possible to determine changes in element distributions along the solder edge and the study permitted the determination of element diffusion in steel samples.

Glow discharge mass spectrometry (GD-MS) and glow discharge optical emission spectroscopy (GD-OES) have also been used for the direct surface analysis of solid samples and depth profiling[66, 67]. Remaining problems are the analysis of nonconducting layered systems and the quantification. Direct helium GD-MS has been used by Itoh and co-workers to determine analytes in steel[68]. The relative sensitivity factors have been calculated from elements in a variety of steel reference materials. The concentrations measured in various steel samples by GD-MS have been in agreement with those measured by XRF spectrometry.

Mixed CeO_2-ZrO_2 systems have attracted widespread interest because of their use in three-way catalyst technology that converts automotive exhaust gases into nontoxic products. Barison et al. described the chemical vapour deposition of a thin film of this material onto cordierite (material which is commonly used in mufflers) so that a high surface to volume ratio material has been produced[69]. The multilayers of the material have been studied using scanning electron microscopy (SEM), x-ray photoelectron spectroscopy (XPS) and SIMS so that the surface and at-depth chemical compositions could be identified.

2.2.2. Capability of LA-ICP-MS for surface analysis

LA-ICP-MS is applied as a bulk and micro local analytical technique in materials research and for geological, biological, medical and environmental materials[70-75]. The use of LA-ICP-MS as a surface analytical technique for the determination of lateral element distribution has also been described for ceramic layers[76] and for profiling of metal layers[77].

Karasev and Suito[78] used LA-ICP-MS to measure the size of Al_2O_3, MgO and complex CaO, MgO, Al_2O_3 inclusions located on the surface of iron and glass samples. Authors state that their

approach allowes calibration between the analytical signal for the inclusion type and for the inclusion particle size has been achieved. SEM and single particle optical sensing (SPOS) methods have been used to verify the LA-ICP-MS results. Good agreement has been reported between LA-ICP-MS and SEM for particles 10–40 μm in diameter. However, the 2–20 μm range provide only reasonable agreement.

Ghazi et al. reported the use of LA-ICP-SFMS to detect nano-leakage at the dentin adhesive interface[79]. Here, a study of the diffusion of silver nitrate into sub-micron voids beneath resin-bonded composite restorations has been carried out. The authors determined ^{43}Ca as well as both Ag isotopes using a Nd:YAG laser operating at 266 (frequency quadrupled) and 213 nm (frequency quintupled) for ablation. Precisions for the analytes ranged from 2.8 to 7.1% RSD in the samples, but were somewhat better (1.8–2.5%) for the NIST 612 glass standard. The LA-ICP-SFMS results of this study allowed to conclude that the amount of Ag increased with the acid-etching time and indicates that this technique is suitable to quantifying the amount of nano-leakage of bonded restorations.

LA-ICP-MS has been successfully applied for quantitative mapping of the lateral elemental distribution of trace elements in multi-phase magnesium-based alloys[80]. A lateral resolution of 32 μm has been sufficient to achieve LOD in the lower mg kg^{-1} range for Ti, Cr, Mn, Fe, Co, Ni, and Cu. Quantification of elements by LA-ICP-MS has been carried out by measuring all elements within the sample and using a sum (100 wt%) normalization calibration procedure. Multi-element mappings over an area of 350 μm x 350 μm have been performed and results for the major elements Mg, Al, and Zn have been compared to EPMA measurements (e.g. 2.2% for MG) and demonstrate the suitability of LA-ICP-MS for this type of analysis.

However, to generate precise and accurate data using LA-ICP-MS, standard reference materials with similar matrix composition should be used for calibration. For example, for trace analysis of zeolites by Pickhardt et al.[81] transferred zeolithes and the reference materials into fused lithiumtetra-borate targets in order to have a similar matrix.

In geology, the NIST glass standard reference materials are most often applied as external calibration standards for the analysis of minerals, glass samples or geological powders transferred in to glasses, e.g. basalt glasses[82]. For calibration purposes, Jochum et al.[83] prepared new geological glass reference materials for micro and local analysis, which have been successfully validated to be applicable as calibration standards for LA-ICP-MS. A good summary of the

application of LA-ICP-MS for the analysis of minerals and inclusions has been given by Heinrcih et al. (2003)[84].

However, in case were no suitable matrix-matched certified reference material (CRM) are available, the quantification is a challenging task in LA-ICP-MS. This is mainly based on the different ablation behaviour of different matrices, which leads to differences in the amount of samples material, different particles size distributions, different aerosol transport and of course to differences in the excitation within the ICP[85]. In such cases therefore, synthetic laboratory standards have been and still are prepared for calibration. One example for the quantitative analysis of trace impurities in ceramic layers of solid oxide fuel cells is given in[76]. Furthermore, alternative quantification strategies using solution-based calibration have been developed for the determination of Rare Earth Elements (REE) in polyethylene materials[86],impurities in geological samples[87] , in silicates[88] and for the determination of platinum nanoclusters[89].

3. Fundamentals

3.1. ICP-MS

During more than 20 years of commercialization, ICP-MS has become the most successful method in many analytical laboratories for the accurate and precise trace element and isotopic determinations in a wide variety of different applications. There are a number of different ICP-MS instruments commercially available, providing a number of pros and cons for specific applications. In general function they consist of many similar components (e.g. nebulizer, spray chamber, plasma torch, interface and detector), but differ fundamentally in the design of the mass spectrometer and in particular the mass analyzer. Generally, the inductively coupled plasma mass spectrometer can be subdivided in the following 5 parts: (i) sample introduction, (ii) ion source (iii) ion extraction, (iv) ion separation and (v) ion detection[90]. In the following paragraph the individual parts of ICP-MS instruments will be described in more detail.

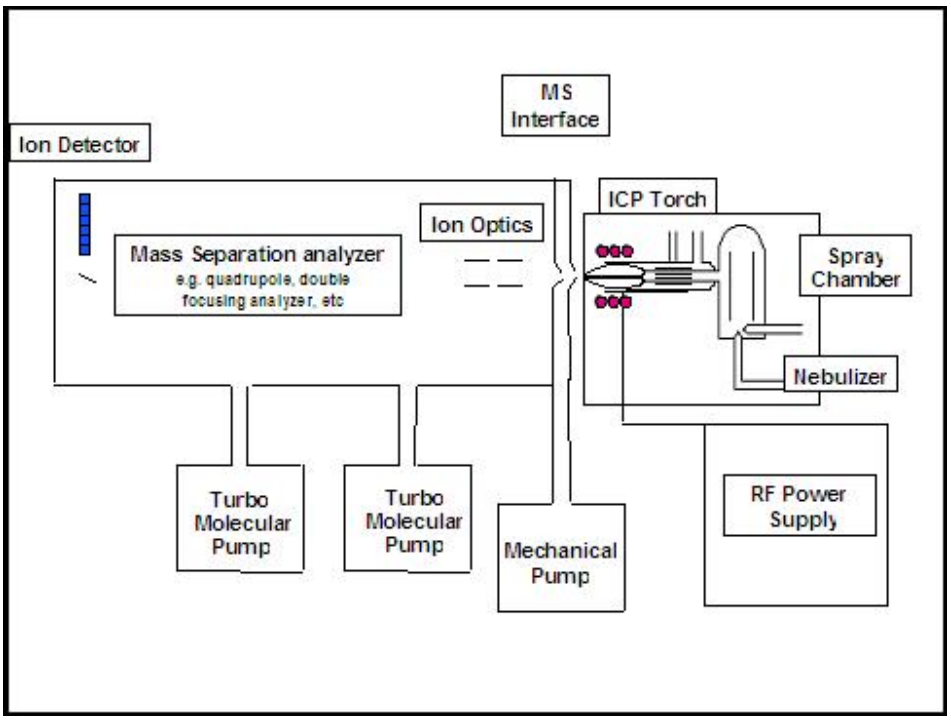

Fig. 3.1.1. Schematic drawing of an ICP-MS.

3.1.1. Sample introduction systems

A variety of sample introduction devices have been coupled to an ICP-MS for gaseous, liquid or solid samples[91].

Generally, liquids are dispersed into fine aerosols using various types of nebulizers and using argon as sample carrier gas at about 1 L/min before being introduced into the ICP. In Fig. 3.1.2 the schematic view of a microconcentric nebulizer (MCN-100) is shown[35].

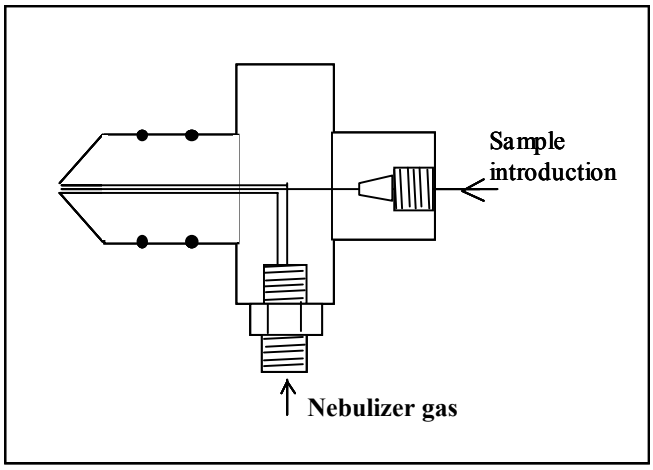

Fig. 3.1.2. Schematic arrangements of a microconcentric nebulizer (MCN-100).

The most common type of liquid sample introduction devices used for ICP spectroscopy are pneumatic nebulizers (PNs) and ultrasonic nebulizers (USNs)[90].

Pneumatic nebulizers used in combination with ICPs have two basic configurations:

- concentric type
- crossflow type

In the concentric type (e.g. Meinhard[92] nebulizer or Micromist), the sample solution passes through a capillary surrounded by a high-velocity gas flow parallel to the capillary axis. The crossflow type nebulizer[93] has a liquid-carrying capillary which is placed 90° to the tube carrying the high-velosity gas stream. These different nebulizers and their figures of merit are extensively described in the literature are applied accordingly to the type of sample of interest[91, 94-96].

The nebulizers are mostly applied in a combination with a spray chamber to remove larger droplets produced during nebulization (e.g. “Scott-Type”) or in combination with desolvation

systems (e.g. “Aridus”[3]) to remove the solvent from the analyte. Recently, microconcentric nebulizers, such as Direct Injection High Efficiency Nebulizer (DIHEN)[97] and DS-5[98] have been introduced. Their major advantage is based on the significantly reduced sample consumption to volumes as low as sub-µl, However, for applications where lowest limits of detection are necessary, ultrasonic nebulizers[99] are preferentially used due to their higher aerosol transport efficiency. This nebulizer is therefore mostly combined to a desolvation device, which is essential for removing excess solvent from the analyte to avoid plasma cooling[90].

For solid sample introduction in ICP-MS different sampling approaches exist such as LA-ICP-MS[70, 72, 100, 101], ETV-ICP-MS[102-104] arc and spark ablation ICP-MS[105, 106], slurry nebulization ICP-MS[107] and direct sample insertion (DSI).

The feasibility of coupling ETV with ICP spectrometry has also been reported as a very efficient sample introduction system. The improved sample transport achievable by this technique permits microvolume sampling and provides detection limits superior by orders of magnitude to those reported for pneumatic nebulization[91]. Similar to ETA-AAS, the initial volatilization of the sample is performed by the controlled heating of a sample supporting device. Such devices may include filaments, boats, ribbons, braids, rods, or tubes constructed of a high-melting-point metal or graphite[91]. A measured weight or volume of sample, solid or liquid, is placed on in vaporizer unit and mobilized through a controlled heating sequence that produces vapor or a highly dispersed aerosol. The aerosol is subsequently transported into the ICP by the carrier gas, usually argon, where it undergoes decomposition, atomization, ionization, and excitation. As in direct sample insertion, ETV-ICP signals are transient. Therefore, simultaneous detection of all analytes of interest is of advantage[90].

Research activities have been also focused on the use of electrical discharges for introduction of solid samples into the ICP. Interaction of the discharges with the sample surface creates a plume of vaporized and particulate matter, which is transportable in a gas stream into the ICP[108].

The types of discharges are classified into two categories: arcs and sparks. Discharge conditions are chosen to remove material from the sample surface in a reproducible manner. Depending on conditions, material can be vaporized, eroded, or sputtered. Discharges are usually operated in an oxygen-free atmosphere, such as argon. As a result, the transport process from the discharge area to the ICP is simplified because the argon is suitable for both discharges.

In order to perform ablation, the sample must by conductive, either naturally or through addition of a conductive matrix material, such as powdered copper or graphite to form of a homogeneous mixture. Transport of sample from the discharge to the ICP is achieved by a flow of argon

through connective tubing, which can vary in length from a few centimeters to several meters. The analytical response is often time–dependent, which is related to element volatility, discharge conditions, discharge stability, and matrix composition. Although much of the published data refers to ICP-AES, spark ablation has recently been extended to ICP-MS[90].
Laser ablation as a solid sampling technique for ICP spectrometry is reported in the respective following chapter.

3.1.2. Ion generation in inductively coupled plasma

The fine aerosol droplets produced by nebulization can represent 2 to nearly 100% of the sample depending of the nebulizer type. These aerosols are introduced into an ICP consisting of a plasma, in which atoms are present in an ionized state. The basic set up of an ICP torch consists of three concentric tubes to support the plasma with cool gas, auxiliary gas and carrier gas. The torch is placed within a water- or argon-cooled rf-coil. As flowing gases are introduced into the torch, the RF field is activated and the gas in the coil region is made electrically conductive by introducing a spark (plasma ignition). After spark-initiated ignition the plasma is formed as a result of a snowball-like increase in the number of ionized species in the RF-field. The formation of the plasma is dependent upon an adequate magnetic field strength and the pattern of the gas streams follows a particular rotationally symmetrically pattern. The plasma is maintained by inductive energy coupling to the flowing gases. In order to prevent possible short-circuiting as well as melting of the torch, the plasma must be thermally insulated from the rest of the instrument. Thermal insulation is achieved by applying an cool gas flow between the inner side of the plasma and the outer tube of the torch at a relatively high flow rate between 15 L/min and 20 L/min. Argon is commonly used for both the intermediate gas and carrier gas. The chemical compounds contained in the aerosol are decomposed into their atomic constitutes in the ICP and ionized with a high degree of ionization (>90% for most chemical elements) and a low fraction of multiply charged ions (~1%)[109]
The plasma acts as a reservoir of energy provided by the rf field, and transfers the energy to the analyte (M). Various ionization processes have been suggested resulting from the presence of species that are obtained during the plasma generation. The major species are not only the argon ions (Ar^+), and the electrons (e), but also the excited Ar^* and metastable Ar^m argon atoms. The main ionization processes can be described as[91]:

1. *Electron impact ionization*

   $e(fast) + M \rightarrow M^+ + e(slow) + e(slow)$

2. *Penning –ionization*

   $Ar^m + M \rightarrow M^{+*} + Ar$

3. *Charge transfer ionization*

   $Ar^+ + M \rightarrow M^+ + Ar$

Different atoms require different ionization energies. Such difference can be successfully applied for improving analytes in comparison to interferences by tuning of the rf-power for preferable ionization of analyte. Based on that it is possible to partially separate potential interfering isotopes or molecules. For instance, Vanhaecke et al.[110] reduced sufficiently the formation of the $^{40}Ar^{12}C^+$ diatomic ions that interfered with the determination of the major chromium isotope at m/z = 52 by using lower rf power of 750 W.

3.1.3. Ion extraction

The ions produced in the plasma are extracted and directed into the mass spectrometer via the interface region, which is maintained at a vacuum of about 0.5 Pa. The interface region consists of two metallic cones (usually nickel), the so-called the sampler and the skimmer cone, which extract the ions through a small orifice (0.6-1.2 mm) into the analyzer. The ion extraction in the interface region is the most critical part of an ICP mass spectrometer, because the ions must be efficiently extracted from the plasma, which is at atmospheric pressure (about 1 MPa) to the mass spectrometer analyzer region at a pressure approximately 5×10^{-6} Pa. The positively charged ions extracted from the ICP have different kinetic energies and trajectories and therefore, before entering the mass analyzer the ions are focused with the ion optics. The principle of such ion focusing (e.g. using the ion lenses) is shown in Fig. 3.1.3. The potentials V_1 and V_2 are different (and lower than $V_{initial}$), forming a non-homogeneous field (see curved dashed lines). The ions will be deflected by the electric field and therefore, focused in the direction of the central path.
In all ICP-MS instruments photons emitted by excited argon atoms result in a high background signal when they reach the detector. To minimize this background, a so-called photon-stop is

utilized in many quadrupole based ICP-MS instruments[111, 112], which is a small metal plate placed in the centre of the ion beam, which prevents photons from reaching the detector.

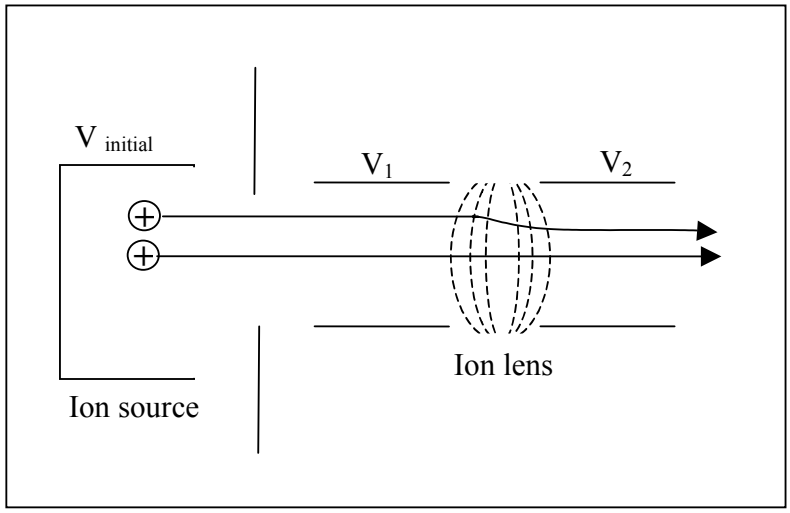

Fig. 3.1.3. Principle of ions focusing with ion lens in ICP-MS[113].

The positive ions are guided around the photon-stop by positively charged cylinder lenses. In other instruments (e.g. Platform, GV) the ion optic system is constructed using a defined angle or off-axis les stack, which also prevents photons from reaching the detector.
In double focusing ICP-SFMS instruments background contributions from photons are significantly reduced (0.2 cps) due to the specific geometry of the mass separation system[114].

3.1.4. Mass analyzers

Ions extracted from the interface region are directed through the ion optics into the mass separation analyzer. The vacuum in this region is maintained at about 10^{-6} Pa. The most common mass separation devices used in ICP instruments are quadrupole, double focusing sector field and time of flight mass spectrometers[115].

3.1.4.1. Quadrupole mass spectrometer

Quadrupole analyzers are mainly used in ICP-MS due to the relatively low costs, their simple operation and their relatively fast m/z separation. However, mass peaks in quadrupoles are not flat-top and request stable mass calibration. Small changes in operating conditions can significantly alter the ion transmission into the analyzer and the mass resolution is low in comparison to other configurations ($m/\Delta m = 300$).

The general layout of the quadrupole mass analyzer is shown in Fig. 3.1.4. Ideally, the four rods should have a hyperbolic profile to generate most stable electric field distribution. In practice, many systems are manufactured using round rods with an interelectrode spacing to produce the best approximation to the optimum hyperbolic field[116].

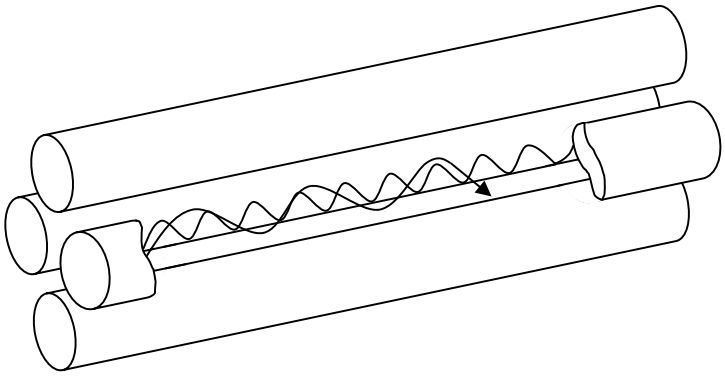

Fig. 3.1.4. Schematic of the quadrupole mass analyzer with cylindrical rods[116].

The potential in a quadrupole field may be expressed in rectangular coordinates by the following equation[117]:

$$V = \frac{V_0}{r_0^2}(x^2 - y^2) \tag{3.1.1}$$

where V_0 is the voltage applied to each rod, and the parameter r_0 is half the distance between opposite rods. The electric field components in the x, y and z directions are therefore [91]:

$$E_x = -\frac{dV}{dx} = -\frac{2V_0 x}{r_0^2} \tag{3.1.2}$$

$$E_y = -\frac{dV}{dy} = -\frac{2V_0 y}{r_0^2} \tag{3.1.3}$$

$$E_z = -\frac{dV}{dz} = 0 \tag{3.1.4}$$

In the static case, the equation of motion in the x and y directions become:

$$\frac{d^2x}{dt^2} = -(\frac{2V_0 x}{r_0^2})(\frac{e}{m}) \tag{3.1.5}$$

$$\frac{d^2y}{dt^2} = -(\frac{2V_0 y}{r_0^2})(\frac{e}{m}) \tag{3.1.6}$$

where e and m refer to the magnitude of charge and ion mass, respectively.
The solution of equation (3.1.5) yields a sinusoidal oscillation in the x-z plane, while the solution of equation (3.1.6) provides an exponentially increasing trajectory in the y-z plane [91].
The mass to charge ratio (m/e) corresponding to the tip of the stability region is given by [117]:

$$\frac{m}{e} = \frac{0.1435V}{f^2 r_0^2} \tag{3.1.7}$$

where m/e, atomic mass units, V, volts; r_0, centimeters; and f (frequency) megahertz.

3.1.4.2. Double-focusing sector field mass spectrometer

The double focusing instruments have been introduced to ICP-MS due to the significant amount of interferences, which limit the access to a number of elements[91]. With the knowledge of the radius of magnetic sector field *r* as well as the widths of the entrance and exit slits it is possible to calculate the maximal possible mass resolution of the magnetic sector field instrument:

$$R = \frac{m}{\Delta m} = \frac{r_B}{(S_1 + S_2)} \tag{3.1.8}$$

with r_B = mu/zB, m-mass of the ion, z-charge of the ion, u-velocity of the ion, B – magnetic field strength, S_1 and S_2 – widths of the entrance and exit slits, respectively.

The formula 3.1.8 assume, however, that the energies of all ions are equal, but in the reality the energy dispersion $\Delta\delta E/qU_B$ (U_B – potential difference) of the ions in ICP should be taken into account:

$$R = \frac{m}{\Delta m} \approx \frac{1}{(S_1 + S_2)/r_B + \Delta\delta E/qU_B} \tag{3.1.9}$$

The eq. 3.1.9 shows that with the reducing energy dispersion of extracted ions it is possible to improve the mass resolution of the instrument. To achieve this, a combination of magnetic and electrostatic field can be applied. Because the ion trajectory deviation resulting from energy dispersion in an electrostatic analyzer is opposite to that in the magnetic sector, the energy dispersion effects in both analyzers will compensate each other, so that finally the energy dispersion of ions does not change their focusing point any more.

Fig. 3.1.5 presents the schematic view of the combination of magnetic and electrostatic field (double focusing) of the mass separation system as well as the calculated ion trajectories for m/z 90 u, 100 u and 110 u.

The operation conditions have been chosen in this example so that only ions with a mass of 100 u can reach the exit slit S_2, where the detector is located (see Fig. 3.1.5a). In Fig. 3.1.5b the calculation was done with the ion energy spread of 500 eV. In this case the ions are not well focused by the magnet, and for a single magnetic device the resolving power would be worse. Double focusing is achieved by the use of the combination of an energy focusing electrostatic field (electrostatic analyzer) located either prior to or after the magnetic field, and the magnet. The electrostatic analyzer field is used to compensate for the energy spread of the ions.

Based on the placement order of magnetic and electrostatic analyzers several different geometries are used: Nier-Johnson, reverse-Nier-Johnson geometry (the magnetic sector is placed before the electrostatic analyzer), and the Mattauch-Herzog geometry[118-120].

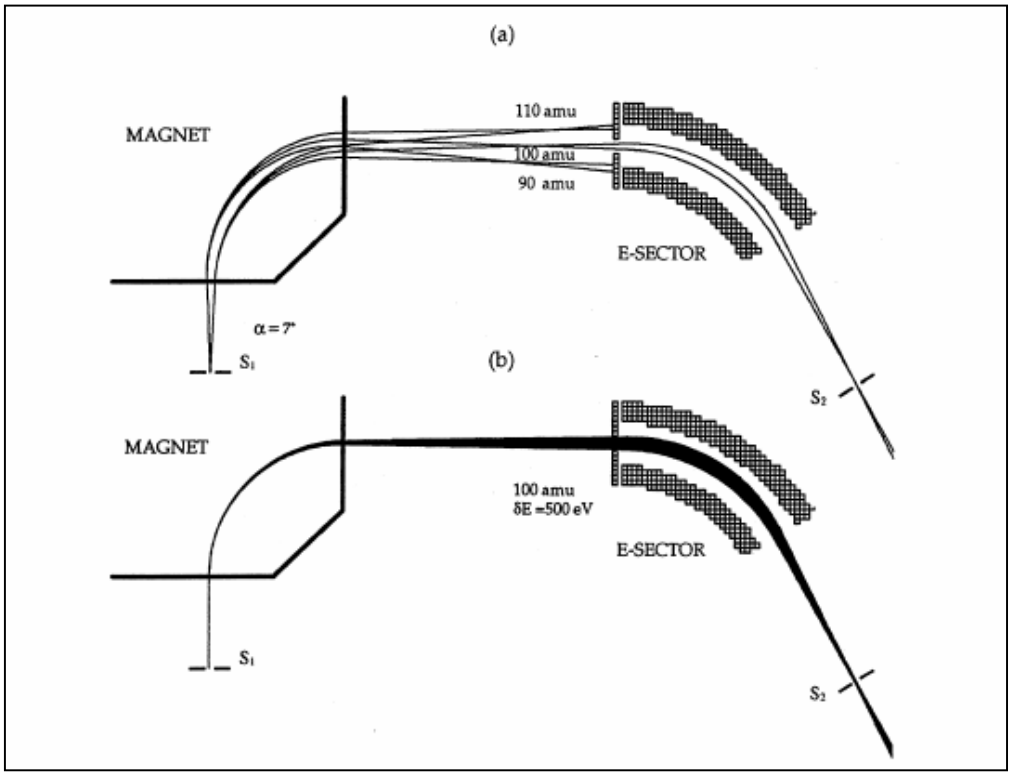

Fig. 3.1.5. SIMION calculations of ion trajectories in a double focusing mass analyzer with a 90°C magnet operated at 4770 Gauss and a 60°C electric sector with a voltage of + and -410 V; U_a = 8000 V; a) ion trajectories for mass 90, 100 and 110 are shown for monoenergetic ions emerging from the entrance slit S_1 with an angle of 7°; b) ion trajectories for mass 100 with an energy spread of 500 eV[121].

3.1.5. Ion detection

The ion beam separated by the mass analyzer is converted to electrical signal using various detectors. The order of magnitude of the signal detectable is in the range from 0.1 ion/s to 10^{11} ions/s. For low signal ranges (< 10^6 ions/s), the ion-counting mode is used, while for higher signals the detector is operated in analogue mode. In the following paragraphs few most commonly applied detector systems are explained in detail.

3.1.5.1. Faraday cup

A Faraday cup detector is shown schematically in Fig. 3.1.7. The Faraday Cup detector is very stable, extremely robust in operation and can very effectively be used for screening unknown samples that may contain high concentrations of elements. The ion beam is directed into a Faraday collector coupled to a true dc amplifier system.

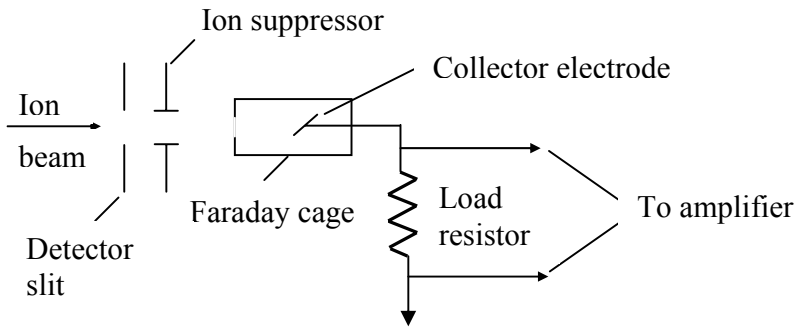

Fig. 3.1.7. Schematic of the Faraday cup[122].

This device can be used to directly measure currents down to 10^{-15} A (corresponding to about 10^4 ions/s). The absolute operating range of the amplifier may be varied by changing the value of the feedback resistor, and the output can be transformed into a series of pulses, which can be handled by the data system using a voltage-to-frequency converter[91].

3.1.5.2. Electron multiplier

In ICP-MS instruments most commonly used ion detectors are a) discrete dynode detectors or secondary electron multiplier (SEM), which consists of a series of metal dynodes along the length of the detector or a continuous dynode electron multipliers (Channeltron). When the ions emerge from the mass separation system, they impinge on the first dynode and are converted into electrons (Fig 3.1.8). As the electrons are attracted to the next dynode, electron multiplication takes place, which results in a very high number of electrons emerging from the final dynode.

This electronic signal is then converted by the data processing system in the conventional way and the readout is in counts (or cps). These cps are directly proportional to concentrations and can be converted into analyte concentrations using comparative measurements of calibration standards. Most detection systems have a dynamic range of up to 6 orders of magnitude in ion counting mode and up to 5 orders of magnitude by combination of ion counting with analog mode (i.e. the measurement of electric current on one of the intermediate dynodes). Therefore, ICP-MS detection can be used to analyze element concentrations ranging from 10^{-12} g/g, up to 10^{-4} g/g.

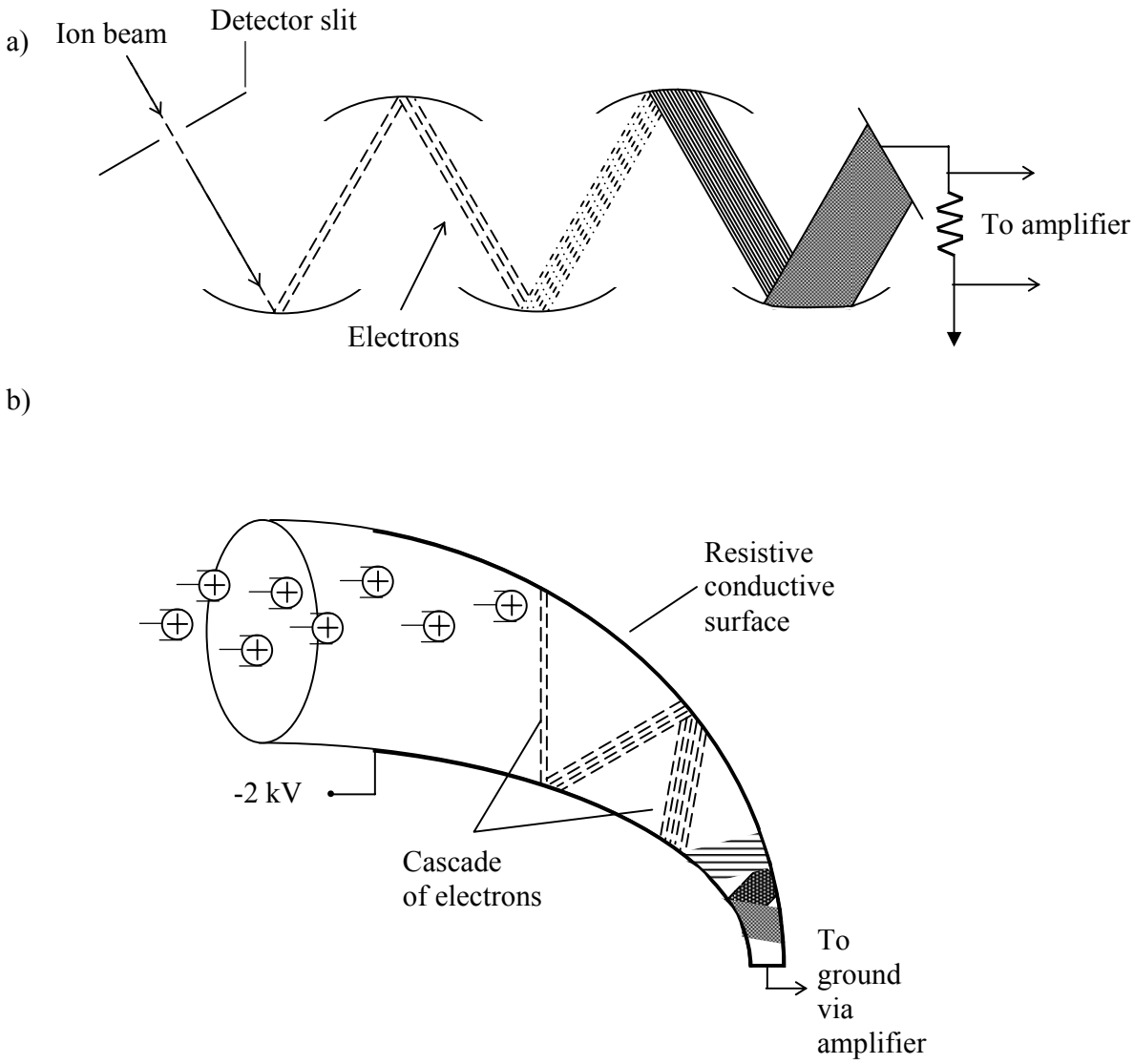

Fig. 3.1.8. Discrete (a) and continuous (b) dynode electron multiplier [122].

3.1.5.3. “Daly”-type detector

Another ion detector type is the “Daly”-type detector, which is used e.g. in the ICP-MS with collision cell Platform (GV Instruments). (Fig.3.1.9) The ion detector consists of a dynode-scintillator and a photomultiplier selectable gain conversion. An incoming analyte ion impacts a conversion dynode, generating a packet of electrons which are accelerated towards a scintillator. The resulting optical emission pulse from the scintillator is detected by the photomultiplier tube. This detection system is also able to work in ion counting and analogue mode. However, due to the relatively long dead time of the ion counting mode, the Daly type detector is only used in analog mode in the ICP-CC-QMS Platform.

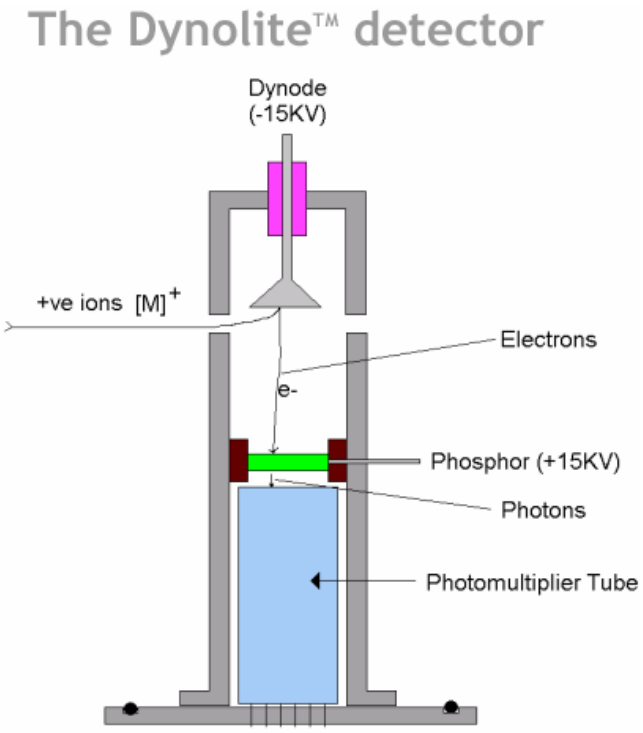

Fig. 3.1.9. Schematic of the Dynolite detector[123].

This detection system operates over a linear dynamic range of 8 orders of magnitude. The detector is able to operate also at high ion intensities ion, even above the linear working range, without the need for protection. The detector operates in a single mode, which does not require cross-calibrations between the analogue and the pulse counting modes.

3.2. Reaction/collision cells in ICP-MS

Application of gas targets in inorganic mass spectrometry was proposed by Becker and Dietze already in 1983[124] for the reduction of the background spectrum and for improving sensitivity in isotopic and trace analysis. The concept was based on the dissociation of interfering molecule ions. The first application of ion molecule reactions have been reported by Rowan and Houk in 1989[125] and was introduced as a instrument in the middle of the 90s. The introduction of a collision gas into rf multipole was found to be useful for improving ion focusing due to a decrease in ion kinetic energy, and for reducing the mean free paths of ions to the dimensions of the rf-multipole when studying the performance of the three-dimensional quadrupole ion trap[126]. The same effect, the so called ‘‘collisional focusing’’, has been found for the linear quadrupole ion guide[127, 128]. The ion-optical properties are well known for quadrupoles utilizing rf and dc operations and were first studied for a hexapole[129]. Although the stability diagram of the hexapole is more diffuse and depends on the initial conditions, the region of ion stability is larger than that for a quadrupole geometry, hence the hexapole is better suited for transporting, guiding and confining low-energy ions beams. In addition to the improvement of the ion transmission ability is also possible to use gas-phase ion molecule chemistry for the neutralization or fragmentation of interfering atomic and molecular ions. The most abundant interferences in ICP-MS are usually caused by argon-based molecular ions (Ar^+ and ArX^+ , where X may be Ar, O, Cl, C, N and so on)[130]. The corresponding ArX neutrals have relatively high ionization potentials. Hydrogen was applied in[131] as a collision gas for removing Ar^+ and ArX^+ ions. By collision with H_2 molecules, Ar^+ ions and argon-based molecular ions ArX^+ can react mainly in three ways:

1. Charge transfer $Ar^+ + H_2 \rightarrow H_2^+ + Ar$
2. Proton transfer $ArH^+ + H_2 \rightarrow H_3^+ + Ar$
3. Hydrogen atom transfer $Ar^+ + H_2 \rightarrow ArH^+ + H$

In particular, the neutralization of the charged argon species allows measurements of Ca, K, Cr, Fe, As, and Se: $^{40}Ar^+$ ($^{40}Ca^+$), $^{40}Ar^{12}C^+$ ($^{52}Cr^+$), $^{40}Ar^{16}O^+$ ($^{56}Fe^+$), $ArCl^+$ ($^{75}As^+$)[132-134]. Furthermore, Kr^+ and Xe^+ ions can also be neutralized by using appropriate gas-phase reactions.

By using collision cell ICP-MS unwanted ions can be removed while operating under normal plasma conditions. The sensitivity of the system remains constant for elements with high ionization energy such as Se and As (in contrast to using “cool” plasma conditions). In addition,

the formation of oxide ions can be reduced. The removal of Kr^+ ions is important for the accurate measurement of Sr isotope ratios due to the overlapping with Kr isotopes.

The collision cell based ICP-MS instruments offer limits of detection of less than 1 ppt for elements such as Pb, In, Sr. For Fe, Ca, K, Cr, Se, and As, detection limits of approximately 10 ppt are reported[129].

Different ICP-mass spectrometric manufacturers have developed reaction/collision cells technologies based on rf-multipoles in order to improve the performance of existing instruments and to extend the application range to elements which have been previously preferred measured by sector field instruments[123 , 135, 136]. Thus, application of a rf-quadrupole filled with reaction gases (hydrogen, ammonia, methane, ethane, ethylene, nitrous oxide and oxygen) in an ELAN 6100 DRC from Perkin Elmer/Sciex allows the effective reduction of the argon ions and argon-based molecule ions by up to 7 orders of magnitude[137]. This is due to application of highly reactive gases as well as due to the band pass filtering of intermediate products of the ion-molecule reaction directly within the reaction cell[133].

In addition, the kinetic energy of the ion can be reduced down to about 1 eV by collision with helium atoms resulting in better abundance sensitivity. This approach is much more effective than for instance increasing the QMS resolution, which would have a significantly lower influence on abundance sensitivity. Thus, when introducing helium into the collision cell a reduction of peak tailing of a high-abundant isotope by up to three orders of magnitude depending on the mass analyzed was observed[138].

The physical features of collision/reaction cells include the number, length, diameter and spacing of the RF multipole rods, the length and the location of the rods relative to the gas filled cell, the position and orientation of the cell within the instrument (distance from differential pumping apertures, beam stop or cell offset/angle applied to stop directed neutral species from the ICP), the use of additional rf/dc fields (e.g. an axial dc field) to supplement the functions of the main multipole ion guiding field, and the design of the ion injection/extraction optics[139].

Several ICP-MS developers have introduced to the market commercial instruments that use quadrupoles, hexapoles and octopoles to serve as reaction/collision cell and to provide the confining fields for ion focusing and guiding. All instruments use specific means to prevent the neutral species from the ICP (Ar metastable atoms) from transforming into the inevitable charged species which could reach the detector, where they might otherwise create new, potentially interfering ions, non-mass-resolved background signals, or detector noise[139]. Various cell entrance/exit ion optics are used, but only few details (design, characterization or modeling) are

available in the open literature. The Perkin Elmer/Sciex instrument uses an axial rf-field and filtering of produced charged species by using a narrow band-pass on a quadrupole-based reaction cell (called dynamic reaction cell)[135]. ThermoElectron uses a high voltage extraction lens followed by a two-element lens in front of the collision cell and a two-element lens behind the cell. Neutrals are separated by steering the ions through a ‘‘jogged’’ path lens (‘‘chicane’’ lens). Agilent and GV Instruments use cells which are directed off-axis so that the ion detector is no longer in the direct line-of-sight view of the ICP. The special lens system at the hexapole exit is aimed to filter the new low-energy charged species created within the collision cell before these ions enter into the quadrupole mass analyzer.

Recently, the construction of the collision cell has been modified for the instrument developed by GV Instrument. The schematic view of the Platform XS instrument with collision cell is shown in Fig. 3.2.1.

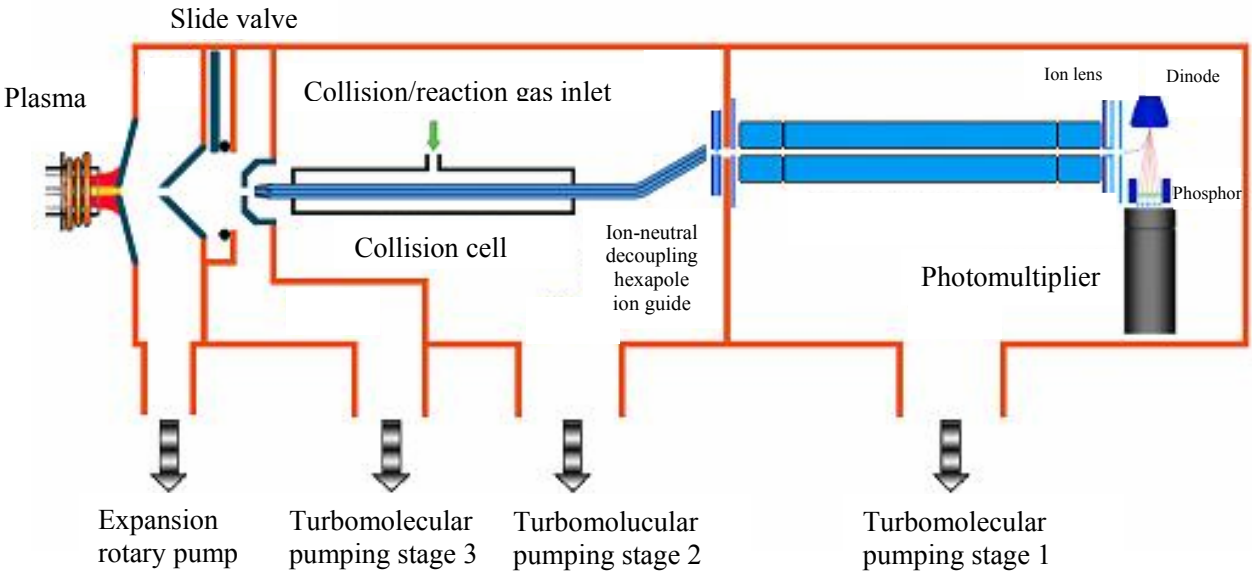

Fig. 3.2.1. Schematic of the Platform XS instrument with collision cell[123].

The hexapole lens assembly is off-axis, with respect to the quadrupole, and is computer controlled. The design does not require a photon stop. A single collimator lens before the hexapole and an asymmetric lens behind the hexapole are the only 2 electrostatic focusing elements.

3.3. Sample introduction in ICP-MS by means of laser ablation (LA-ICP-MS)

3.3.1. Principles

For direct analysis of solid samples laser ablation is potentially the most useful solid sampling technique for ICP spectroscopy[48, 75, 85, 140]. A schematic diagram of LA-ICP-MS arrangements is presented in Fig. 3.3.1.

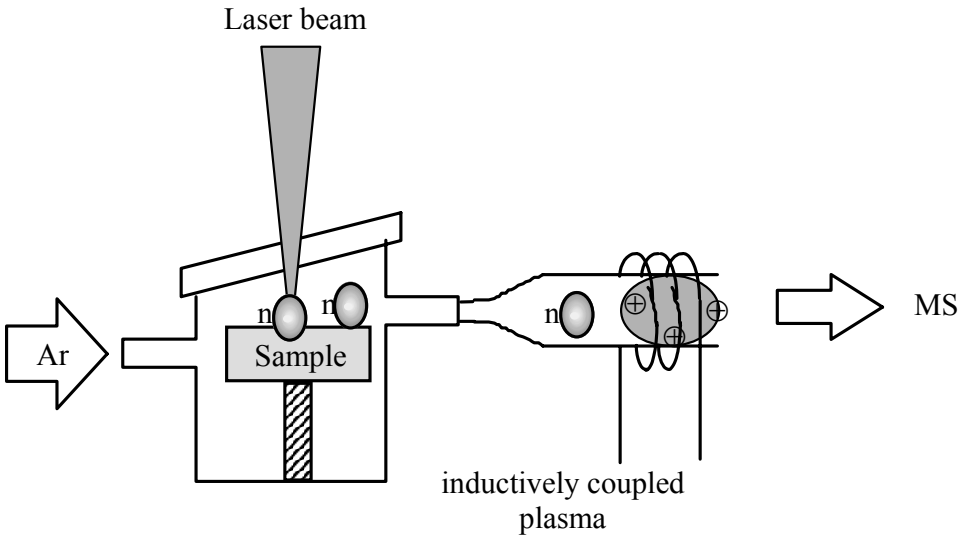

Fig. 3.3.1. Schematic arrangement of the LA-ICP-MS[76].

Similarly to the arc or spark ablation process, sufficient energy in the form of a focused laser beam is directed onto a sample surface to cause the material to be ablated from the surface. The plume of vapor and particulates released from the surface is transported within a carrier gas into an ICP, where the aerosol atomization and ionization takes place. Positively charged ions are then analyzed using the mass spectrometer. This basic principle has been introduced by Gray in 1985 and in various modification used for direct solid analysis[141].

The growing interest in LA is based on the ability to sample a wide range of diverse conducting and non-conducting materials. The main advantage of laser ablation ICP-MS is the possibility to analyze samples directly with low or without sample preparation, thus overcoming the potential

problems related to contamination and analyte losses. This method is particularly useful for the analysis of dissolution-resistant minerals, ceramics or other materials. Additional advantages are the reduction of reagents for dissolution, labor costs, avoiding solvent induced spectral interferences, and the possibility to obtain spatial information of analytes within the sample due to the capability of high spatial resolution analysis using focused laser beams. Furthermore, drilling into the sample, elemental distribution within 3 dimension can be generated, which is in particular of interest for depth profiling of layered structures.

The signal intensity measured is proportional to the amount of ablated and transported material into the ICP. However, the rate and amount of material ablated depends not only on sample type and surface conditions, but also on laser properties and operating conditions[142-150]. These include wavelengths, laser energy, laser pulse duration, repetition rate, focus or image position, laser operating mode (single crater drilling or scanning ablation) and the gas environment during ablation[142-150]. Studies on different ablation cell geometries and the length of the transport tube have shown to be less critical for the material transport into the plasma[151-154].

During the interaction of laser radiation with a solid surface, the sample material is ablated due to photon energy deposition (partially thermal heating) on the sample surface and a "material plasma" consisting of electrons, ions and neutrals is formed. This plasma cools to room temperature within a very short period of time and particles of the sample are formed by nucleation, condensation and agglomeration (Fig. 3.3.2.), which are than transported to the ICP.

In contrast, the visible Ar plasma (with low fractional ionization) arising from interaction of the photons with the argon gas above the material plasma within the laser ablation chamber, consists mainly of metastable excited Ar atoms. This Ar plasma gives no contribution to the ablation of the sample material (to low energy and short lifetime of the excited species). During ablation of different homogeneous samples, researchers observed that the intensity ratios of different elements change upon progressive ablation from a single crater. In order to describe these non-stoichiometric effects in LA-ICP-MS, Fryer[155] introduced the term "elemental fractionation" and calculated a relative fractionation index, which represents the relative degree changes of element ratios over time or progressive ablation into the sample. The fractionation index allows elements to be classified into groups with similar behavior during ablation and ionization[156]. Unfortunatelly, this definition and calculation does not take into account potential elemental fractionation between different matrices and indicates only constancy of the ablation process within a given matrix[155, 156].

Wavelength and related irradiance are the major variables that have been used to study this phenomenon in detail. The fractionation of U versus Pb in silicates was significantly reduced by using shorter laser wavelength. The advantages of the shorter wavelength are based on reduced thermal alteration of the sample material during ns-laser pulse[157].

Improvements are related to an increased coupling of the laser energy into the sample, leading to higher energy densities. This increased absorptivity directly translates to smaller ablation rates in opaque materials at a given irradiance[158, 159] and reduces the heat-affected zone in the sample. NIST glass standard (610, 612 and 614) were ablated using 193 and 266 nm LA system[158]. A comparison of the intensities measured for the analytes are most significantly different for 266 nm ablation, which is related to the different absorptivity of the NIST glass samples. However, these differences become almost insignificant at 193 nm, which indicates that the ablation rates for the lower wavelength are less dependent on absorptivity[158].

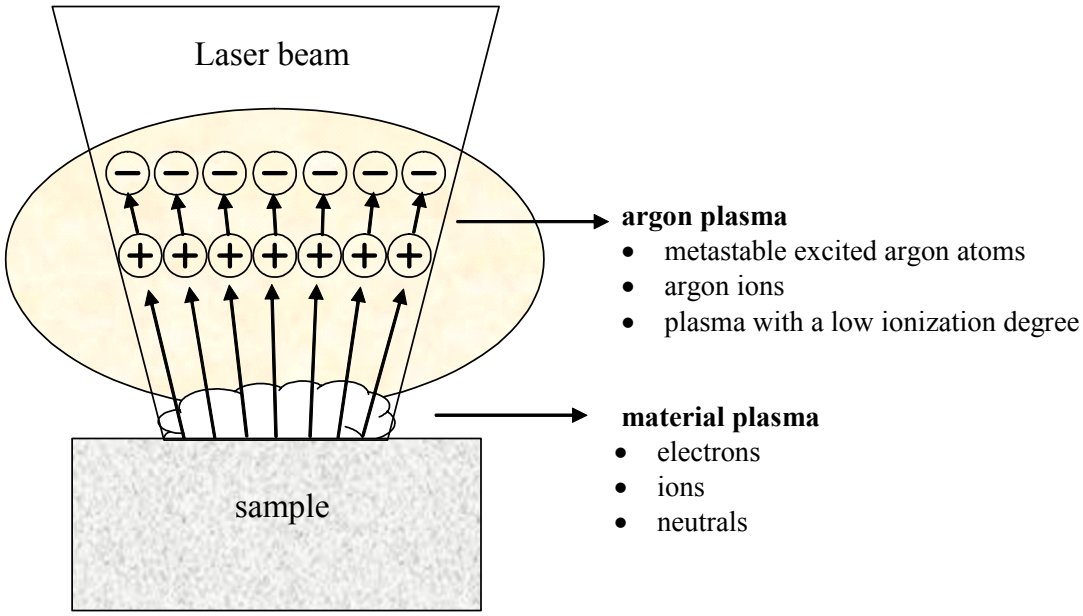

Fig. 3.3.2. Interaction of the laser beam with solid surface[160].

The absorptivity at this wavelength seems to be similar for NIST glasses which are illustrated by the similar sample removal rate per pulse even when having largely different trace element concentration from 450 to 0.7 μg/g (NIST 610 to NIST 614). However, significant differences were observed using 266 nm for ablation. The material removal by the 266 nm laser is dependent

on the absorptivity of the material ablated. In highly UV transparent samples, the laser energy is absorbed in a larger volume leading to higher ablation rates[158].

However, for metallic samples, the wavelength has only a little effect on the ablation characteristics[161] and the pulse duration appears to be the most dominant parameter affecting the formation of molten material in the ablation spot and therefore, the stoichiometry of the generated aerosol. Recently, Koch et al.[162] showed that selective vaporization during LA of brass can be significantly reduced by using femtosecond (fs) instead of nanosecond (ns) laser pulses.

With irradiated laser power densities of $\Phi < 10^9$ W/cm^2, the sample material is only incompletely vaporized and, depending on the material properties, fractionation effects. The occurance of these fractionation effects are significant and limit the quantitative trace analysis capabilities[163]. On the other hand, with irradiated laser power densities of $\Phi > 10^9$ W/cm^2, significantly lower fractionation effects can occur. However, time-dependent signal ratio variation based on the changing particle sizes generated during progressive ablation into the sample is currently the most severe limitation of laser ablation at wavelength such as 266 nm.

3.3.2. Instrumentation

Significant improvements in LA-ICP-MS have been achieved due to the rapid development in laser technology. In the past 20 years, lasers with different wavelengths (Table 3.3.2) have been tested in combination with ICP-MS, however the most widely used are the UV wavelength (266, 213 and 193 nm)[85].

In LA-ICP-MS, different commercial laser ablation systems – mostly solid state Nd-YAG laser ablation systems (e.g., CETAC LSX 200, LSX 500 and LSX 3000, Cetac Technologies, Omaha, NE, USA; Merchantek LUV 266 nm laser microprobe, UP 213, UP 266, UP 266 Macro from New Wave Research/Merchantek, Fremont, CA, USA; VG MicroProbe 2, Thermo Finnigan, Bremen Germany; Ablascope 213 nm, Bioptic, Berlin, Germany) have been coupled to several types of ICP-MS. Furthermore, a few commercial excimer laser ablation systems (e.g. UP 193H, New WaveResearch/Merchantek; GeoLasArF, MicroLas, Göttingen, Germany) are currently available on the analytical market and several home-made[150, 164-166] laser ablation systems have also been developed and are still in use in different laboratories. Application of excimer lasers in laser ablation ICP-MS is increasing because the shorter wavelength lead to smaller particle size

distributions, more complete vaporization of such particles within the plasma and therefore, reduced fractionation effects[167].

Table 3.3.2. Year of first report on the different laser types and wavelengths for analysis with ICP-MS[85]

Year	Laser	λ (nm)	T[a]	References
1985	Ruby	694	Ns	[141]
1992	Nd:YAG	1064	Ns	[168]
1993	Nd:YAG	266	Ns	[169]
1995	ArF	193	Ns	[170]
1996	KrF	248	Ns	[171]
1997	Nd:YAG	532	Ns	[172]
1997	XeCl	308	Ns	[173]
1998	Nd:YAG	213	Ns	[174]
2002	Ti:Sapphire	≈800	Fs	[175]
2003	F2	157	Ns	[176]
2003	Nd:YAG	193	Ns	[177]
2003	Ti:Sapphire	≈260	Fs	[148]

[a] Pulse duration

3.4. Capillary electrophoresis

CE is a method in which ions are separated by differences in their rates of migration through a silica capillary[178, 179]. The capillary is filled with an electrolyte solution and each end of the capillary is placed in an electrolyte reservoir which also contains a platinum electrode. The electrodes at the two ends of the capillary are connected to a high-voltage power supply (0-30 kV). Ions in solution can flow through the capillary to complete an electric circuit. The sample ions migrate at different velocities towards the electrode of opposite charge (electrophoresis flow). The sample ions are detected spectrophotometrically as they pass through a cell near the end of the capillary[178].

Separations by ion chromatography (IC) and CE are both based on differences in the velocities at which ions move through a column or capillary. However, in IC these differences in velocity are the result of differences in partitioning of sample ions between a stationary ion exchanger and the liquid mobile phase. In CE there is no partitioning between the two phases and differences in velocity are the result of differences in electrical mobility (electrophoretic mobility) through a non-packed capillary[178].

CE has several advantages in comparison to IC. For example, separations by CE are fast and it is relatively easy to adjust experimental conditions to obtain an adequate separation of sample ions. However, CE is limited by the choice of detectors, the relatively low sensitivity, problems with reproducibility. Furthermore it has been reported that CE is a somewhat more complicated technique in comparison to IC[178-180].

3.4.2. Principles

Separation of anions is based on differences in electrophoretic flow. Inorganic ions are generally smaller and therefore more mobile than organic ions. The electrophoretic mobilities of inorganic ions are an inverse function of their hydrated ionic radii. Electrophoretic mobility is also affected by the charge of an ion and by the solvent medium. Therefore, tables of ionic conductance are a convenient source for estimating electric mobilities of ions[178].

In addition to electrophoretic flow, a second type of migration occurs in the capillary called electroosmotic flow (EOF). A minute charge on the capillary surface (called the zeta potential) results from ionization of silanol groups, which have a pK_a of 6 to 7[178].

$$-SiOH \leftrightarrows SiO^- + H^+$$

Cations from the bulk solution are attracted to the capillary surface. These cations are forced toward the cathode. Since the cations are hydrated and the inner diameter of the capillary is quite small, their migration induces a bulk liquid flow (a plug flow). This means that all of the liquids and solutes in the capillary flow at the same rate toward the cathode (electroosmotic flow). The mobility of the solute resulting from EOF is termed the electroosmotic mobility (μos)[178]. EOF in fused silica capillaries is pH-dependent. The EOF is very low around pH 3-4, but rises rapidly around pH 5-6 as the silanol groups become progressively more ionized. Finally, the EOF is around pH 8-9. Vectors can indicate the magnitude and direction of electromigration. For sample, for cations in neutral to alkaline solution is the electrophoretic and electroosmotic flow vectors in the same direction, which is called comigration. The electrophoretic vectors of anions are in the opposite direction to the cationic vectors. Usually the electroosmotic vector is larger than the electrophoretic vector, so that the netto movement of anions is still toward the cathode. This is important because the separated sample ions (anions in this case) must all pass through the detector. A separation in which the electrophoretic and electroosmotic vectors are in the opposite directions is called counter migration. A separation with counter migration will take longer than one with comigration, but the separation power of counter migration is usually better[179, 180].

Table 3.4.1. summarizes several equations that apply to CE. Eq. 1 states that the velocity (cm/s) of an moving ion is a function of its mobility and field strength (V/cm), which is defined in Eq. 2. Ionic mobility (cm^2/V s) is defined in terms of column length, migration time and applied voltage (Eq. 3.). Eq. 4 shows that ionic mobility (cm^2/V s) is made up of electrophoretic and electroosmotic mobility. In CE as in other chromatographic techniques, the separation power is often stated by the number of theoretical plates, N[178-180].

Table 3.4.1. The most important fundamental equations that apply to CE

1. Velocity, [cm/s]	$V=\mu E$	μ=mobility, $cm^2/V\ s$ E=field strength, V/cm
2. Field strength [V/cm]	$E=U/L$	U=applied voltage, V L=capillary length, cm
3. Mobility [$cm^2/V\ s$]	$\mu=L_dL/tU$	L_d=length to detector, cm L=length (total), cm t=migration time, s U=applied voltage, V
4. Mobility [$cm^2/V\ s$]	$\mu=\mu_{ph}+\mu_{os}$	μ_{ph} = electrophoretic mobility μ_{os} = electroosmotic mobility

3.4.1. Experimental setup

The essential parts of a CE instrument are shown at Fig. 3.4.1. A background electrolyte (BGE) is placed in reservoirs and then pumped through the capillary to fill it with BGE. A typical capillary is made of fused silica.

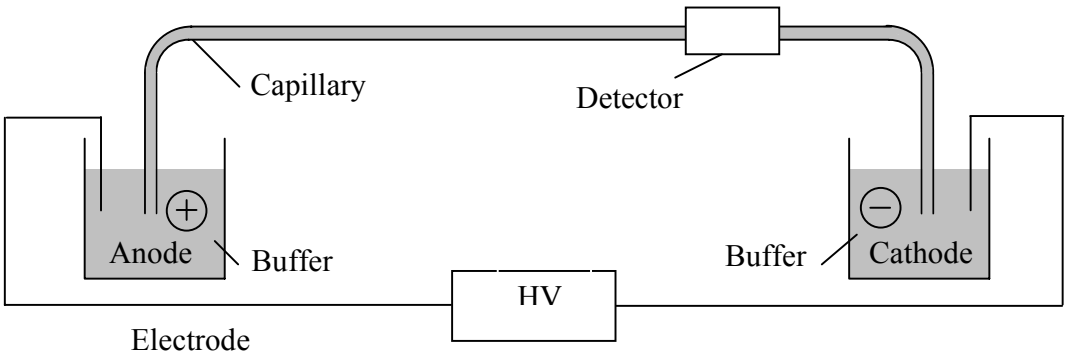

Fig. 3.4.1. Schematic set up of a capillary electrophoresis.

The diameter is often in the order of 50 or 75 μm i.d. and a capillary is approximately 60 cm long. A platinum working electrode is placed in each reservoir and connected to a high-voltage power supply capable of generating voltage of up to 30 kV. A positive power supply makes the electrode (L) the anode (positive charge) and the other electrode (R) the cathode. With a negative power supply these polarities are preserved. Conditions must be always selected in a way that sample anions migrate from left to right and thus flowing towards the detector.

4. Experimental

4.1. Instrumentation

4.1.1. ICP-MS

The instruments used in this work were the following:

- ICP-CC-QMS (Platform ICP, Micromass Ltd., Manchester, UK)
- ICP-SFMS ("Element 1", ThermoElectron, Bremen, Germany)
- ICP-QMS (ELAN 5000, Perkin-Elmer/SCIEX)

and will be described in more detail.

Platform ICP

The Platform (GV Instruments, Manchester, UK) is a quadrupole-based ICP-MS (See.Fig.4.1.1) with an ion transfer system based on a hexapole collision cell (ICP-CC-QMS)[123, 138, 181, 182]. Oxygen and helium were introduced into the hexapole cell as collision gases. Gas input into the hexapole was controlled by built-in mass flow controllers. For solution introduction into the instrument, a Meinhard nebulizer (J.E. Meinhard Associates, Inc, Santa Ana, CA, USA) with a Scott double-pass quartz spray chamber cooled to 4 °C was used. Aqueous solutions were introduced in the continuous flow mode via a peristaltic pump (Perimax 12, Spetec GmbH, Erding, Germany). Sample introduction systems as a solid sampling technique attached for this instrument are reported in a corresponding paragraph (4.1.2).

The sampler cone is made of nickel and is on the back side coated with a copper substrate for efficient cooling of the cone. The skimmer cone is also made from high purity nickel. The region between the two cones is evacuated by a rotary pump. The hexapole lens assembly is off-axis, with respect to the quadrupole and computer controlled. Due to the off-axis geometry a photon stop is not required. For optimum transmission and abundance sensitivity performance, the system employs a four stage differentially pumped vacuum system with three turbo pumps and two stage rotary pump. The detection system (Daly-type) operates at a linear dynamic range of 8 orders of magnitude.

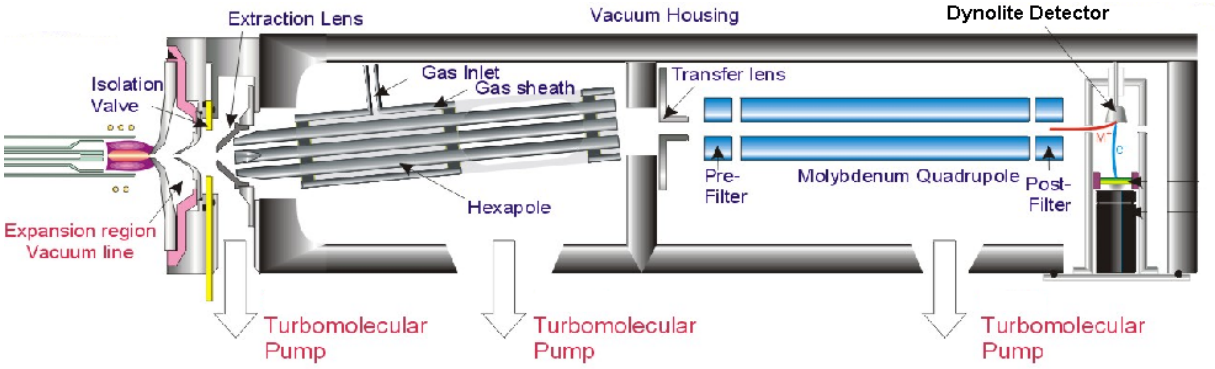

Fig. 4.1.1. Schematic diagram of the Platform ICP, Micromass.

Element 1

The Element 1 (ThermoFinnigan, Bremen, Germany) is a double focusing sector field instrument with a reverse Nier-Johnson-geometry. A schematic set up is given in figure 4.1.2. The argon plasma ion source and sampling interface of the instrument are at ground potential. This enables the straightforward coupling with chromatographic or laser ablation sample introduction systems. A grounded platinum electrode GuardElectrode*2* (GE) from ThermoElectron, is inserted between the quartz torch and rf load coil in order to reduce the plasma potential and for further improvements of sensitivity. The ion transfer optics focus the ions from the plasma interface onto the entrance slit of the double focusing analyzer. The magnet used in this instrument is specifically designed for use in ICP-MS applications. It is relatively small (sufficient for the mass range 0 – 260 u), laminated and efficiently water-cooled for highest mass stability. After passing through the magnetic field the ions enter the electrostatic analyzer for energy focusing. The use of the magnetic sector mass spectrometers offer advantages related to resolution, peak shape and background intensity[114, 183]. Double focusing mass spectrometers permit variable resolution using three different sized entrance slits. Beside the entrance and exit slits a third intermediate slit is installed in the Element 1. Using the fully open intermediate slit the instrument can be operated in low resolution mode, which is characterized by the flat-top peak shape. This peak shape is advantageous when using the instrument in a peak hopping mode because small changes in the mass calibration will not affect the signal intensity. By decreasing the peak widths the resolution

increases and the instrument can be operated in the medium and high resolution modes. Typical mass resolution values R of the Element 1 are 300, 4000 and 11000, respectively.

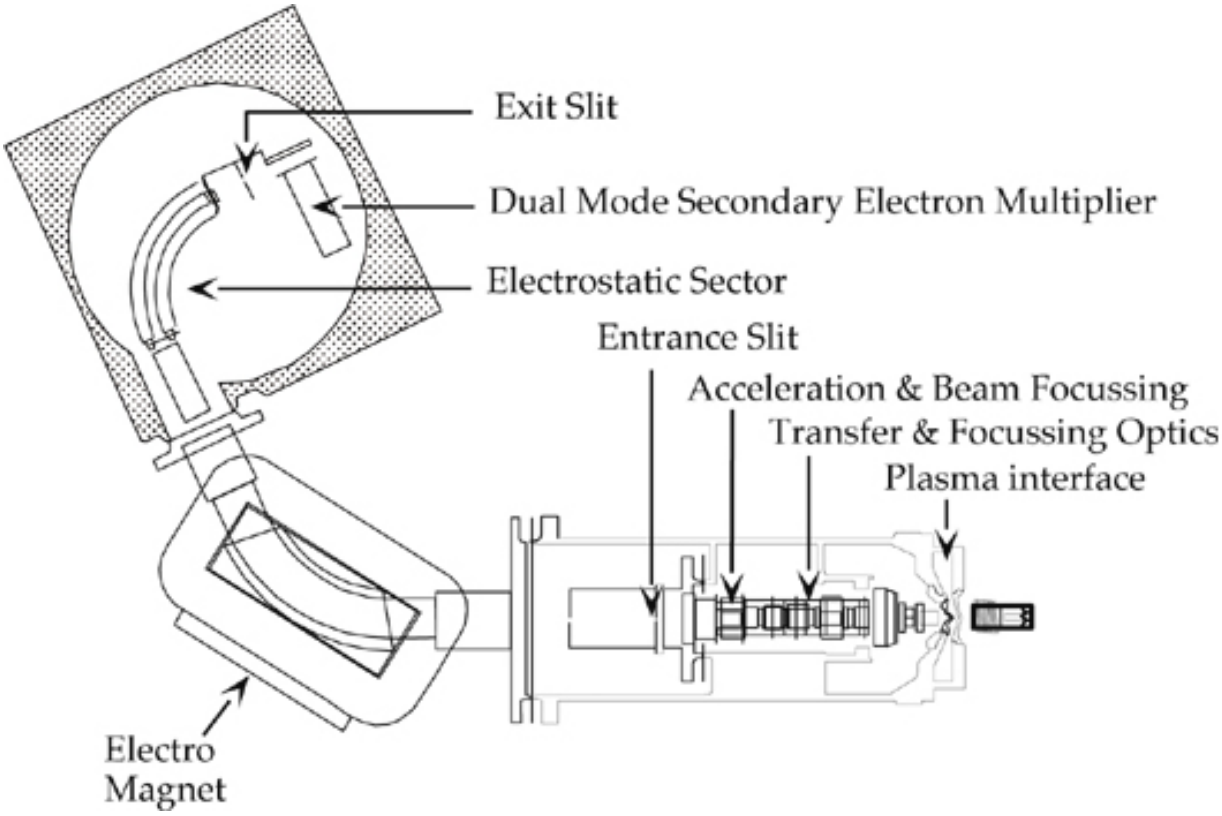

Fig. 4.1.2. Schematic arrangement of reverse Nier –Johnson geometry High Resolution ICP-MS instrument (the Finnigan ELEMENT)[183].

The flat topped peak shape obtained using stable magnetic sector instruments allows also better precision for isotope ratio measurements in comparison to the Gaussian peak shape generated in quadrupole-based instruments, The curved optical axis of the double-focusing geometry greatly reduces the photon background derived from the ICP without reducing sensitivity. For heavy masses, the background counting rate is negligible (< 0.2 cps) leading to high signal/noise ratios and low LOD. The background becomes only significant for elements m/z < 85 due to spectroscopic interferences generated from the plasma and sample matrix introduced[114]. However, some of these interferences can be significantly reduced or resolved by applying the different resolution modes available for this instrument[114]. Further reduction of interferences can be achieved by using dry plasma conditions as used in laser ablation[184].

ELAN 5000

The schematic operation principle of the ELAN 5000 is presented in Fig. 4.1.3.

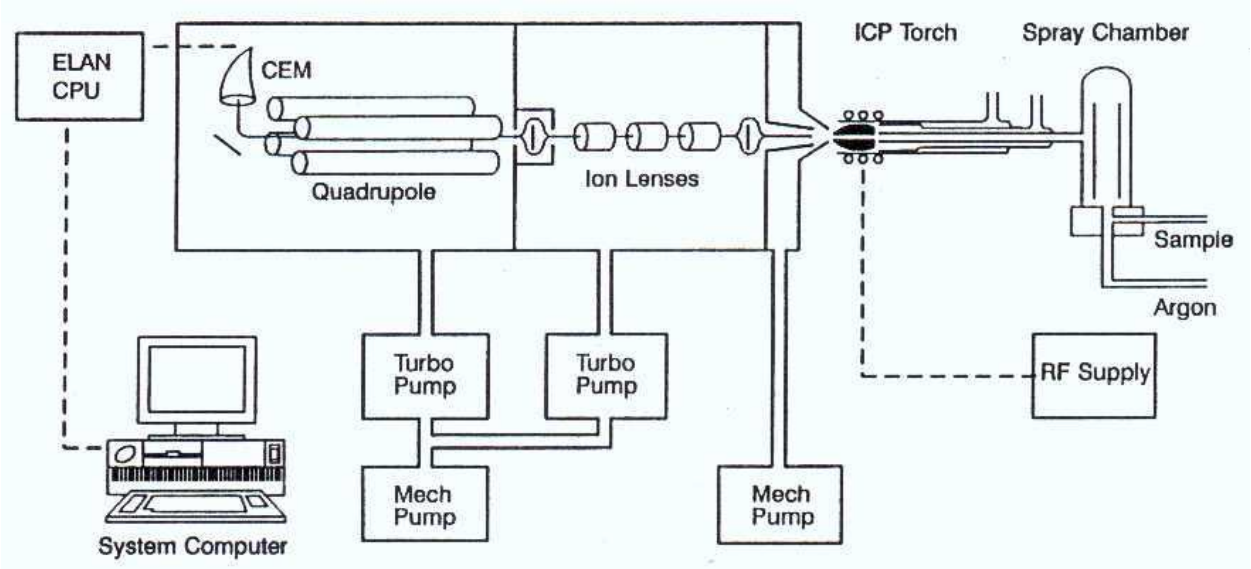

Fig. 4.1.3. Schematic diagram of the quadrupole ICP-MS ELAN 5000.

This instrument has been first launched in 1990 and has been a "work-horse" over a long period of time. The general principle has been described in a large number of publications[185-190]. However it should be mentioned that a photon stop blocks the photons coming from the ICP,and the ions are focused by a block of electrostatic lenses (positively charged). The number of lenses in current instruments is significantly reduced, which is based on the fact that each lens contributes to background. Furthermore, the quadrupole mass analyzer (4 rods, approximately 1 cm in diameter and 30 cm long) is longer incomparison to current systems, which leads to increased quadrupole settling times longer than those commonly applied today. Once the ions have been separated according to their mass-to-charge ratio, they are detected by the channel electron multiplier (CEM).

4.1.2. Sample introduction systems

4.1.2.1. Design of sample introduction device for iodine isotopic measurements

Within this work a special sample introduction device for iodine thermal desorption from solid materials and on-line introduction of iodine into the ICP-MS via the gas phase was designed and realized. The experimental configuration is shown in Fig. 4.1.4.a. For example, a solid soil sample (1–5 g) can be placed into an oven and heated to T ~ 1000 °C over approximately 20 min. After this period a high purity oxygen (Linde Gas AG) was introduced into the oven acting as an oxidant and carrier gas at a flow rate of 80 ml min^{-1}. The evaporated iodine was transferred into the ICP-CC-QMS for on-line measurement of transient signals of $^{129}I^{+}$ and $^{127}I^{+}$ and $^{129}I/^{127}I$ isotope ratios.
Furthermore, the developed sample introduction device was equipped with a cooling finger which was placed behind the oven for iodine hot extraction and in front of the ICP-CC-QMS for online measurements. Experimental arrangement is shown in Fig. 4.1.4.b The evaporated iodine was enriched in the cooling finger and trapped by using liquid nitrogen cooling. During the warming sequence of the cooling finger, the iodine was again mobilized and transferred to the ICP-CC-QMS.

4.1.2.2. Capillary electrophoresis

The schematic drawing of the CE-ICP-QMS interface is shown in Fig 4.1.5. The interface consists of a PEEK tubing, PEEK finger tight fitting and a PEEK four way adapter (Upchurch Scientific, Oak Harbor, WA, USA).
Orange PEEK tubing (0.50 mm id x 1.6 mm od) were used as a sleeve around the CE capillary into the four way adapter. The makeup electrolyte was aspirated through a 20 cm Teflon tubing (1.0 mm id x 1.6 mm od). The 0.50 mm platinum interface electrode was sealed via a PEEK sleeve (orange = 0.50 mm id x 1.6 mm od) and sealed inside the back of the nebulizer via a 1.5 cm Tygon peristaltic pump tubing. It is important to make all the fittings air tight since slight leaks affect the self aspiration of the nebulizer. The platinum electrode was grounded in the CE instrument by using a copper wire fitted with alligator clips. All the CE solutions were degassed and filtered through a 0.45 mm filter paper.

(a)

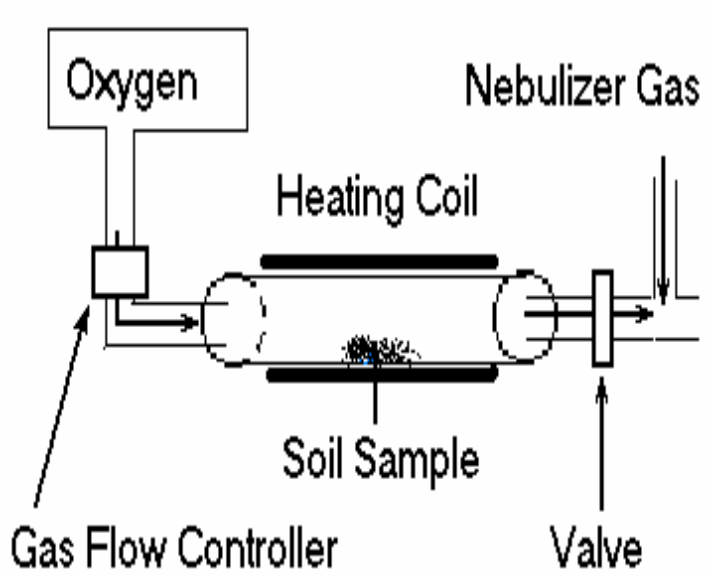

(b)

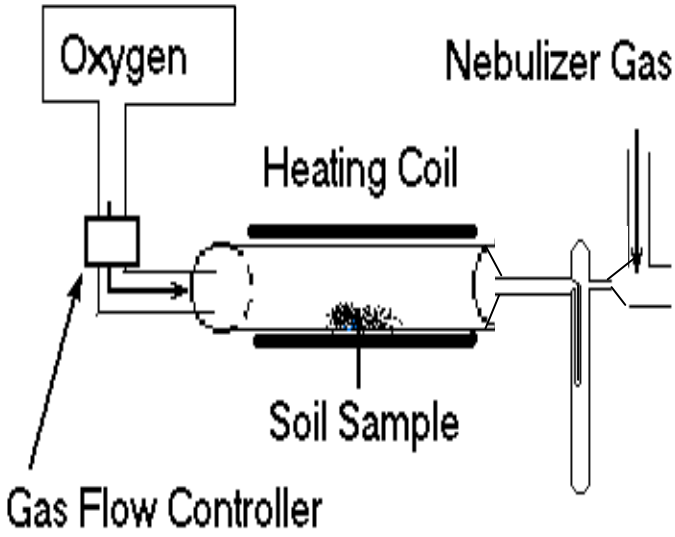

Fig. 4.1.4. Schematic diagram of the sample introduction device without (a) and with (b) cooling finger for iodine introduction via gas phase in the ICP-CC-QMS.

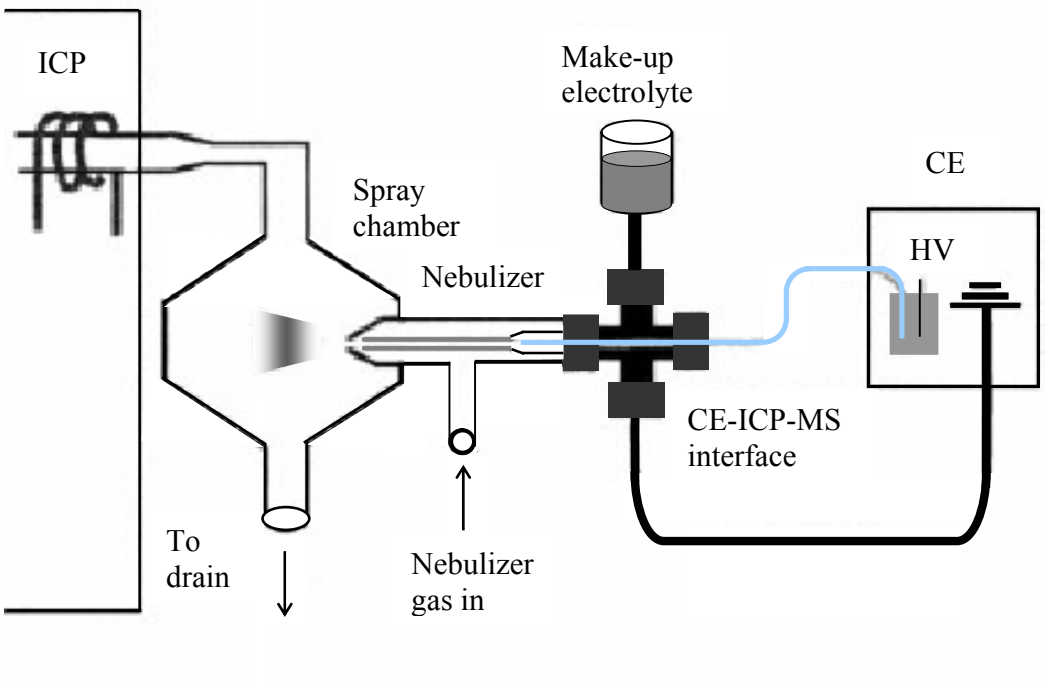

Fig. 4.1.5. Schematic diagram of CE coupled to ICP-MS[33].

New capillaries were conditioned by purging with 0.1 M HCl for 5 min, 0.1 M NaOH for 5 min and CE electrolyte (fresh) for 5 min. After each run the capillary was disconnected, washed with electrolyte for 2 min and then connected to the interface. Both ends of the CE capillary were put at the same level to prevent a hydrostatic imbalance (siphoning) when combined to ICP-MS.

4.1.2.3. Laser ablation ICP-MS with cooled LA-chamber

LA-ICP-SFMS with cooled LA-chamber was used for the determination of uranium isotope ratios on biological samples. In order to analyze biological surfaces, a cooled PFA laser ablation chamber was developed[73]. The cooling system of the ablation chamber is achieved by using two Peltier elements in serial connection below the target holder, which was made of aluminum. Using this setup at a current and voltage of 0.6 A and 16 V applied to the Peltier elements, a

temperature of the target holder of about -15ºC was reached. The experimental set up of the cooled ablation cell in combination with LA-ICP-SFMS is shown in Fig. 4.1.6.

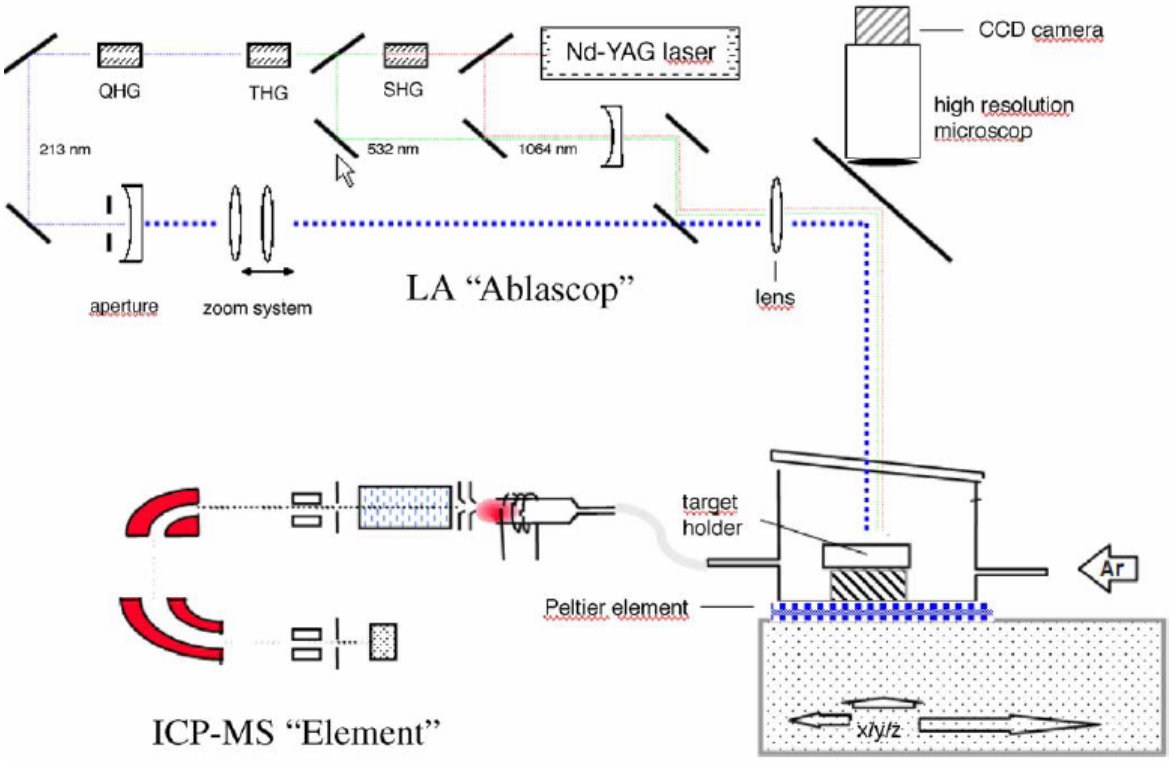

Fig. 4.1.6. Experimental arrangement of LA-ICP-MS with cooled laser ablation chamber[74].

The laser ablation system from Bioptic (Ablascope, Bioptic Laser System, Berlin, Germany) with the standard laser ablation chamber coupled to ICP-SFMS (Element 1, Thermo Electron, Bremen, Germany) was also used for the analysis of the lateral element distribution within NiCrAlY-based coatings on high-temperature alloys.

4.1.2.4. Laser ablation using a microflow nebulizer adapted on an ablation chamber

For on-line isotope dilution in laser ablation ICP-MS, a microflow nebulizer DS-5 (CETAC Technologies, Omaha, NE, USA) was inserted into the ablation chamber as described

elsewhere[191]. The microflow nebulizer was implemented onto the laser ablation chamber on the opposite side of the gas outlet and transfer line to the ICP (see Fig. 4.1.7.).

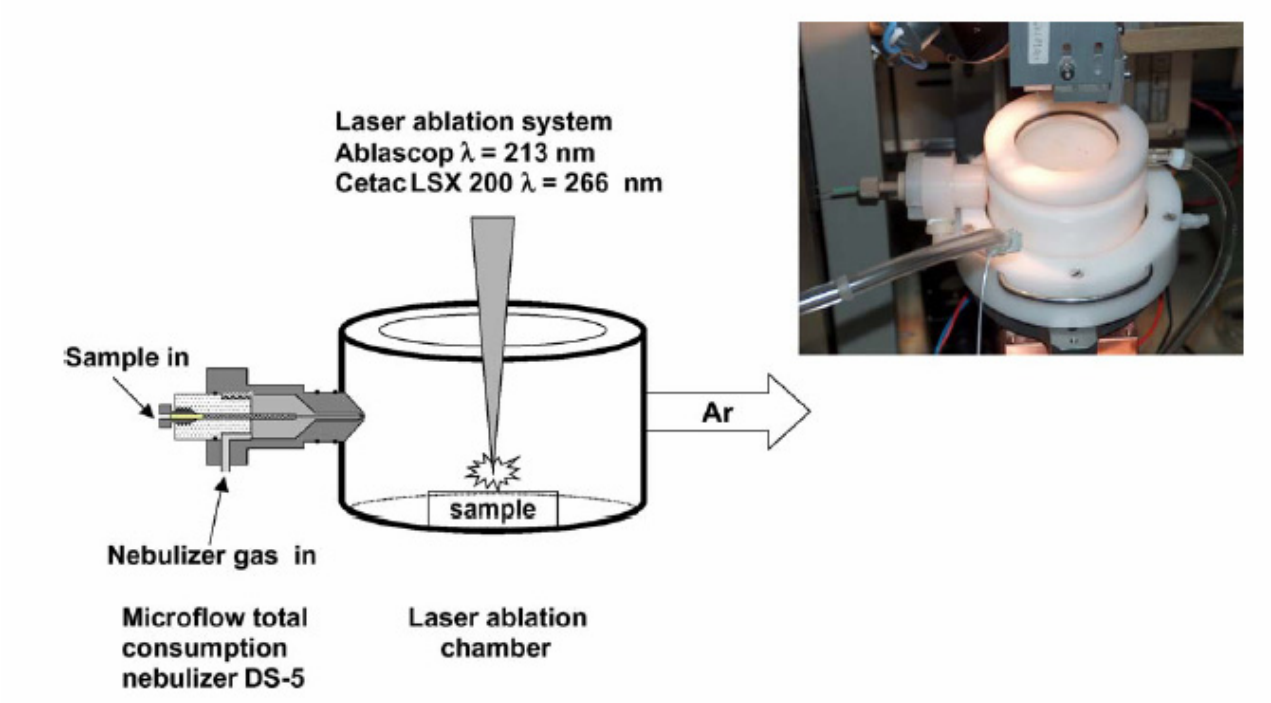

Fig. 4.1.7. Experimental set-up of a laser ablation chamber with microflow nebulizer DS-5 for on-line isotope dilution analysis[191].

A low and constant nebulizer solution uptake rate of 7 μl min^{-1} was provided by a high precision syringe pump (CMA-100, Carnegie Medicine, Solna, Sweden). A photograph of the micronebulizer inserted in the cooled laser ablation chamber is shown in Fig. 4.1.7.

In order to determine the uranium concentration of NIST-SRM 1515 doped to apple leaves, the laser ablation system LSX 200 (266 nm, CETAC Technologies, Omaha, NE, USA) was coupled to the Platform ICP-CC-MS described in[191]. Ablation of sample material was performed by scanning the focused laser beam across the sample surface (single line scan modus) using the following laser parameters (repetition rate 20 Hz, crater diameter 300 μm, laser power density 1.1×10^{9} Wcm^{-2}).

4.2. Samples, standard reference materials and sample preparation

A ^{129}I standard solution from Amersham International (Buckinghamshire, UK) was used for calibration and for preparing of laboratory standards. Aqueous standard solutions of iodine (^{127}I) were prepared by diluting NaI from Merck (Darmstadt, Germany). Synthetic laboratory standards (aqueous solutions and soil samples) with different ^{129}I concentrations and different $^{129}I/^{127}I$ isotope ratios were prepared to investigate the accuracy achievable for $^{129}I/^{127}I$ isotope ratio measurements. Therefore, 6 contaminated soil samples were analyzed for their $^{129}I/^{127}I$ isotope ratio by ICP-CC-QMS using the sample introduction device without cooling finger.
SRM 4357 (Ocean Sediment Environmental Radioactivity Standard) from NIST and two contaminated soil samples of unknown origin were analyzed for the $^{129}I/^{127}I$ by ICP-CC-QMS with the developed sample introduction device using the cooling finger.

All solutions were diluted with deionized Milli-Q water (18MΩcm^{-1}, Millipore Milli-Q-Plus water purifier, Millipore Bedford, MA, USA). The solutions were acidified with subboiled HNO_3 immediately before the introduction into the Meinhard nebulizer due to the observation that this acidification of the NaI solution before the determination resulted in improved sensitivity by a factor 3 and better reproducibilities. No further sample preparation was required for soil samples.
The chemicals used for the CE experiment (HNO_3, HCl, NaOH) were from Merck (Darmstadt, Germany). MilliQ plus deionized water was used for solution preparation and dilution. The electrolyte solution used for CE was 6 mM hydroxyisobutyric acid (HIBA) complexing electrolyte (Fluka, Neu-Ulm, Germany) with 5 mM CIA-Pak UV Cat 1 chromophore (Waters) adjusted to pH = 4.0 with 0.1 M HCl. Lanthanide standards with natural isotope were prepared by mixing of single element standard solution from Merck.

The LA-ICP-SFMS measurements using the cooled LA chamber were carried out using small volumes (20 µL, uranium concentration 100 ng ml^{-1}) of the isotope standard reference materials NIST U-350, NIST U-930 and CCLU-500[192, 193] as well as uranium with natural isotopic composition. The standards were placed onto the surface of the biological samples, e.g. flower leaves. For mass bias correction, one droplet of isotopic standard reference material NIST U-020 (20 µl, uranium concentration 100 ng ml^{-1}) was added in addition. After drying in an oven (T=75ºC, 2h) the samples were analyzed immediately by LA-ICP-SFMS.

The on-line isotope dilution LA-ICP-MS experiments were carried out using the NIST SRM 1515 (apple leaves) with a certified uranium concentration of 0.006 μg g^{-1}. A uranium standard solution from Merck was added to the sample material in order to obtain a doped uranium concentration of 10 μg g^{-1}. The mixture was then homogenized, dried and placed on a high-purity carbon ribbon for direct laser ablation measurements. A solution of isotope-enriched tracer ($^{235}U/^{238}U$: 0.5465), a U concentration containing 6 mg l^{-1} in 2% nitric acid was prepared from NIST U-350 standard solution by diluting with MilliQ water and sub-boiled nitric acid. The tracer concentration was prepared to obtain an isotope ratio in the mixture of sample and the tracer solution close to one.

NiCrAlY-based coatings on high-temperature alloys (base material) were analyzed by LA-ICP-MS after oxidation in air at a temperature of 980 °C for 300, 1000, 5000 and 15000 hours. Fig. 4.2.1 shows a cross section graph SEM with the structure of the analyzed sample (bond coat (BC) and base material (BM)). The thickness of the bond coat was approximately 200 μm. The initial matrix composition of the BC and BM before oxidation, the composition of the alloy certified reference material BAM-328-1 (Bundesanstalt für Materialprüfung, Berlin), used for quantification via RSCs, and the concentration of other BAM reference material used for the acquisition of the calibration curves are summarized in Table. 4.2.1.

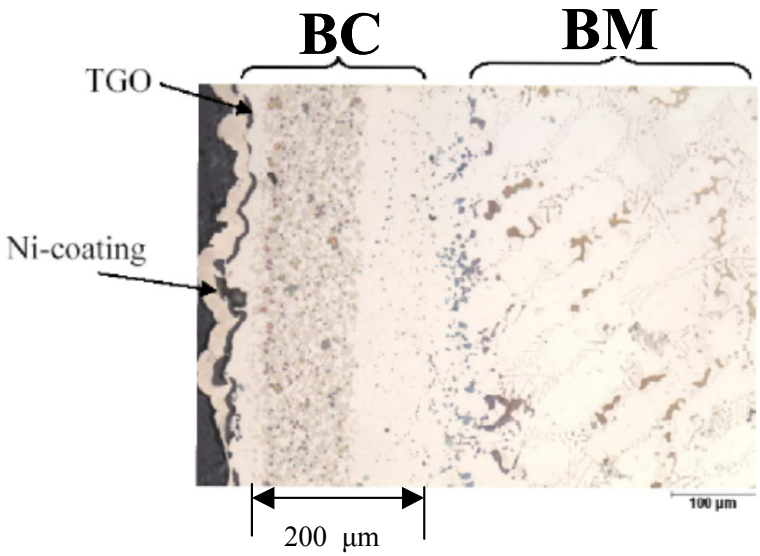

Fig. 4.2.1. Bond coat (BC) and base material (BM) layout in analyzing sample.

Table 4.2.1. Composition of sample and reference material (Concentration, wt-%)

Element	Concentration, wt-%							
	Bond coat	Base material	BAM-328-1	BAM-327-2	BAM-277-1	BAM-178-1	BAM-128-1	BAM-237-1
Ni	50	60	20.38	19.72	10.43	0.048	0.046	10.32
Co	25	8.3	41.65	0.16	0.15	-	-	0.22
Cr	17	16	20.54	24.35	18.04	0.92	0.10	17.24
Al	10	3.4	0.7	0.7	-	0.04	0.286	-
Re	1.5	-	-	-	-	-	-	-
W	-	2.5	4.16	-	-	-	-	-
Ta	-	1.7	0.18	-	-	-	-	-
Ti	-	3.2	-	-	-	-	0.896	-
Mo	-	1.7	4.41	0.17	0.22	-	-	0.306

5. Results and discussions

5.1. Application of ICP-MS and LA-ICP-MS to environmental science

5.1.1. Determination of $^{129}I/^{127}I$ isotope ratios in liquid solutions and environmental soil samples by ICP-CC-QMS

The determination of ^{129}I is very difficult due to low ^{129}I quantities present at high ^{127}I concentrations. In particular, the precise and accurate determination of $^{129}I/^{127}I$ by ICP-MS is restricted by xenon impurities ($^{129}Xe^+$) present in the argon plasma gas[33, 50] or samples[194] and also by the influence of peak tailing of ^{127}I on ^{129}I. Thus selective removal of Xe is required for ultratrace detection of ^{129}I. Removing the isobaric interference of ^{129}I and ^{129}Xe by high resolution ICP-mass spectrometry is currently impossible and would require a mass resolution of approx. 600000[195].

A principal possibility for improving the abundance sensitivity is the application of a pressurized ion-guide before the quadrupole mass analyzer in ICP-MS. According to a previous study [138] the ion kinetic energy has been reduced to about 1 eV by collision using helium atoms resulting in improved abundance sensitivity. Thus, when introducing helium into the collision cell a reduction of peak tailing of the high-abundant isotope by up to three orders of magnitude depending on the mass analyzed has been observed. However, increasing the QMS resolution had a significantly lower influence on abundance sensitivity than reducing the ion energy by collision with helium atoms. Therefore, the reduction of background to its minimum is of major importance. In addition, gas-phase ion-molecule chemistry in pressurized rf-multipoles can be used for selective removal of interfering isotopes[132, 134, 196]. Thus, oxygen was applied as a collision gas for selective reduction of xenon ions, whereby the reaction of $^{129}Xe^+$ with O_2 was studied[195]. It was observed that $^{129}Xe^+$ reacts at least 10^4 times faster with O_2 than the analyte of interest $^{129}I^+$. The main reaction scheme of $^{129}Xe^+$ with O_2 is based on charge transfer reaction. However, when the cell is pressurized with O_2 for suppression of $^{129}Xe^+$, the formation of $^{127}IH_2^+$ by reactions with gas impurities limits the detection of ^{129}I[139].

The aim of this work was focused on a rapid and high-sensitive method based on ICP-CC-QMS for the determination of low $^{129}I/^{127}I$ isotope ratios in synthetic and environmental samples.

Optimized experimental parameters of the ICP-CC-QMS using different sample introduction systems are summarized in Table 5.1.1.

Table 5.1.1 Typical experimental parameters of the ICP-CC-QMS (Platform, Micromass)

Sample introduction system	Meinhard nebulizer with Scott double-pass spray chamber	Device for gas-phase sample introduction
RF power	1400 W	1400 W
Coolant gas flow rate	13.5 l min^{-1}	13.5 l min^{-1}
Auxilary gas flow rate	1.0 l min^{-1}	1.0 l min^{-1}
Nebulizer gas flow rate	0.85 l min^{-1}	0.85 l min^{-1}
Solution uptake rate	0.9 ml min^{-1}	-
Sample weight	-	2-10 g
O_2 sample gas flow	-	80 ml min^{-1}
Oven heating temperatute	-	1000 °C
Cone lens	300 V	300 V
Hexapole exit lens	400 V	400 V
Hexapole bias potential	1.0 V	1.0 V
Ion energy lens	2.0 V	2.0 V
Multiplier voltage	470 V	470 V
O_2 collision gas flow	0.9 ml min^{-1}	0.9 ml min^{-1}
He collision gas flow	6 ml min^{-1}	6 ml min^{-1}
Dwell time, s	0.2	0.2
Settle time, s	0.02	0.02
Mass resolution, m/Δ	300	300

The experimental parameters (cool, auxiliary and nebulizer gas flow rates) were first optimized with respect to maximum ion intensity of $^{127}I^+$. The ICP-CC-QMS optimization was carried out using an 80 mg l^{-1} iodine standard solution (1% HNO_3) introduced by a Meinhard nebulizer in combination with a cooled spray chamber. Secondly, an optimization was performed using helium only and later oxygen was introduced into the hexapole collision cell. The ICP-CC-QMS does not allow direct control of the operating gas pressure in the hexapole and therefore flow rates of collision gases were externally controlled. Flow rates of helium and oxygen for optimization of $^{129}I/^{127}I$ isotope ratio measurement were varied between 0 and 10 ml min^{-1} and between 0 and 2 ml min^{-1}, respectively. The ICP-CC-QMS performance (sensitivity, background and precision) was measured and optimized every day before the measurements.

5.1.1.1. Figures of merit of ICP-CC-QMS for determination of ^{129}I

For optimization of experimental conditions, the intensity of $^{127}I^+$ was measured in comparison to the noise intensity at mass 129 (caused by $^{129}Xe^+$ and molecular ions $^{127}IH_2^+$ and by detector

noise) as a function of nebulizer gas flow, rf power at constant helium addition and as a function of the oxygen flow rates applied.

Fig. 5.1.1. shows the dependence of $^{127}I^+$ intensity and signal-to-noise ratio on the nebulizer gas flow rate.

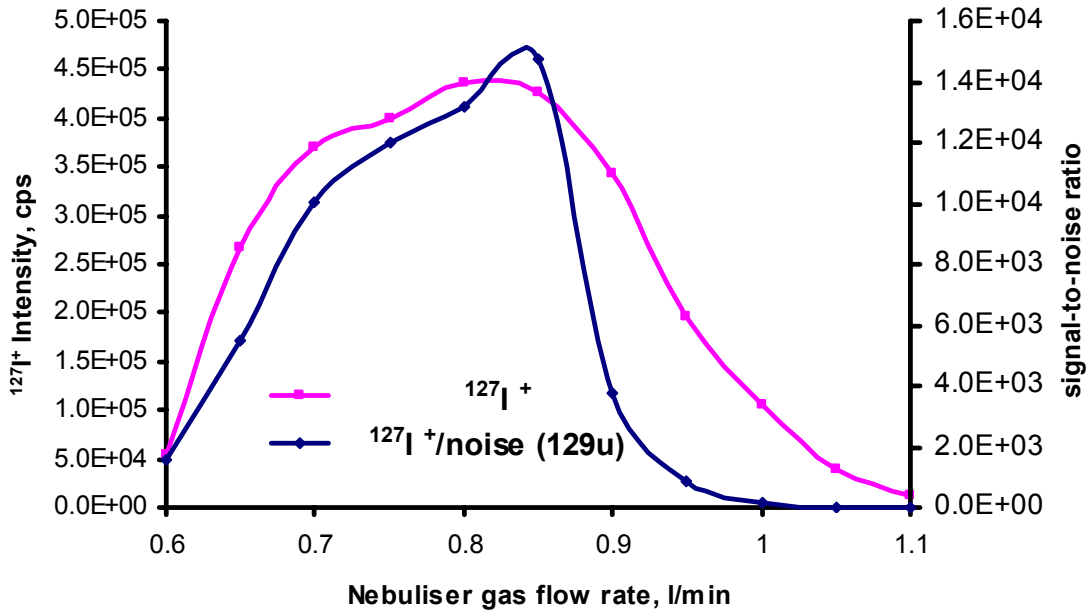

Fig. 5.1.1. Dependence of $^{127}I^+$ intensity and $^{127}I^+$/noise (129 u) on the nebulizer gas flow rate (He flow rate: 6 ml min^{-1}, O_2 flow rate: 0.9 ml min^{-1} , rf power: 1400 W, hexapole bias: 0).

When increasing the nebulizer gas flow from 0.6 l min^{-1} to the optimum value of 0.85 l min^{-1} an increase of analyte ion intensity for $^{127}I^+$ and of signal-to-noise-ratio by a factor of 10 was measured, whereas the noise intensity at mass 129 increased by a factor of 4 only.

Fig. 5.1.2. presents the dependence of $^{127}I^+$ intensity and signal-to-noise ratio on the rf power using the same He and O_2 flow rates. The optimum rf power was determined at 1400 W. An improvement in signal-to-noise ratio for $^{129}I^+$ by a factor of 10 in comparison to 1000 W was found.

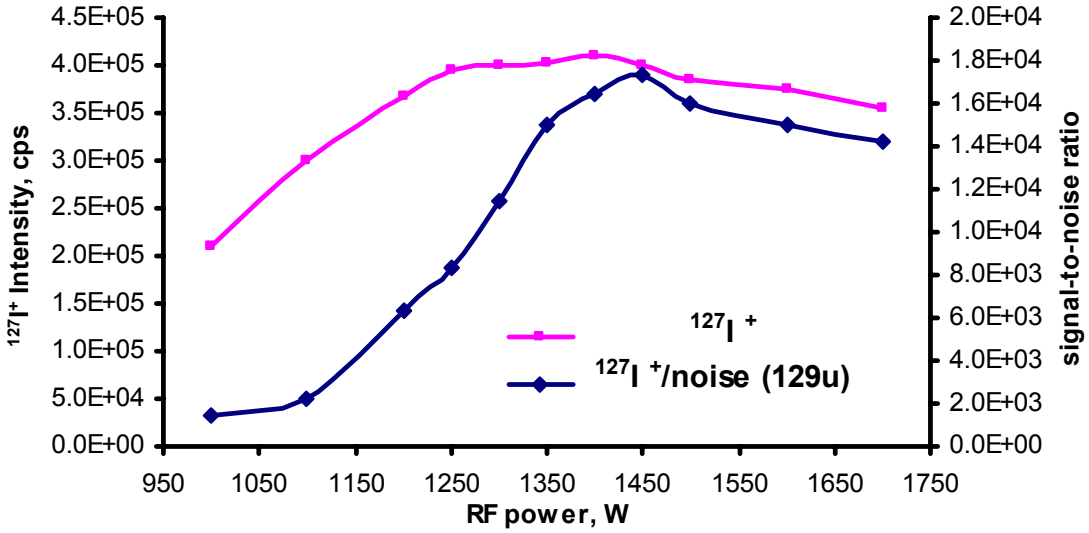

Fig. 5.1.2. Dependence of $^{127}I^+$ intensity and $^{127}I^+$/noise (129 u) on rf power (He flow rate: 6 ml min^{-1} , O_2 flow rate: 0.9 ml min^{-1} , hexapole bias: 0, nebulizer gas flow rate: 0.85 l min^{-1}).

The dependence of $^{127}I^+$ intensity and signal-to-noise-ratio on helium and oxygen flow rate is shown in Fig. 5.1.3. and Fig. 5.1.4.

Ion transmission of $^{127}I^+$ was improved when introducing helium and oxygen into collision cell due to decrease of the kinetic energy of the ion and better focusing of the ion beam by hexapole ion guide[134, 138]. The increasing He flow rate (at O_2 flow rate of 0 ml min^{-1}) lead also to an minor increase of the noise intensity at m/z = 129, but the signal-to-noise-ratio improved by a factor of 2 to 3. This mainly due to the collision induced neutralization of xenon ions within the collision cell. Significantly higher improvement of signal to noise ratio for $^{129}I^+$ was found when introducing O_2 at a flow rate of 0.9 ml/min. In this experiment, the noise intensity at mass 129 was about 25 ± 3 cps, which corresponds to the noise intensity of the Daly type detector in analogue mode as used for these experiments. The influence of extraction lens potential and hexapole bias potential on $^{129}I^+$ intensity and signal-to-noise ratio is summarized in Fig. 5.1.5.

In addition, the effect of the potential applied to the extraction lens (extraction cone) was studied. The maximum value of signal-to-noise ratio for ^{129}I determination was observed at a cone potential of 300 V.

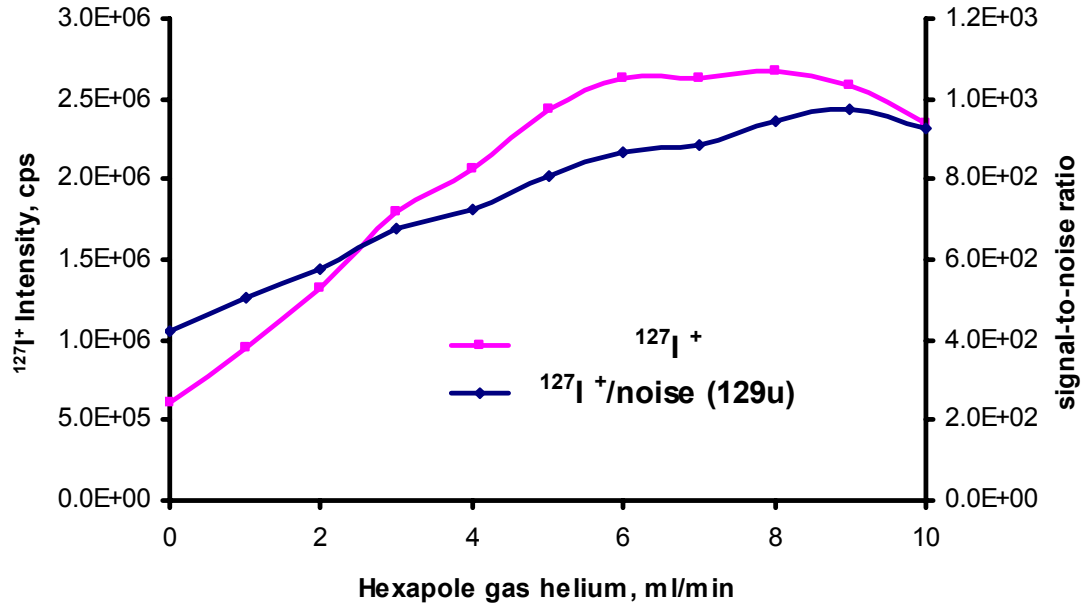

Fig. 5.1.3. Dependence of $^{127}I^+$ intensity and $^{127}I^+$/noise (129 u) on the helium flow rate (O_2 flow rate: 0 ml min^{-1}, rf power: 1400 W, nebulizer gas flow rate: 0.85 l min^{-1}).

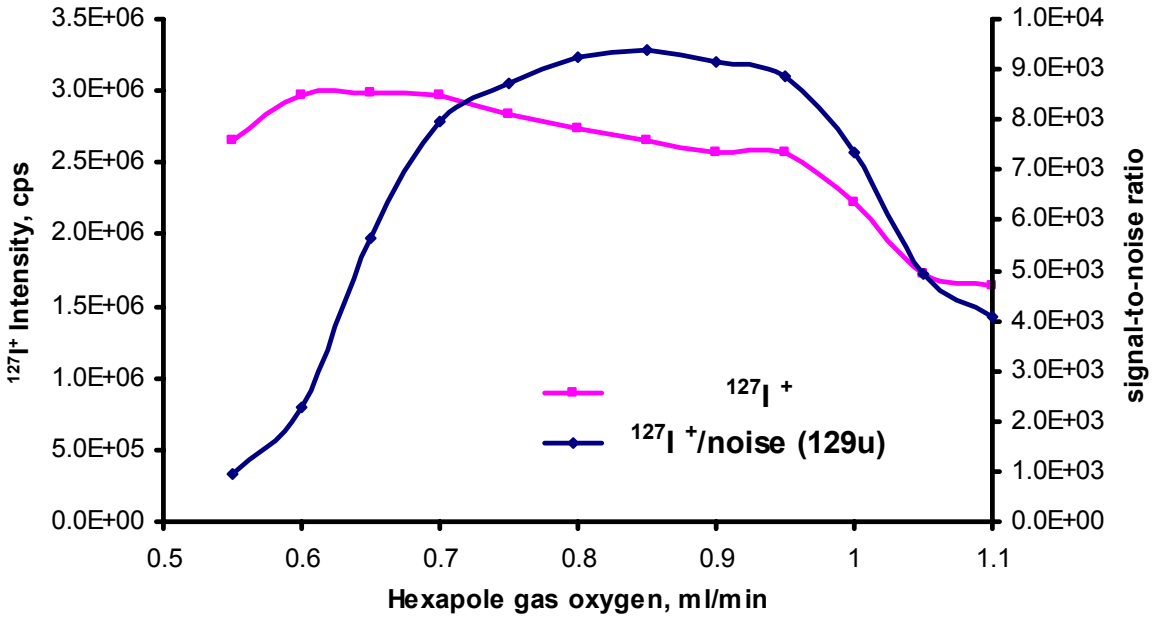

Fig. 5.1.4. Dependence of $^{127}I^+$ intensity and $^{127}I^+$/noise (129 u) on oxygen flow rate (He flow rate: 6 ml min^{-1}, rf power: 1400 W, nebulizer gas flow rate: 0.85 l min^{-1}).

(a)

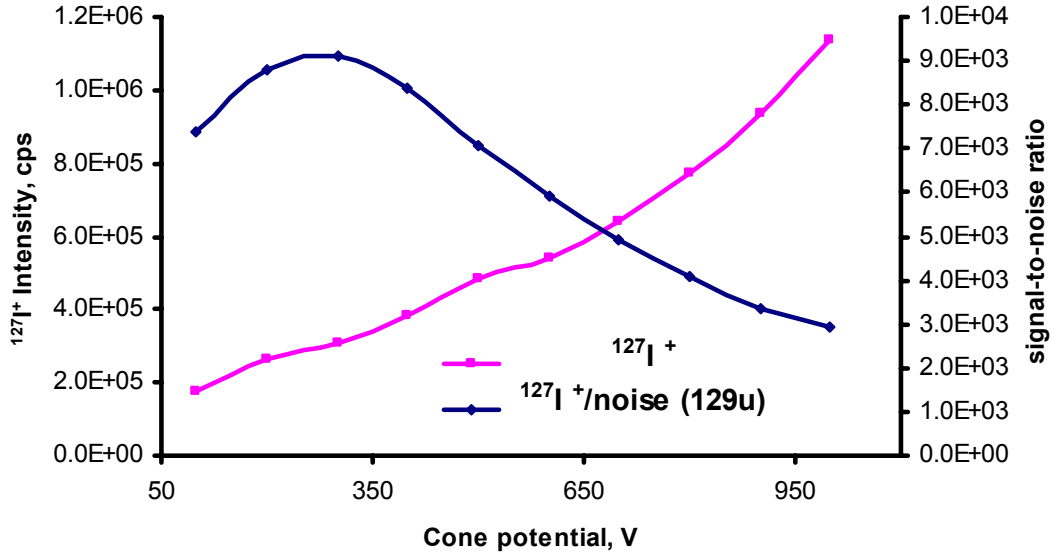

(b)

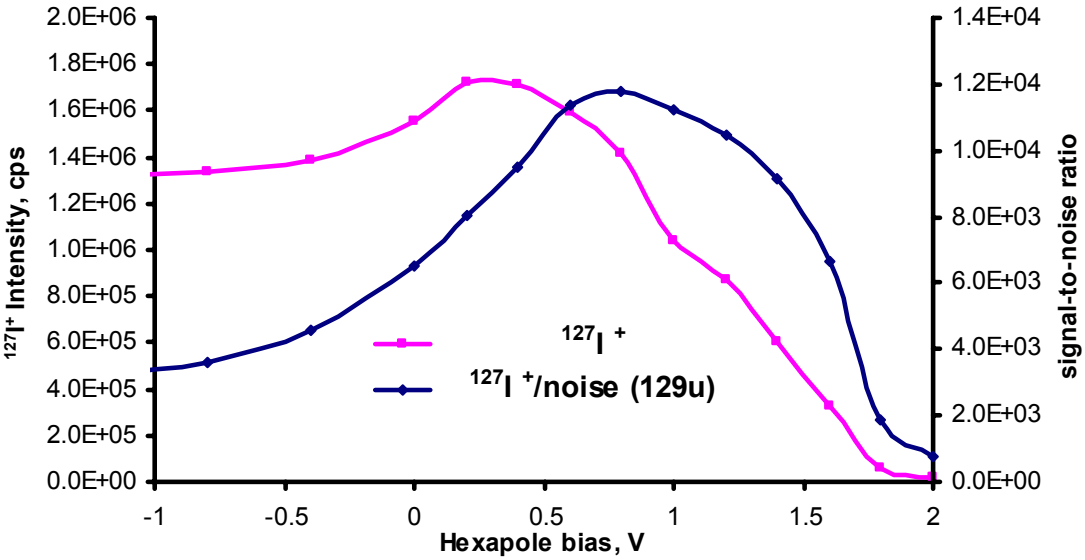

Fig. 5.1.5. (a) Dependence of $^{127}I^+$ intensity and $^{127}I^+$/noise (129 u) on cone potential (He flow rate: 6 ml min^{-1} O_2 flow rate: 0.9 ml min^{-1} , rf power: 1400 W, nebulizer gas flow rate: 0.85 l min^{-1} ; (b) Dependence of $^{127}I^+$ intensity and $^{127}I^+$/noise (129 u) on hexapole bias (He flow rate: 6 ml min^{-1} , O_2 flow rate: 0.9 ml min^{-1} , rf power: 1400 W, nebulizer gas flow rate: 0.85 l min^{-1}).

Higher extraction voltage increases the intensity of iodine ions but also results in a reduction of the signal-to-noise ratio. This is caused by the fact that the $^{129}Xe^{+}$ obtains too high kinetic energy and can not be removed efficiently within the collision cell. In contrast, application of hexapole bias potential of about 1 V resulted in an improvement of the signal-to-noise ratio due to the suppression of IH_2^{+} ion formation.

The application of a positive hexapole bias lead also to a suppression of analyte ion intensities, The IH_2^{+} molecular ions formed in the collision cell have lower kinetic energy and they are moderated more stable due to a larger collision cross section in comparison to analyte ions. Therefore, the molecular ions are stronger influenced by the hexapole bias. Thus, application of O_2 as collision gas allowed the most effective reducing of the background intensity (mainly caused by $^{129}Xe^{+}$ ion intensity) to the level of detector noise. The detection limit for ^{129}I determination in aqueous solutions was determined to be 8 x 10^{-13} g ml^{-1} (0.8 ppt). For comparison, when using the same instrument with hydrogen and helium collision gases the detection limit for ^{129}I determination was reported to be 3 ppt[50]. The use of ICP-SFMS lead to limits of detection for ^{129}I in aqueous solution of approx. two orders of magnitude higher (100 ppt) than the developed CC-based methode, which is due to the high $^{129}Xe^{+}$ background intensity (Xe impurities within the gas), which cannot be reduced[33].

The described method was further applied to $^{129}I/^{127}I$ isotope ratios measurements for ratios as low as 10^{-6} in synthetic aqueous solutions. These samples were prepared from known concentrations of NaI and doped with long-lived a ^{129}I radionuclide. The results of isotope ratio measurements in aqueous solutions are summarized in Table 5.1.2.

Table 5.1.2. Figures of merit of isotope ratios measurements of $^{129}I/^{127}I$ in aqueous solutions, which were prepared in our laboratory

Sample	Expected	Measured	Accuracy (%)	RSD (%)	Concentration of ^{129}I ($g\ g^{-1}$)
LS1	1.18 x 10^{-6}	1.18 x 10^{-6}	0.23	4.1	1 x 10^{-11}
LS2	2.45 x 10^{-6}	2.53 x 10^{-6}	3.19	3.4	2 x 10^{-11}
LS3	4.65 x 10^{-6}	4.75 x 10^{-6}	2.03	3.07	5 x 10^{-11}
LS4	1.18 x 10^{-6}	1.19 x 10^{-6}	1.31	2.17	10 x 10^{-11}
LS5	2.35 x 10^{-6}	2.38 x 10^{-6}	1.29	1.83	20 x 10^{-11}
LS6	4.71 x 10^{-6}	4.51 x 10^{-6}	4.17	1.75	50 x 10^{-11}

The measured isotope ratios are in good agreement (within 5 %) with the expected values. The smallest $^{129}I^+/^{127}I^+$ isotope ratio which can be determined by ICP-CC-QMS in aqueous solution was 10^{-6}.

5.1.1.2. Sample introduction device for direct determination of $^{129}I/^{127}I$ isotope ratio in soils

In this work a special sample introduction device (see Fig. 4.1.4) for iodine thermal desorption from solid material and on-line introduction of iodine into the ICP-MS via the gas phase was applied for direct determination of $^{129}I/^{127}I$ isotope ratios in solid samples. For the experimental parameter see Table. 5.1.1. The advantage of this arrangement consists in a possibility to extract volatile analyte from soil matrix which allows a direct $^{129}I^+/^{127}I^+$ isotope ratio measurement via desorption of iodine from solid sample and introduction of the analyte into the ICP-MS directly. This optimized analytical method reduces matrix effects, improves detection limit for ^{129}I for solid sample analysis and for $^{129}I/^{127}I$ isotope ratio measurements. In addition to reducing the $^{127}IH_2^+$ ion formation due to the absence of a sample dilution step, the procedure reduces also analyte losses and analysis time.

Fig. 5.1.6. presents an example of a chromatogram of transient signals of $^{127}I^+$ and $^{129}I^+$ acquired when introducing iodine vapour extracted by oxidation with O_2 from a contaminated solid soil by sample heating in an oven at a temperature of 1000 ºC.

The maximum sensitivity observed during the measurements of transient I signals was 10^7 cps/ppm. The detection limit for ^{129}I in soil samples was 30 pg g^{-1} (30 ppt). To determine the accuracy of the $^{129}I/^{127}I$ isotope ratio measurements, synthetic soil samples doped with NaI solution and ^{129}I were prepared. The ^{129}I concentrations in the synthetic samples was between 50-200 ppt. The results of $^{129}I/^{127}I$ isotope ratio measurements in three synthetic soil samples are summarized in Table 5.1.3.

Table 5.1.3. Isotope ratios of $^{129}I/^{127}I$ in synthetic soil samples (S)

Sample	Expected	Measured	Accuracy (%)	RSD (%)	Concentration of ^{129}I (g g^{-1})
S1	2.3×10^{-6}	2.1×10^{-6}	1.9	11.5	5×10^{-11}
S2	1.2×10^{-6}	1.1×10^{-6}	2.6	7.8	10×10^{-11}
S3	4.7×10^{-6}	4.5×10^{-6}	3.0	3.0	20×10^{-11}

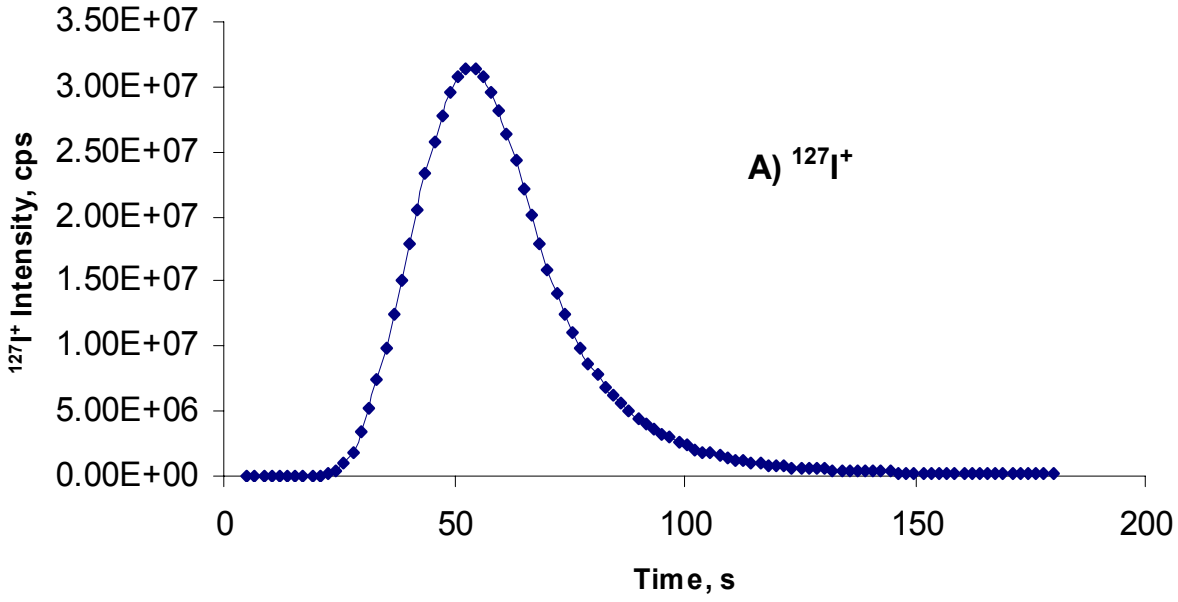

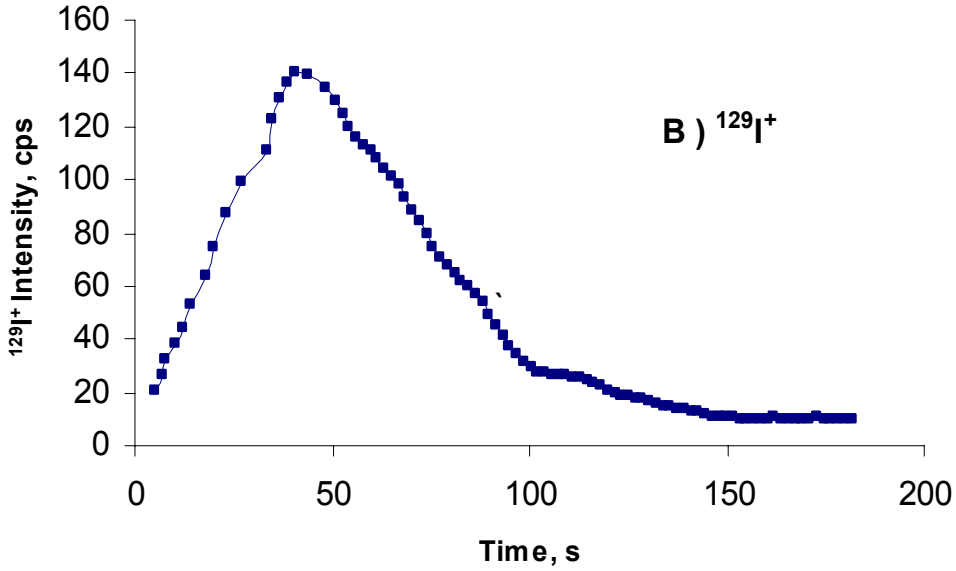

Fig. 5.1.6. Transient signals of $^{127}I^+$ and $^{129}I^+$ measured by ICP-CC-QMS using iodine extraction from a solid sample (oven temperature T=1000 ºC, flow rate of oxygen: 80 ml min^{-1}).

The relative standard deviation for the measured $^{129}I^{+}/^{127}I^{+}$ isotope ratios (from $1.2x10^{-5}$ to $4.7x10^{-6}$) was in the low % range and the accuracy varied between 1.9 % and 3.0 %.
For a further testing of the method towards lower samples sizes, the amount of contaminated soil (sample 3) was varied between 5 and 1 g. The $^{129}I/^{127}I$ isotope ratios of $5x10^{-6}$ were determined with a standard deviation of about 10 %. Most important, the reduction of the sample amount was not resulting in significant increasing of RSD (Table 5.1.4.).

Table 5.1.4. Isotope ratios of $^{129}I/^{127}I$ in soil sample 3 from contaminated area in dependence of the sample amount

Sample	Amount of sample (g)	$^{129}I/^{127}I$	SD	RSD (%)
3	5	5.0×10^{-6}	4.7×10^{-7}	9.4
3	2.5	5.2×10^{-6}	5.4×10^{-7}	10.4
3	1	5.1×10^{-6}	5.4×10^{-7}	10.6

The results of the $^{129}I/^{127}I$ isotope ratio measurements in four environmental soil samples (5 g of each soil was analyzed) are summarized in Table 5.1.5.

Table 5.1.5. Isotope ratios of the $^{129}I/^{127}I$ ratio in contaminated soil samples

Sample	$^{129}I/^{127}I$	SD	RSD (%)
1	4.1×10^{-5}	2.3×10^{-6}	5.8
2	3.9×10^{-6}	8.4×10^{-8}	2.2
3	5.0×10^{-6}	4.7×10^{-7}	9.4
4	2.0×10^{-6}	8.7×10^{-8}	4.4

The ^{129}I concentration in the soil samples was in the pg/g range. The $^{129}I^{+}/^{127}I^{+}$ isotope ratios in the contaminated soil samples varied between 4×10^{-5} and 2×10^{-6}. The precision of these small isotope ratios at ultratrace concentrations was in most cases better than 6%. Using the described ICP-CC-QMS method it was possible to determine $^{129}I^{+}/^{127}I^{+}$ isotope ratios as low as 10^{-6}.

5.1.1.3. Improvement of the LOD for ^{129}I in sediments

In order to improve the performance of the direct analyte introduction system and the LOD for ^{129}I in solid soil samples, a cooling finger was added to the set up and placed between the oven and ICP-MS. The figures of merit of this device and its performance were studied. Fig.5.1.7. contains an example of transient signals of $^{127}I^+$ and $^{129}I^+$ obtained when introducing iodine vapor extracted by oxidation with O_2 from a contaminated soil sample after heating in an oven at T=1000 ºC. When applying the cooling finger, the transient signals were significantly shorter and thus, the signal-to-noise ratio was improved. This is especially important in case of the low ^{129}I signals, which could not be distinguished from the noise using the previous set up. Therefore, the developed sample introduction system allows separating and intermediate enrichment of the volatile iodine from the soil matrix before introduction into the inductively coupled plasma. The achieved LODs were as low as 0.4 pg g^{-1} for ^{129}I, which is a factor of 7 better than the previously detection limits without applying a cooling finger. LODs were calculated using 3σ criteria, where the sensitivity S was obtained for ^{127}I (with account that for the sensitivity for ^{127}I and ^{129}I) and 3 standard deviation of blank for mass 129 was used (see eq. 5.1)

$$LOD=(3\sigma+\text{blank (u129)})/S \qquad (5.1)$$

Detection limits for ^{129}I using different set ups are summarized in Table 5.1.6.

Despite RNAA and particularly AMS provide lower detection limits for this radionuclide, the ICP-CC-MS allows ^{129}I concentration and $^{129}I/^{127}I$ isotope ratios to be determined at the ultratrace level in solid samples by ICP-CC-MS directly and rapidly without any additional sample preparation step. The gas-phase sample introduction minimizes matrix effects significantly, which makes this technique applicable for quantification of a wide variety of different matrices without matrix-matched calibrations.

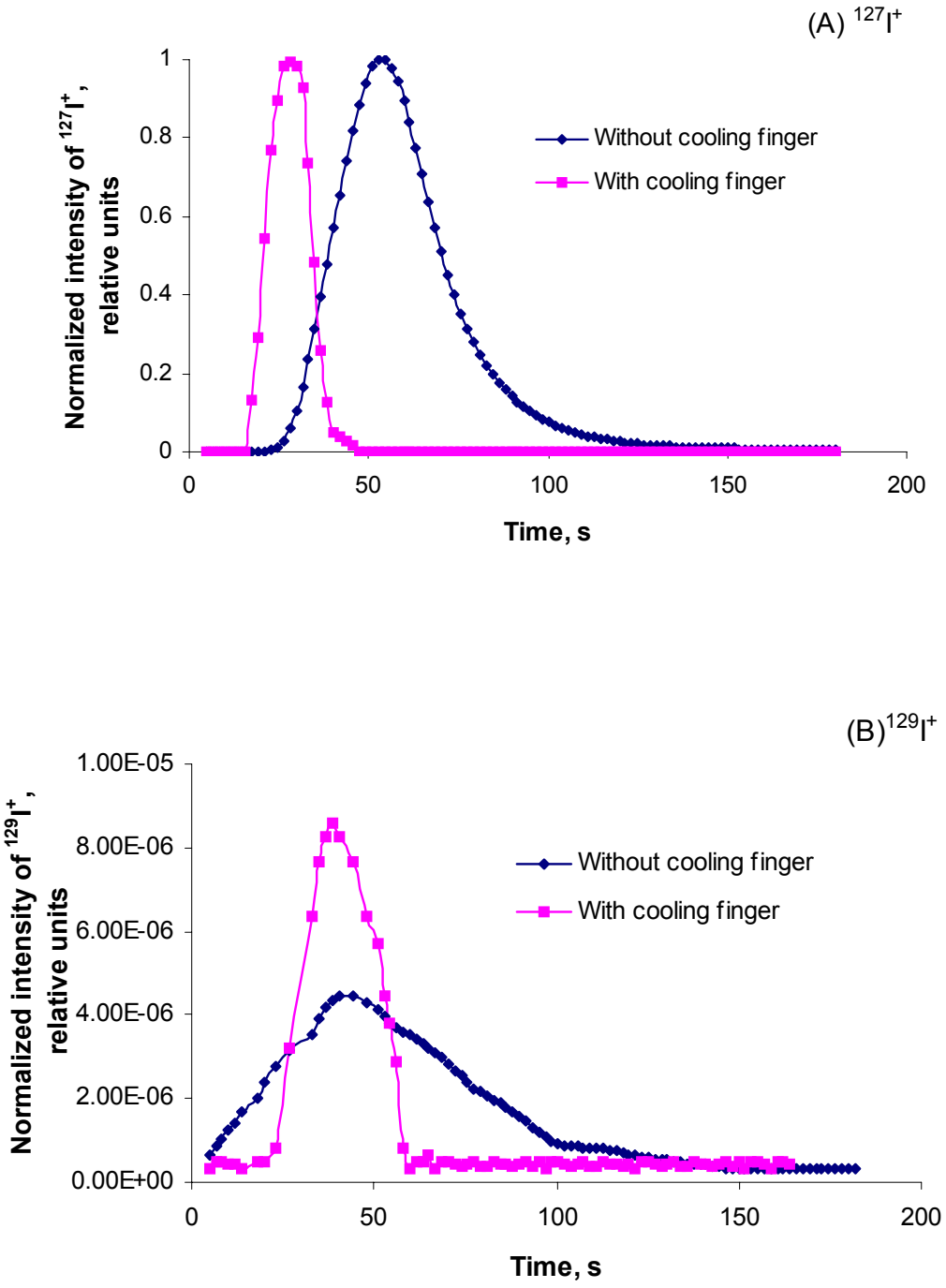

Fig. 5.1.7. Transient signals of two iodine isotopes measured after extraction with and without colling finger by ICP-CC-QMS for two different soil samples. A) $^{127}I^{+}$ and B) $^{129}I^{+}$.

To further validate the method, SRM 4357 (Ocean sediment) was used to estimate the accuracy of the $^{129}I^{+}/^{127}I^{+}$ isotope ratio measurements using a cooling finger.

Table 5.1.6. LODs for ^{129}I in liquid and soil samples using different mass spectrometric techniques

Matrix	Instrumentation	LOD, pg g^{-1}	Reference
Aqueous solution	ICP-SFMS	100	Kerl et al., 1996[33]
Aqueous solution	ICP-CC-MS (reaction gas H_2, He)	3	Becker, 2002 [50]
Aqueous solution	ICP-CC-MS (reaction gas H_2)	0.8	Izmer et al., 2003[181]
Sediment	ICP-CC-MS (reaction gas O_2)	30	Izmer et al., 2003[181]
Sediment	ICP-CC-MS with cooling finger (reaction gas O_2)	0.4	Izmer et al.,2004[197]
Sediment	RNAA	0.125	Szidat et al., 2000 [21]
Sediment	AMS	0.000023	Szidat et al., 2000 [21]

Table 5.1.7 summarizes the results of the $^{129}I/^{127}I$ ratio analysis in this sediment in comparison to the expected $^{129}I/^{127}I$ isotope ratio. Since the iodine isotope ratio is not certified in SRM 4357, it was calculated based on the concentrations of ^{129}I and ^{127}I.

Table 5.1.7. Comparison of estimated and measured isotope ratio $^{129}I/^{127}I$ in SRM 4357 using ICP-CC-MS

Material	Instrumentation	Required sample mass, g	Expected $^{129}I/^{127}I$	Measured $^{129}I/^{127}I$
Ocean sediment (SRM4357)	ICP-CC-MS with cooling finger	1-5	4.4×10^{-7}	5.34×10^{-7}

The measured isotope ratio of 5.3×10^{-7} using the cooling finger configuration is within 20 % of the estimated $^{129}I/^{127}I$ isotope ratio of 4.4×10^{-7}. Using the measured isotope ratios and the certified concentration of ^{127}I, a concentration of ^{129}I of 1.65×10^{-12} g/g was calculated. However, it needs to be mentioned that the reported concentration of ^{129}I in this reference material showed a variation between 0.92-1.84 pg/g[198]. The results of the $^{129}I/^{127}I$ isotope ratio measurements within two contaminated soil samples are summarized in Table 5.1.8.

Table 5.1.8. Isotope ratio of $^{129}I/^{127}I$ in soil samples from a contaminated area measured by ICP-CC-QMS using the cooling finger

Sample	$^{129}I/^{127}I$	SD	RSD (%)
1	2.1×10^{-6}	2.0×10^{-7}	9.4
2	6.9×10^{-6}	5.3×10^{-7}	7.6

The isotope ratios $^{129}I/^{127}I$ in the contaminated soil samples varied between about 2×10^{-6} and 6×10^{-6}. The precision of these small isotope ratio measurements at the ultratrace concentrations were better than 10% and the minimum detectable $^{129}I/^{127}I$ isotope ratio was 10^{-7}. However, the present study was limited by a relatively high background of the Daly-type ion detector and the linear dynamic range of the ICP-CC-QMS of 10^8. An ion detector possessing lower background and wider linear dynamic range would be more suitable for further studies of $^{129}I/^{127}I$ isotope ratio measurements in environmental and radioactive waste samples.

In summary, this study confirms that an oxygen and helium collision gases are an efficient mixture for $^{129}Xe^+$ background reduction and therefore most promising for low LOD. Accuracy and precision determined using the described method are sufficient for routine ^{129}I measurements in polluted and non-polluted environmental samples.

5.1.2. Determination of lanthanides in standard samples by CE-ICP-MS

The ELAN 5000 ICP-QMS instrument was used mass spectrometric detector for all CE measurements and the operating conditions shown in Table 5.1.9 were used throughout the measurements. The nebulizer gas and ICP-MS conditions were optimized by introducing a solution of La, Tb and Tm (10 ng ml^{-1}). ICP rf power adjusted with respect to the $^{139}La^+$ signal to minimize the oxide formation. The CE separation conditions are shown in Table 5.1.10.

The advantages of the capillary electrophoretic PEEK interface coupled to ICP-MS were extensively discussed in the introduction and it was found that the developed method can be successfully applied for the direct analysis of the environmental samples after passing them through a 45 μm filter. The normal current of 4.5 μA was maintained across the interface and it increased up to 9.0 μA. The make-up electrolyte solution of 0.005% HNO_3 was sufficient to reduce the amount of HIBA and UV Cat-1 reagent before entering the ICP-MS. Furthermore, it

reduces the salt or carbon deposits on the sampler and skimmer cones and provides therefore low background signals.

Table 5.1.9. Operating conditions and data acquisition parameters for ICP-MS measurements

RF power, W	1200
Nebulizer gas flow, L/min	0.80
Nebulizer type	MicroMist (liquid uptake rate 200 μl/min)
Mass resolution, m/Δm	300
Optimization criterion	Maximum ion intensity for 10 ng/ml $^{139}La^{+}$, $^{159}Tb^{+}$, $^{169}Tm^{+}$

The other parameters affecting the separation and the peak shape are the position of the capillary within the nebulizer and the height of the make-up electrolyte. The best peak shapes were acquired when the capillary was positioned about 1 mm from the inner capillary of the nebulizer. Uptake of the make-up electrolyte and flow of the nebulizer gas into the spray chamber stops after further inserting the capillary into the nebulizer. Thus in must be concluded that it is very important to control the position of the capillary in the nebulizer for optimum performance of the set up.

Table 5.1.10. CE operating conditions

CE instrument	Water Quanta 4000 Capillary Ion Analyzer
Power supply	Positive 25 kV
Injections	30 s hydrostatic (≈ 35 nl injection volume)
Capillary	id 75 μm; od 365 μm; 75 cm long
Electrolyte solution	6 mM HIBA, 5 mM UV Cat 1, pH=4.3 with diluted HCl
ICP-MS make-up buffer	0.005 % HNO_3
Temperature	22 ^{o}C

As already mentioned, the height of the makeup electrolyte also influences the electrical conductance and the peak shape. Experiments were performed using increasing heights of the

makeup electrolyte. The peak shapes were improved when the level of the make-up electrolyte was higher than the level of the end of the capillary into the nebulizer.

Fig.5.1.8. show an electropherogramm of a run where only dysprosium isotopes were monitored in a 1 µg/ml standard mixture additional 13 lanthanides with natural isotope ratios. Atomic isobaric and molecular interferences were separated and are shown. A standard capillary electropherogram resolving all 13 lanthanides with natural isotope abundances is shown in Figure 5.1.9. These results demonstrate that CE separation prior to the ICP-MS detection is very beneficial for lanthanides analysis, especially for nuclide abundances and concentrations occurring in spallation products. This information is necessary for accessing the dose levels and for assuring irradiation safety when analysing these types of samples.

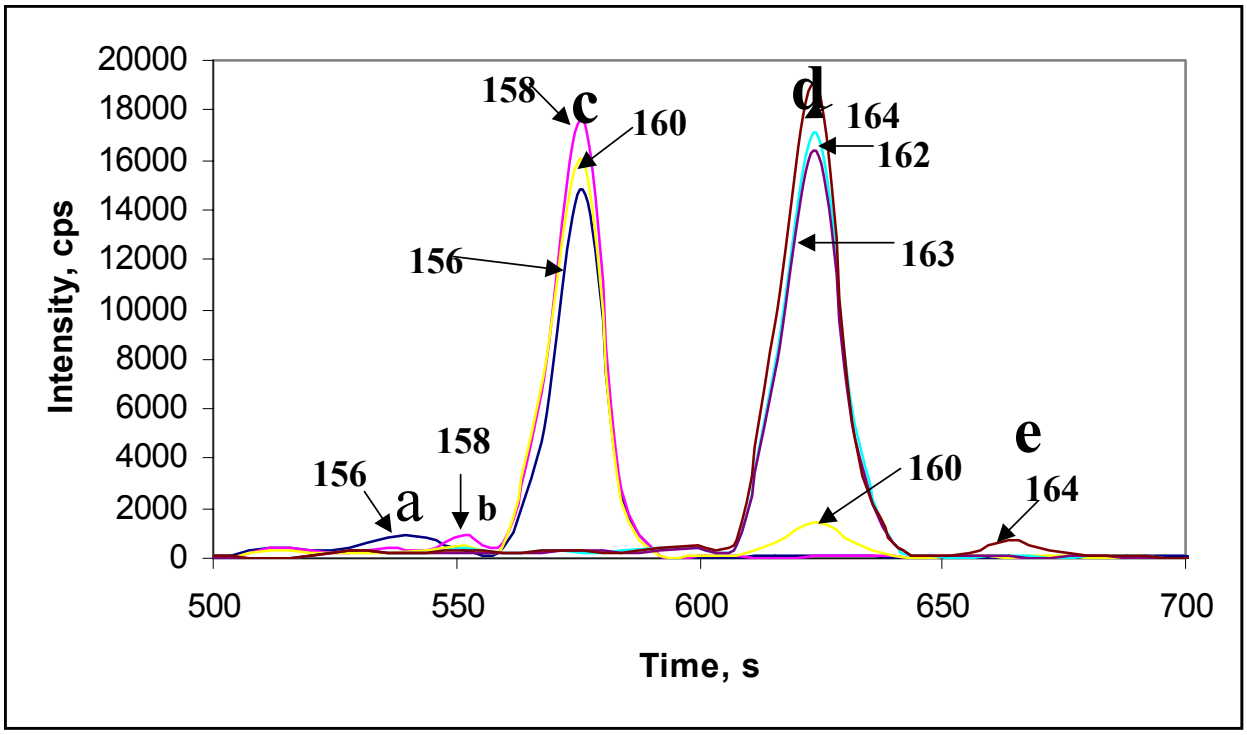

Fig. 5.1.8. CE-ICP-MS electropherogram of m/z from 156 to 164 showing the isotopes of Dy separated from potential isobaric and polyatomic interferences in a standard sample containing 14 lanthanides (a) $^{140}CeO^{+}$, (b) $^{142}NdO^{+}$, (c) Gd isotopes, (d) Dy isotopes (e) $^{164}Er^{+}$.

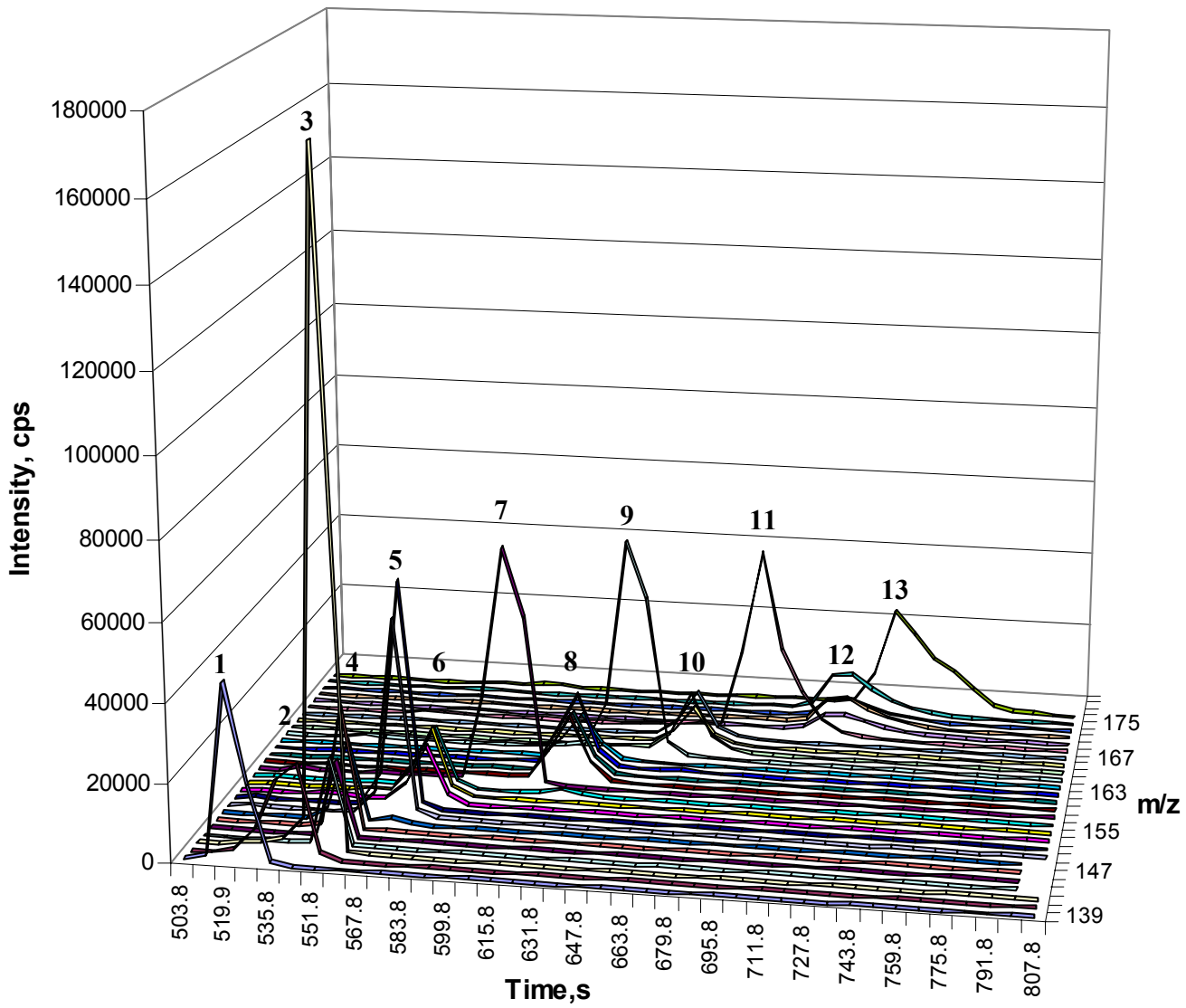

Fig. 5.1.9. CE-ICP-MS electropherogram of 13 lanthanides with natural isotope abundances (1) $^{139}La^{+}$, (2) $^{140}Ce^{+}$, (3) $^{141}Pr^{+}$, (4) Sm^{+} , (5) Eu^{+}, (6) Gd^{+}, (7) ^{159}Tb, (8) Dy^{+}, (9)$^{165}Ho^{+}$, (10)Er^{+} , (11) $^{169}Tm^{+}$, (12) Yb^{+}, (13) $^{175}Lu^{+}$.

5.1.3. Determination of ^{90}Sr by ICP-MS

The use of ICP-MS eliminates many of the problems encountered with radiochemical detection of "middle-lived" radionuclides (with a half-life of a few dozens years) and both ICP-SFMS and ICP-CC-QMS have been found selective and sensitive enough for determination of such nuclides[50, 199]. However, difficulties arise from isobaric interferences of atomic ions or molecular ions that originate from the matrix of the sample or from the plasma. Most critical is the occurrence of radioactive and stable nuclides at the same mass. The LOD, accuracy and precision of ^{90}Sr determination in ICP-MS are mainly affected by the occurrence of isobaric atomic and molecular ions that increase the background signal at m/z = 90 (see Table 5.1.11). All of these interferences have to be considered and eliminated for accurate analysis of radioactive strontium at m/z = 90. ^{90}Y is the first decay product of the ^{90}Sr decay. Although yttrium may be removed by the use of strontium-specific resins, once the procedure is completed ^{90}Y will be produced by the decay of ^{90}Sr. This is of concern when using radiochemical detection techniques[200]. Detection of ^{90}Sr is difficult by radioanalytical techniques, because this isotope has no gamma and relatively low energetic betta-irradiation. Therefore, the amount of ^{90}Sr in samples is analyzed by detecting ^{90}Y after equilibrium between ^{90}Sr and ^{90}Y, which is reached after 2–3 weeks.

Table 5.1.11. Possible interferences on the ^{90}Sr radionuclide and the required mass resolution

Nuclide	Interferences	Required mass resolution (m/Δm)
^{90}Sr	$^{180}W^{++}$	1370
	$^{180}Hf^{++}$	1372
	$^{58}Ni^{16}O_2^{+}$	2315
	$^{74}Ge^{16}O^{+}$	10765
	$^{52}Cr^{38}Ar^{+}$	19987
	$^{50}V^{40}Ar^{+}$	49894
	$^{54}Fe^{38}Ar^{+}$	155548
	$^{50}Ti^{40}Ar^{+}$	158287
	$^{90}Zr^{+}$	29877

Isobaric interferences can be corrected by using mathematical correction algorithms. However, considering the very low ^{90}Sr concentration, such an approach will not provide the required accuracy. For ^{90}Y no correction is required, because the $^{90}Y/^{90}Sr$ concentration ratio is 0.025% in the activity equilibrium and ICP-MS will not be sensitive enough to detect the yttrium ingrowth that would be expected from typical ^{90}Sr concentrations.

$^{90}Zr^{+}$ represents another isobaric interference and its removal may be accomplished by several approaches. One would be again a specific separation technique prior to analysis[201]. However, the current techniques utilized for strontium isolation prior to the measurements, such as precipitation, ion exchange or solvent extraction[202, 203] cannot be considered selective or safe and, additionally, may require large amounts of resins/acids, solvents and are time-expensive. A new advance in the isolation of radioactive strontium has been the use of extraction chromatography[204]. Although this preparation technique may serve to eliminate some of the zirconium it has been reported that similar resins may not completely remove all interfering isotopes[204]. Instrumental techniques used for interference elimination may include ICP-SFMS at its maximum mass resolution ($m/\Delta m$) of 12 000, the application of a collision cell or cool plasma conditions[205]. A sector field ICP-MS has been used to accomplish measurements using the required mass resolution and successful interference separation from the isotopes of interest has been achieved[206]. However, the proposed instrumentation is generally not suitable for isobaric singly charged ions separation, such as $^{90}Sr^{+}$ from $^{90}Zr^{+}$. This mainly due to the low mass difference (mass of ^{90}Sr = 89.9077 u and ^{90}Zr = 89.9047 u) which would require a mass resolution of approximately 30 000.

5.1.3.1. Application of the ICP-MS with collision cell for ^{90}Sr determination

A possible way to solve the interference problem is the application of ICP-CC-QMS because unwanted ions produced in the plasma can be selectively removed or shifted in m/z ratio prior to mass spectral analysis by the addition of specific reagent gases[207].

For the present task oxygen was introduced into the collision cell of the ICP-CC-MS as a collision and reaction gas. For solution introduction into the instrument, a Meinhard nebulizer (J.E. Meinhard Associates, Inc, Santa Ana, CA, USA) with a Scott double-pass quartz spray chamber cooled to 4 ºC was used. Aqueous solutions were introduced in the continuous flow

mode via a peristaltic pump (Perimax 12, Spetec GmbH, Erding, Germany). Specific instrument operating conditions are shown in Table 5.1.12.

Table 5.1.12. Experimental conditions

RF power	750 W
Coolant gas flow rate	13.5 L min^{-1}
Auxiliary gas flow rate	1.0 L min^{-1}
Nebulizer gas flow rate	0.8 L min^{-1}
Solution uptake rate	0.9 mL min^{-1}
Sampling and skimmer cones	Nickel
Dwell time	0.2 s per isotope
Extraction lens (cone) potential	-600 V
Transfer lens (hexapole exit) potential	-400 V
Hexapole bias potential	-0.8 V
Quadrupole bias (ion energy) potential	-2.0 V
Nebulizer	Meinhard
Spray chamber	Scott double-pass
Cell gas	O_2
Flow rate of cell gas	1.9 mL min^{-1}

In previous ion/molecule reaction studies by Eiden et al[195]., it has been shown that Y and Zr react with O_2 by two orders of magnitude faster than Sr. Our initial experiments using a collision cell pressurized with O_2 was also successful and a flow rate of 1.9 mL min^{-1} O_2 was sufficient to promote the oxide ion formation of zirconium (see Fig. 5.1.10). With increasing O_2 gas flow rate, the $^{90}Zr^+$ intensity decreases. The zirconium is oxidized and will therefore be measured as $^{90}ZrO^+$ at m/z 106. Introduction of oxygen into collision cell resulted also in an increase of Sr ion intensity due to collisional focusing as described in a previous chapter. However, an increase in the oxygen gas flow leads to further scattering of analyte ions on oxygen molecules which is accompanied by reduced transmission of the ion beam. Based on the optimized oxygen flow it was possible to calculate LOD for strontium in the order of 2 ng L^{-1} with ICP-CC-MS. The LOD's were primarily due to the relatively high background count rate of the Daly-type detector[138]. Here the LOD are also defined as the equivalent concentration of three times the standard deviation of the blank response. The standard deviation was calculated from six consecutive measurements of the blank solution at m/z = 90.

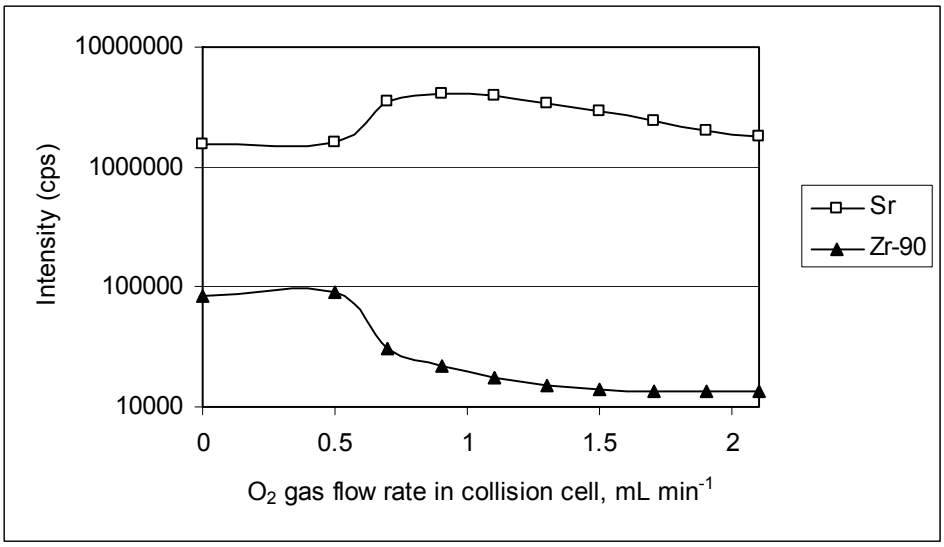

Fig. 5.1.10. Response of $^{88}Sr^{+}$ and $^{90}Zr^{+}$ with increasing flow rate of O_2 in the collision cell. Both elements are at a concentration of 50 mg L^{-1}.

5.1.3.2. Cool plasma mode for separation of Sr and Zr

An alternative approach to the collision cell for the removal of interferences is the use of cool plasma conditions (plasma which operates at lower forward powers to suppress ions of elements with higher ionization potentials). The elimination of isobaric interference of $^{90}Zr^{+}$ and "Ar-based interferences" (e.g. $^{52}Cr^{38}Ar^{+}$, $^{50}Ti^{40}Ar^{+}$, *etc*) was of special interest due to their relatively high abundance. The ionization potentials of strontium and zirconium are 5.7 eV and 6.8 eV, respectively, therefore Zr^{+} should theoretically be suppressed under cool plasma conditions. Therefore, the plasma forward power was varied and correlated to the ion intensity of the elements of interest. All other operating conditions were kept constant. In the second experiment, oxygen was added to the plasma at various percentages of the total flow rate of the nebulizer gas (argon). In a previous work it has been noted that mixing argon and oxygen for the nebulizer gas, cool plasma conditions can also be achieved[9]. Results of both experiments are summarized in Fig. 5.1.11.

a)

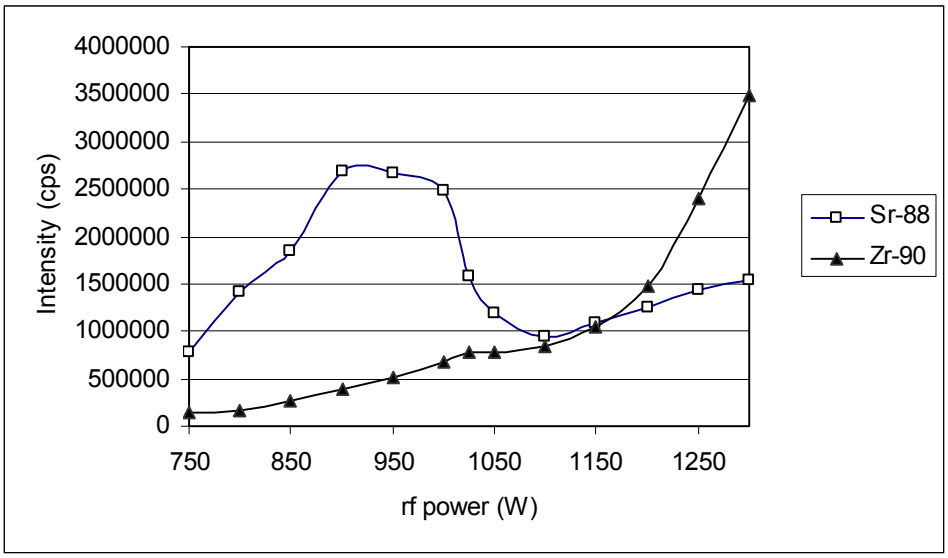

b)

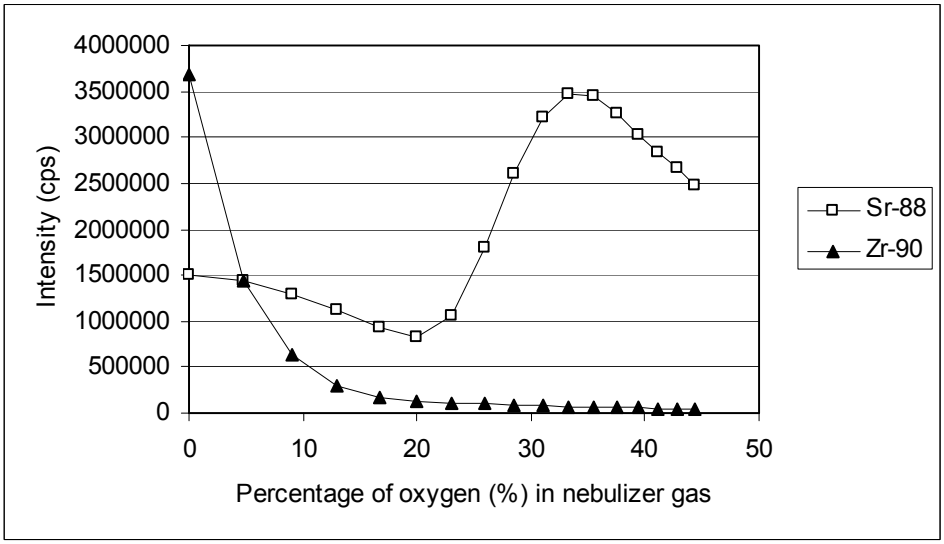

Fig. 5.1.11. Effect of rf power (a) and O_2 addition to the nebulizer gas flow (b) on the response of $^{88}Sr^{+}$ and $^{90}Zr^{+}$ using a ICP-CC-MS. Strontium concentration used for the experiment was 50 mg L^{-1} and 1000 mg L^{-1} Zr, respectively.

The results shown in Fig. 5.1.11. b) are possibly due to the combination of cool plasma conditions and oxide formation as pointed out in a previous work[208]. Becker and Dietze found a general increase in the oxide formation rate of other radionuclides using a shielded torch under hot plasma conditions[209]. Other researchers have noted that the strong bonds of oxides usually withstand plasma conditions[205]. There exists also the potential for formation of argon–carbon based interferences such as $^{38}Ar^{40}Ar^{12}C^{+}$. However, cool plasma conditions generally inhibit the formation of argon-based polyatomic ions[210]. Vanhaecke et al.[110] applied an rf power of 750 W, which was sufficient to reduce the formation of the $^{40}Ar^{12}C^{+}$ interferring with major chromium isotope at m/z = 52. The formation of $^{38}Ar^{40}Ar^{12}C^{+}$ was investigated by the introduction of a 0.01 % trichloroacetic acid for cool plasma conditions and an increase of the background at m/z = 90 was not observed[211]. Other potential molecular ions, such as $^{38}Ar^{52}Cr^{+}$, $^{36}Ar^{54}Fe^{+}$, $^{40}Ar^{50}Ti^{+}$ and $^{40}Ar^{50}Cr^{+}$, were also investigated by analysis of solutions containing these elements. However, also this multielement approach showed no increase in the background at m/z = 90. Other potential contributions to the background at m/z = 90 was assumed from the formation of nickel-based interferences, such as $^{58}Ni^{16}O_2^{+}$ or $^{60}Ni^{16}O^{14}N^{+}$, due to the use of nickel cones. This was most pronounced when O_2 was added in various percentages to the nebulizer gas flow of the ICP-CC-MS instrument (see Fig. 5.1.12).

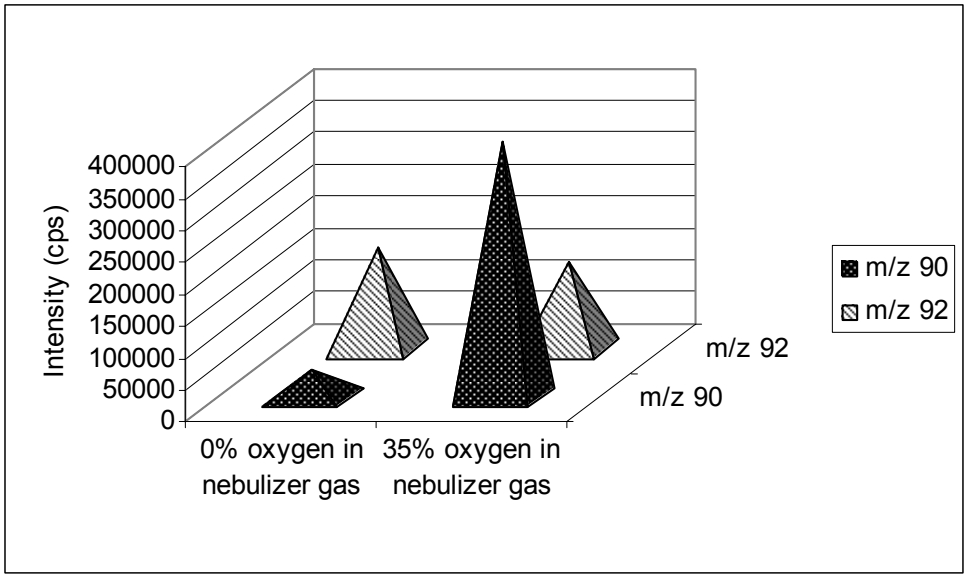

Fig. 5.1.12. Effect of oxygen in the nebulizer gas on the background at m/z = 90.

Using the addition of oxygen, the interferent at m/z = 90 increases by approximately one order of magnitude. Interestingly, there is no change in the abundance of the interferent at m/z = 92, as would be expected due to $^{60}Ni^{16}O_2^+$. Therefore it can be assumed that this may be due to the elimination of the carbon-based interference under the cool plasma conditions generated by the addition of oxygen. The calculated LODs (3s; blank Milli-Q water) are given in Table 5.1.13.

Table 5.1.13. LODs of ^{90}Sr in water samples using ICP-CC-QMS

Collision cell	RF power, W	Percentage of O_2 in nebulizer gas, %	Limit of detection, ng L^{-1}
1.9 ml min-1 O_2	1350 900 750	40	3 2 5
0.9 ml min-1 O_2	900 1350		3 2

However, if the application of ICP-CC-QMS and cool plasma conditions reduces the influence of isobaric interferences on m/z=90, the peak tailing of $^{88}Sr^+$ and in particular the Daly detector noise was considered to be the critical factors for the determination of relatively short-lived ^{90}Sr using the described method. If the concentration of natural strontium in a sample is higher than 25 ng ml^{-1}, which is very often the case, then other methods would be required (e.g. use of MC-ICP-MS with better abundance sensitivity and significantly lower instrument background).

5.1.4. Determination of U isotopic ratios on the surface of biological samples by LA-ICP-MS

A method for the determination of precise uranium isotope ratio measurements on a thin uranium layer on a biological samples was developed. The experimental parameters of LA-ICP-MS were optimized with respect to maximum $^{238}U^+$ ion intensity and minimum uranium hydride formation rate $^{238}UH^+/^{238}U^+$. These experiments were carried out using uranium with natural isotopic composition. Optimized experimental conditions are summarized in Table 5.1.14.

Table 5.1.14. Optimized operating conditions of LA-ICP-SFMS using a cooled laser ablation chamber for uranium isotope ratio measurements on the surface of biological samples

	LA-ICP-SFMS
Laser ablation system	Ablascope, (Bioptic^{tm})
Wavelength of Nd-YAG laser, nm	213
Laser power density, W cm^{-2}	3.5×10^{9}
Laser pulse duration, ns	5
Number of laser shots	100
Repetition frequency, Hz	20
Temperature of laser ablation chamber, ºC	~ -15
ICP-MS	Element 1, (Finnigan)
RF power, W	1200
Cooling gas flow rate, L·min^{-1}	18
Auxiliary gas flow rate, L·min^{-1}	1.25
Nebulizer gas flow rate, L·min^{-1}	1.20
Extraction lens potential, V	2000
Sampler cone	Nickel, 1.1 mm orifice diameter
Skimmer cone	Nickel, 0.9 mm orifice diameter
Mass resolution, m/Δm	300
Mass window, %	10
Runs	400
Passes	1
Scanning mode	peak hopping
Analysis time, min	5

The measured uranium isotopic ratio was corrected for UH^+ formation, mass bias, and detector dead time. The mass bias factor (based on an exponential correction[212] was determined using the NIST U020 standard solution, which was added to a flower leaf. The dead time of the ion detector was determined using a method described by Ketterer et al.[213] and was determined to be 45 ns using 0.1 $ngmL^{-1}$ of NIST U020 isotopic standard reference material.

A relatively high laser power density (3.3×10^9 W cm^{-2}) and a small laser crater diameter (down to 5µm) were applied for the experiments in order to reduce possible fractionation effects. In Fig 5.1.13, the dried droplet of CCLU 500 and the laser craters generated using the optimized ablation conditions (see table 5.1.14.) are shown.

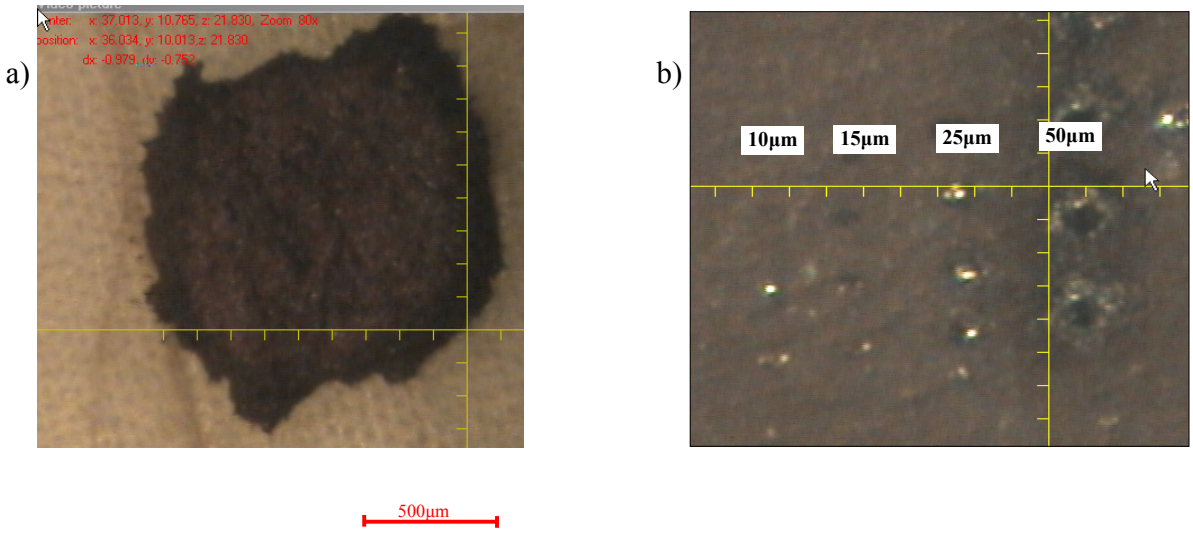

Fig. 5.1.13. Dried droplet of CCLU 500 isotopic standard reference material deposited onto a flower leaf (a) and craters of different diameters produced on the leaf under optimized ablation conditions (b).

In focus, the laser produced well-defined craters of 10, 15, 25 and 50 µm diameter on the sample surface. Variation of the laser beam diameter influenced directly the amount of ablated material when scanning the sample surface. Since the energy density of the laser remains constant it can be expected that the intensity is a function of the crater diameter. Fig 5.1.14a shows the dependence of the $^{238}U^+$ ion intensity signal on the different spot size, measured on the dried droplet of natural uranium solution on flower leaf surface. However, it needs to be mentioned that the crater diameter increase by a factor of 4 did not provide a signal enhancement by a factor of 4, which is mainly due to the fact that the U standards were dried on the surface of the leaf and are not homogeneously distributed throughout the entire ablated volume. A good correlation

between the measured ion intensity of $^{238}U^{+}$ and the diameter of the laser crater of the analyzed sample was determined with a correlation coefficient (R) of 0.9988 (Fig 5.1.14b).

(a)

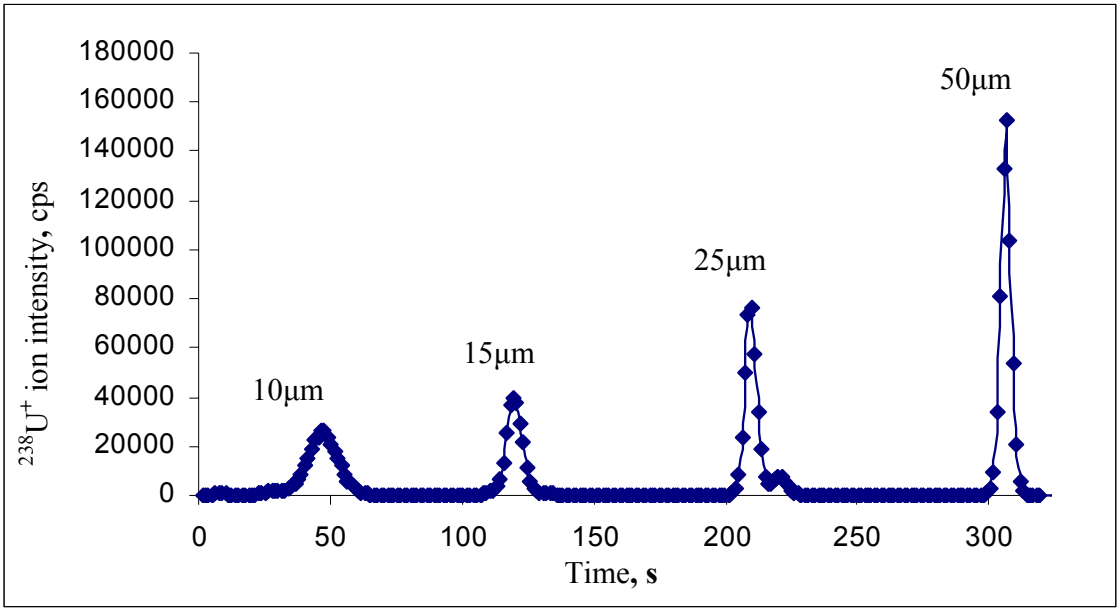

(b)

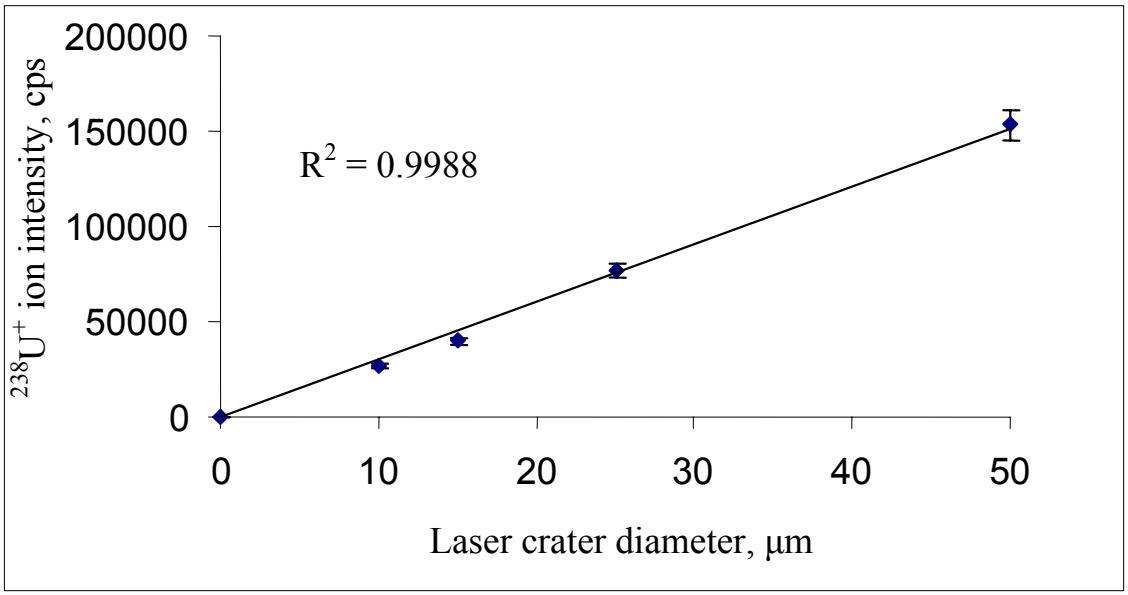

Fig. 5.1.14. (a) Dependence of $^{238}U^{+}$ ion intensity signal on the spot size (100 laser shots, repetition frequency 20 Hz) measured by LA-ICP-MS with cooled laser ablation chamber on the dried droplet of natural uranium standard solution (20 µl, U concentration 100 ng mL^{-1}) deposited onto the flower leaf and (b) Correlation curve of uranium ion intensity as a function of laser crater diameter measured by LA-ICP-MS with cooled laser ablation chamber.

If a substantial amount of material is transported into the plasma, it may cause a change in the plasma conditions and would result in a reduction of the ionization efficiency. In our experiment, the dependence of laser crater diameters does correlate linearly to the intensity of the peaks (R^2= 0.9988).

The results of the measurements on the NIST U-350, U-930 and CCLU-500 standard as well as natural uranium are presented in Table 5.1.15. and Fig 5.1.15. For the experiments with the non-cooled laser ablation chamber, the precision (relative standard deviation n = 6) and accuracy were in the range of 4.0% - 12.7% and 6.1% – 16.1% for the uranium isotopic standards reference material and 6.7% - 15.8% and 8.2% – 12.1% for natural uranium, respectively. The measured accuracies and RSDs were strongly dependent on the isotopic ratios as well as on laser crater diameter. Accuracy and precision were better with the higher uranium isotopic ratio in samples and larger crater sizes. The obtained data for precision and accuracy correspond to previous measurements[81, 214, 215]. An improvement of analytical results was observed when the ablation chamber of the laser ablation system was cooled to about -15ºC (see Table 5.1.15). The accuracy and precision in all measured samples were improved by up to one order of magnitude compared to the non-cooled LA chamber. For the measured uranium isotopic standards, precision of the $^{235}U/^{238}U$ ratio with 50 µm spot size ranged from 0.4 - 0.9 % RSD, whereas accuracies were in the range of 0.5 – 1.1 %. For the uranium with natural isotopic composition the best precision and accuracy were also achieved for $^{235}U/^{238}U$ ratios with 50 µm laser crater diameter and found to be 0.9 and -0.2%, respectively. for a similar precision and accuracy was observed for $^{234}U/^{238}U$ ratios, which were 3.2% and 1.8% for cooled LA chamber experiments (50 µm laser crater) in comparison to 11.0% and 8.8% under normal conditions.

The most probable reason for this improvement in precision and accuracy is that in the case of the non-cooled LA chamber the water vapor produced during the laser ablation of the leaf is very difficult to control and leads to changes in the plasma conditions and ionization efficiencies. However, when the ablated sample is cooled, these vapors have less effect on the plasma and, therefore, result in increased precision and accuracy. In addition, the adsorption properties of the laser energy in ice is significantly better than in a water matrix[216, 217], which would improve the amount of ablated material and therefore, precision and accuracy. However, since the standard was placed on the sample surface, a higher ablation rate would not lead to an increase in the count rates.

(a)

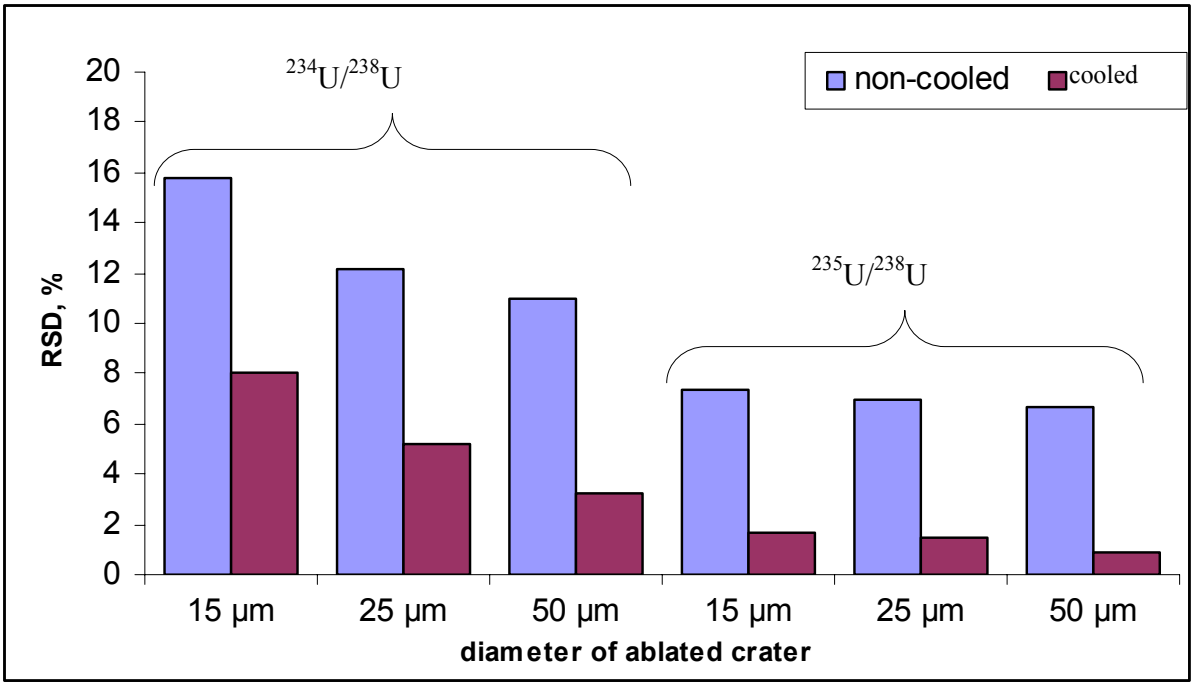

(b)

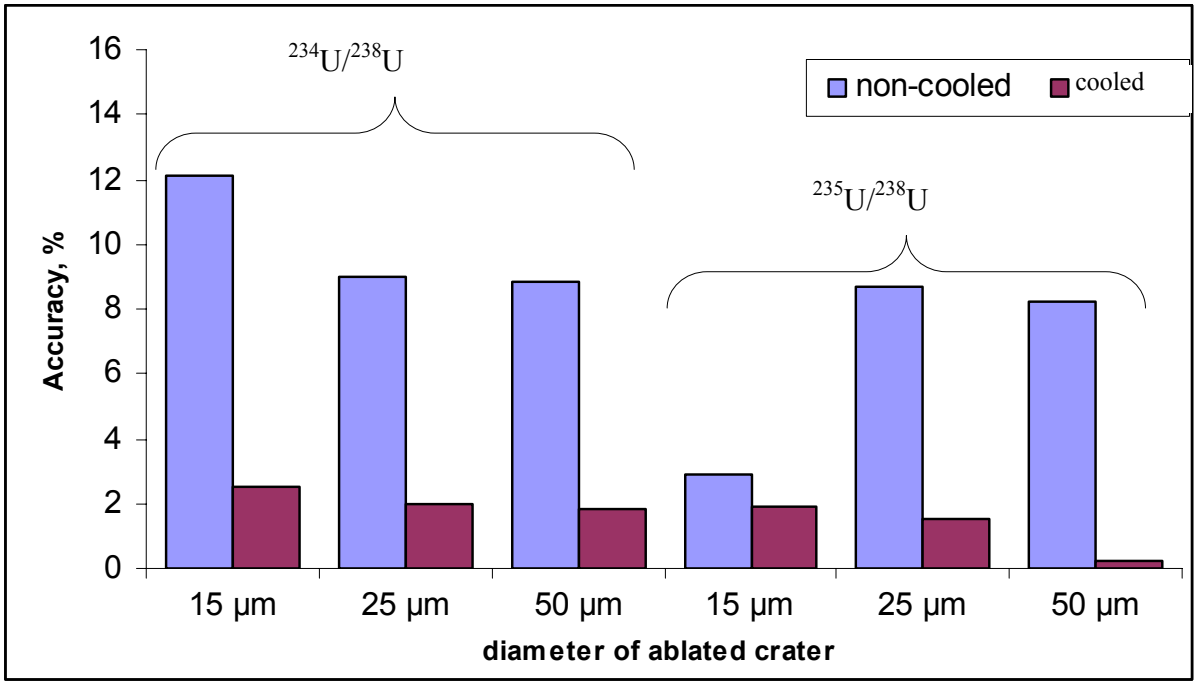

Fig. 5.1.15. Precision (a) and accuracy (b) of $^{234}U/^{238}U$ and $^{235}U/^{238}U$ isotope ratios, measured by LA-ICP-MS in dried droplet of uranium with natural isotopic composition using cooled and non-cooled laser ablation chamber.

Table 5.1.15. Precision and accuracy of uranium isotope ratios, measured in dried droplet of NIST U-350, NIST U930 and CCLU-500 uranium isotope reference materials using cooled and non-cooled ablation chamber

Standard reference material	Isotopic ratio	Measured isotopic ratio			RSD %			Accuracy %			Recommended isotopic ratio
		15[a]	25[a]	50[a]	15[a]	25[a]	50[a]	15[a]	25[a]	50[a]	
Non-cooled laser ablation chamber											
NIST U350	$^{234}U/^{238}U$	0.00324	0.00340	0.00350	9.4	8.2	8.1	16.1	12.3	10.0	0.00387
	$^{235}U/^{238}U$	0.50713	0.50768	0.57982	6.3	6.1	5.9	7.2	7.1	-6.1	0.54648
	$^{236}U/^{238}U$	0.00285	0.00284	0.00281	7.9	7.3	6.9	-10.2	-9.4	-8.0	0.00259
NIST U930	$^{234}U/^{238}U$	0.17886	0.17906	0.18207	10.7	9.2	9.0	11.0	10.9	9.4	0.20097
	$^{235}U/^{238}U$	15.63	15.92	15.92	5.1	4.9	4.5	9.9	8.2	8.2	17.34
	$^{236}U/^{238}U$	0.04103	0.04091	0.04069	9.9	9.8	9.0	-8.9	-8.6	-8.0	0.03767
CCLU-500	$^{234}U/^{238}U$	0.00946	0.00966	0.00971	12.7	9.7	8.3	14.9	13.1	12.7	0.01112[b]
	$^{235}U/^{238}U$	0.89792	0.90091	0.90191	5.7	5.5	4.0	10.2	9.9	9.8	0.99991[b]
	$^{236}U/^{238}U$	0.00313	0.00268	0.00302	5.5	5.2	5.0	-12.1	3.9	-8.2	0.00278[b]
Cooled laser ablation chamber											
NIST U350	$^{234}U/^{238}U$	0.00372	0.00369	0.00276	2.0	1.6	1.4	4.2	4.7	3.2	0.00387
	$^{235}U/^{238}U$	0.5344	0.5366	0.5524	1.3	1.2	0.9	2.2	1.8	-1.1	0.54649
	$^{236}U/^{238}U$	0.00272	0.00265	0.00252	2.1	2.0	1.9	-4.8	-2.1	3.2	0.00259
NIST U930	$^{234}U/^{238}U$	0.19453	0.19494	0.19594	1.8	1.6	1.1	3.2	3.0	2.5	0.20097
	$^{235}U/^{238}U$	17.07	17.19	17.21	1.0	0.8	0.4	1.6	0.9	0.8	17.34
	$^{236}U/^{238}U$	0.03851	0.03715	0.03809	1.5	1.3	1.0	-2.2	1.4	-1.1	0.03767
CCLU-500	$^{234}U/^{238}U$	0.01083	0.01137	0.01124	1.5	2.0	1.6	2.6	-2.2	-1.1	0.01112[b]
	$^{235}U/^{238}U$	0.9889	0.9909	1.0049	1.3	1.2	0.9	1.1	0.9	-0.5	0.99991[b]
	$^{236}U/^{238}U$	0.00285	0.00284	0.00276	1.4	2.0	1.6	-2.4	-2.1	1.2	0.00278[b]

[a] laser crater diameter in μm

[b] recommended value

5.1.5. Determination of uranium by on-line LA-ID-ICP-MS in NIST-SRM 1515

In addition to the described method for the uranium determination in sample NIST-SRM 1515 (apple leaves) and isotope dilution LA-ICP-MS technique was tested. On-line isotope dilution in LA-ICP-MS consists of a sequence of three measurements:

1. Laser ablation of the sample and nebulization of 2% nitric acid in order to determine the $^{235}U/^{238}U$ isotope ratio in the sample (S).
2. Nebulization of isotope-enriched tracer solution NIST U-350 and simultaneous laser ablation of the sample for the determination of the $^{235}U/^{238}U$ isotope ratio in the mixture (X).
3. Nebulization of isotope-enriched tracer solution NIST U-350 while the laser is not operating for measurement of the $^{235}U/^{238}U$ isotope ratio in the tracer solution (T).

The LSX 200 laser ablation system with the microflow total consumption nebulizer DS-5 (see Experimental) was combined with Platform ICP-CC-QMS. Experimental parameters are summarized in Table 5.1.16.

Table 5.1.16. Experimental parameters for on-line isotope dilution LA-ICP-CC-QMS

ICP-CC-QMS "Platform"		Laser ablation system "LSX 200"	
RF power	1200	Wavelength (nm)	266
Coolant gas flow rate (l min^{-1})	13.55	Pulse energy (mJ)	4
Auxiliary gas flow rate (l min^{-1})	1.09	Laser energy density (W cm^{-2})	1.1 x 10^9
Carrier gas flow rate (l min^{-1})	0.85	Repetition frequency (Hz)	20
He gas flow rate (ml min^{-1})	10	Spot diameter (μm)	3000
Dwell time (ms)	200		

Experimental parameters in ICP-MS were optimized with respect to maximum ion intensity of $^{238}U^+$ using a 1 μg l^{-1} uranium solution nebulized with a DS-5 directly coupled to the laser ablation chamber. This quick and easy way of optimizing ICP-MS parameters in LA-ICP-MS is possible using the mono gas sample introduction system because the optimized conditions (rf power, carrier or nebulizer gas flow rate) were found to be the same for nebulized solutions and ablated solid samples[87, 215]. Furthermore, the mono gas sample introduction system offers optimum mixing of nebulized isotope-enriched tracer solution and laser-ablated solid sample directly within the ablation chamber, which is of importance in the case of isotope dilution analysis.
Based on this procedure, an apple leave sample was doped with 10 μg ml^{-1} of liquid uranium standard with a natural $^{235}U/^{238}U$ isotope ratio, properly mixed and dried in the heating oven.

Then the sample was placed onto the target holder and the $^{235}U/^{238}U$ isotopic ratios were measured using the LA-ICP-CC-QMS.

The $^{235}U/^{238}U$ isotopic ratios measured during the ablation of the sample and the nebulization of 2% HNO_3 and NIST U350 tracer solution were determined to be 0.0077 and 0.4660, respectively. During nebulization of only NIST U-350 tracer solution without ablation of the sample $^{235}U/^{238}U$ isotopic ratios was determined to be 0.5218. In Fig. Fig. 5.1.16b, the results of the measured $^{235}U/^{238}U$ isotope ratios obtained by LA-ICP-CC-QMS for the quantitative analysis of uranium via on-line isotope dilution in NIST apple leaves SRM 1515 (doped U concentration: 10 µg g^{-1}) are summarized.

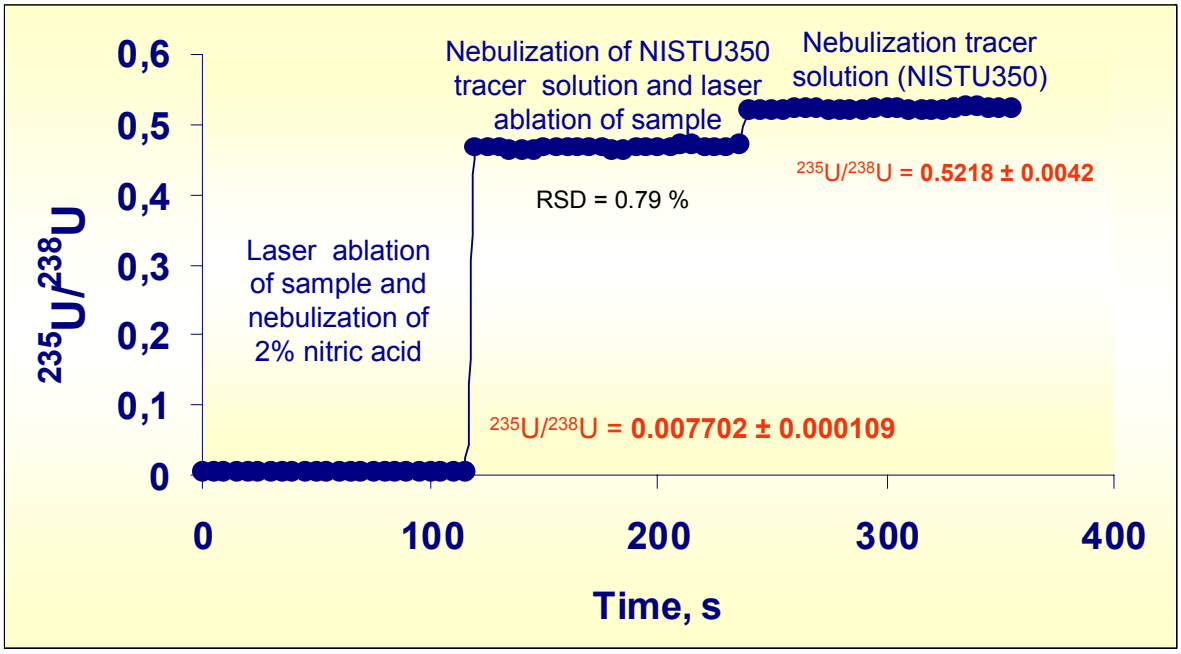

Fig. 5.1.16. $^{235}U/^{238}U$ isotope ratio measured during LA-ID-ICP-QMS analysis of the NIST SRM 1515 (apple leaves) sample.

Using these data the uranium concentration in the sample was calculated using the isotope dilution formula:

$$C_s = KC_T[(T - X)/(X - S)](m_s / m_T) \qquad (5.2.1)$$

where

C_s and C_T are concentration of uranium in the sample and tracer, respectively;

T, X, S are $^{235}U/^{238}U$ isotopic ratios in the tracer solution, the mixture and in the sample, respectively;

m_s and m_T are the relative atomic masses in the sample and tracer, respectively.

K is correction factor determined via internal standardization

Taking into consideration that there is a difference in ion intensity for laser ablation of the sample and nebulization of U standard using DS-5 nebulizer the barium concentration in the analyzed sample was determined and used as internal standard element. Correction factor was calculated as ratio between true Ba concentration and measured Ba concentration.

$$K = C_{true}/C_{meas}, \quad (5.2.2)$$

where

C_{true} -true Ba concentration

C_{meas}-measured Ba concentration

As shown in Table 5.1.17, a concentration of 11.19 ± 1.11 μg g^{-1} was determined in the apple leaves sample investigated, which is in good agreement with the doped uranium concentration of 10 μg g^{-1}.

Table 5.1.17. Results of uranium determination in NIST apple leaves SRM 1515 doped with uranium by on-line LA-ID-ICP-MS

Uranium concentration (μg g^{-1})			
NIST SRM 1515 Apple leaves	Certified value	Doped U	On-line LA-ID-ICP-MS
	(0.006)[a]	10±0.5	11.19±1.11

[a] Informative value

5.2. Application of LA-ICP-MS in materials science

Interdiffusion between coating and substrate (base material) after oxidation in air at a temperature of 980 °C for several thousand hours affects the coating life and causes the formation of new, frequently brittle phase at and close to the coating and the substrate interface. Several effects, especially the interdiffusion of matrix elements at high temperature, can result in an alteration of the mechanical properties and or oxidation performance. Therefore, the lateral element distribution and diffusion profiles between coating and substrate material are of special interest as a function of oxidation time. The aim of this study was to develop an method for the characterization of NiCrAlY-based coatings on high-temperature alloys to study element interdiffusion at interfaces. The ICP-SFMS was coupled to the Ablascope laser ablation system (Bioptic, Germany) was used for the analysis of lateral element distribution in NiCrAlY-based coatings. The optimization of the experimental parameters (rf power and carrier gas flow rate) was performed with respect to maximum ion intensities of analytes (Table 5.2.1).

Table 5.2.1. Optimized experimental parameters of LA-ICP-SFMS

Laser ablation	**Ablascope**
Wavelength, nm	213
Pulse duration, ns	5
Repetition frequency, Hz	20
Energy pulse, mJ	2-4
Diameter of laser crater, µm	25
ICP-SFMS	**ELEMENT 1**
Mass resolution, m/Δm	300
RF power, W	1050
Carrier gas flow rate, L/min	0.92
Dwell time, ms	50
Sweeps	1
Replicates	400

5.2.1. Investigation of diffusion processes in NiCrAlY-based alloys using LA-ICP-MS

5.2.1.1. Optimization of the surface analytical method

The surface of the certified reference material BAM-328-1 was scanned by a focused laser beam in "line scan" and "single point" mode in order to study different sampling methods. The measured $^{27}Al^{+}$ ion intensity as a function of ablation time for "line scan" (sample is moved relatively to the focused laser beam along a defined line on the sample) and "single point" (continuous ablation at a single point) mode for different laser energies (2 mJ and 4 mJ) is shown in Fig. 5.2.1 and Fig. 5.2.2 respectively.

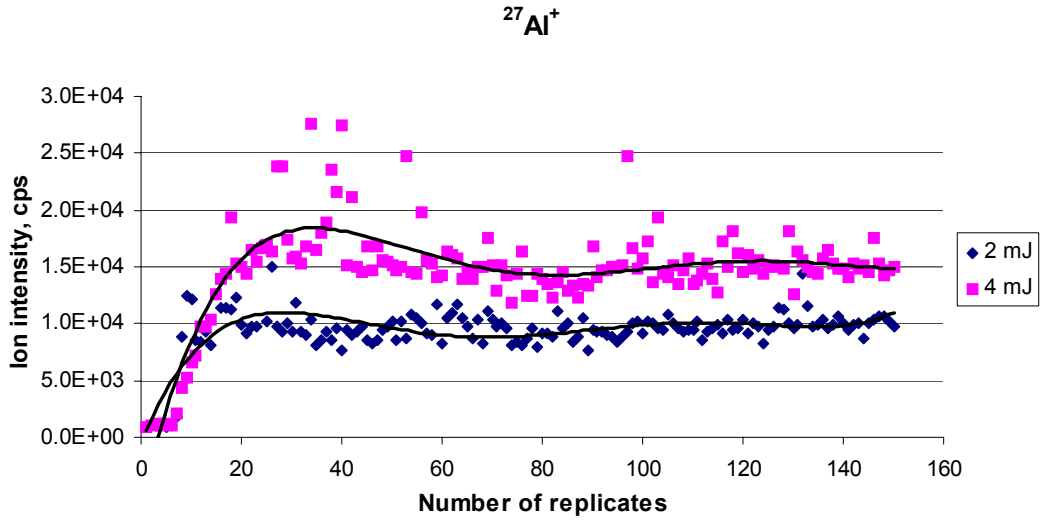

Fig. 5.2.1. $^{27}Al^{+}$ - ion intensity as a function of laser ablation time for different laser energies (line scan mode).

During the preablation of the sample surface after starting the measurements, the ion intensity of analyte increases as found by the analysis of high-purity quartz glasses in ref.[160] . In general, for 4 mJ laser energy, higher ion intensities were observed. Nevertheless, 2 mJ laser energy results in better stability of the ion beam and a better precision for both sampling methods. The relative standard deviations (RSD in %) of measured ion intensities at a laser energy of 2 and 4 mJ on alloy certified reference material BAM-328-1 are compared for "line scan" and "single point" mode and are summarized in Table 5.2.2.

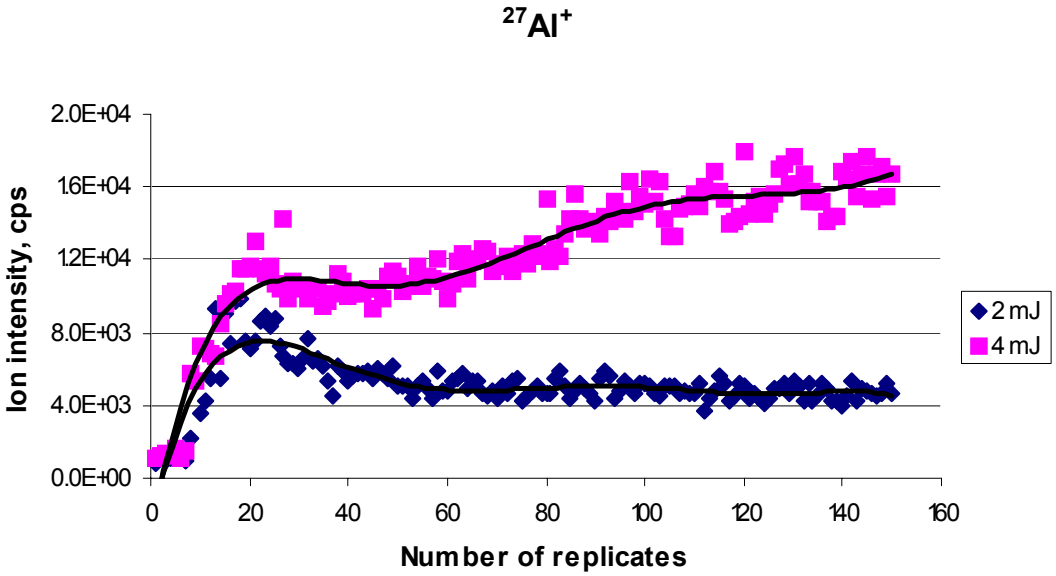

Fig. 5.2.2. $^{27}Al^{+}$ - ion intensity as a function of laser ablation time for different laser energies (single point mode).

In general, using the "line scan" mode the RSDs varied for both laser energies between 8 and 20 %. It should be considered that fractionation effects are possible at lower laser energy[85, 158, 159]. A further loss of ion intensities was observed when the laser beam was defocused using a "single point" mode due to decreasing laser power density during laser ablation.

Table 5.2.2. Relative standard deviations (RSD, %) of measured ion intensities (100 replicates). Measurements were performed using the certified reference alloy BAM 328-1

Element		Al	Cr	Co	Ni	Mo
RSD, % Line scan mode	2 mJ	10.2	8.4	9.4	8.9	20.6
RSD, % Single point mode		12.2	9.3	19.4	16.9	31.5
RSD, % Line scan mode	4 mJ	17.1	8.7	11.7	9.8	20.9
RSD, % Single point mode		17.5	27.8	37.8	34.9	54.8

In order to study the laser ablation of alloys, the dependence of RSCs on the rf power of ICP and carrier gas flow rate was investigated using the certified reference alloy BAM-328-1. The results of the measurements are presented in Fig. 5.2.3 and Fig. 5.2.4, respectively.

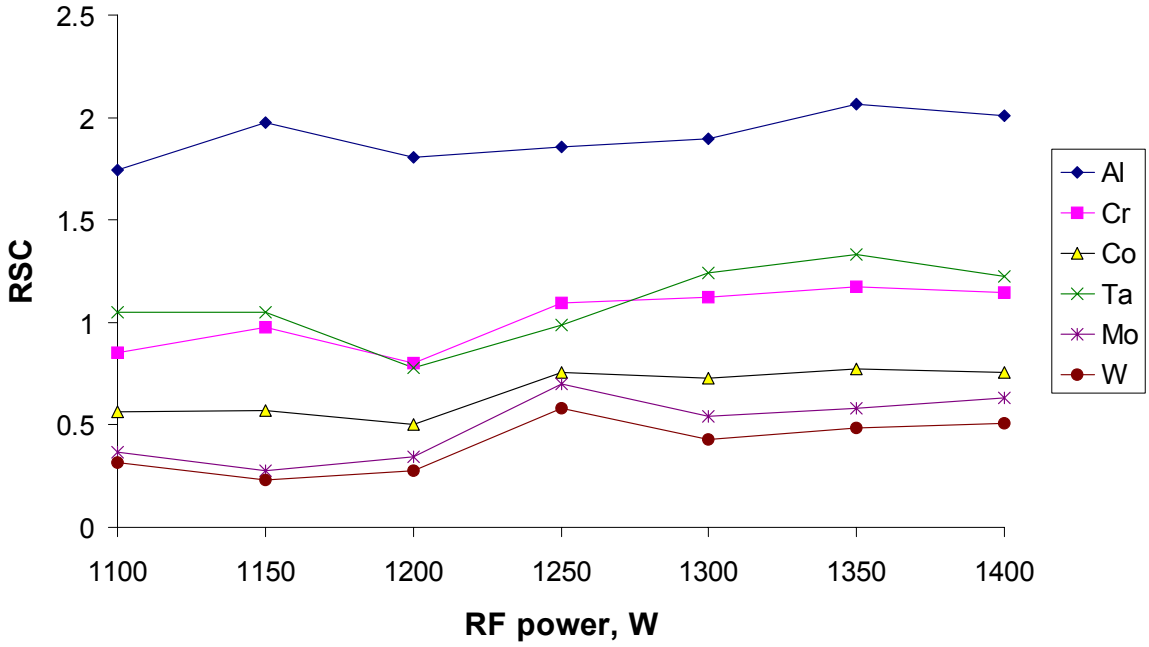

Fig. 5.2.3. Dependence of RSCs on the rf-power measured by LA-ICP-MS (alloy standard BAM-328-1).

All elements studied showed no large variation of RSCs as a function of rf power and carrier gas flow rate. Values of RSCs for different elements were in the range from 0.2 to 2, which means that a semi-quantitative determination of elements without reference material would be possible within this range. Under the experimental condition applied it was observed that elements with a high melting point (such as W, and Mo) lead to RSCs lower than 1, whereas for Al with relatively low ionization potentials lead to RSCs always higher than one. The RSCs determined on the certified reference material were applied as correction factors for the “real “ samples.

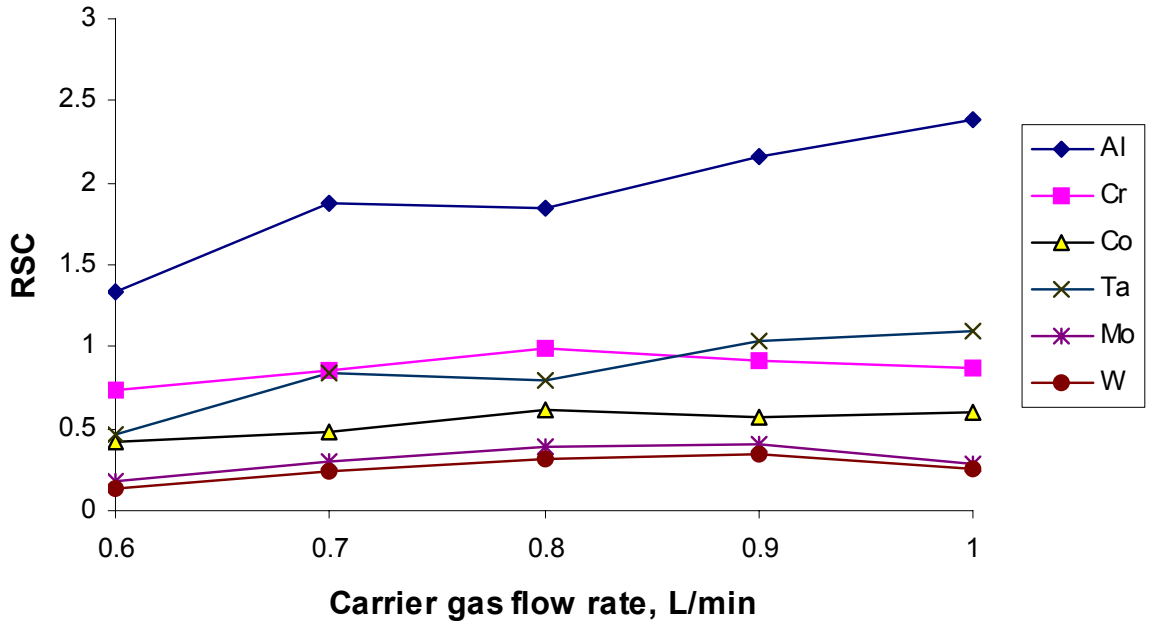

Fig. 5.2.4. Dependence of RSCs on the carrier gas flow rate measured by LA-ICP-MS (alloy standard BAM-328-1).

The certified reference material BAM-327-2 was analyzed by LA-ICP-MS in order to verify the method. The sample was quantified via RSCs used as the correction factor determined on alloy reference material BAM-328-1. The results of bulk analysis on CRM BAM-327-2 yielded accuracies between 4-22% in the alloy as demonstrated in Fig 5.2.5.

Further possible calibration strategies via external calibration and solution-based calibration were also studied. As the result, correlation coefficients (R^2) of the calibration curves measured in the "single point" mode and "line scan" mode at 2 mJ laser energy are presented in Fig. 5.2.6.

Analysis of CRM BAM-327-2 by external calibration generally yields better accuracy in comparison with the RSC quantification method (see Fig.5.2.5), but the technique is more time-consuming and the possibility of quantification is limited by the availability of certified alloy reference standards.

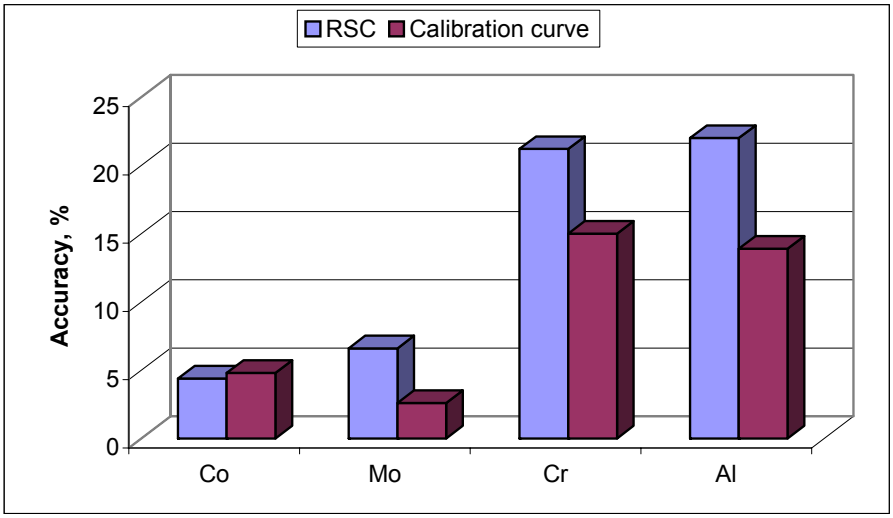

Fig. 5.2.5. Accuracy of quantitative element determination in CRM BAM-327-2 using RSCs for correction of measured values.

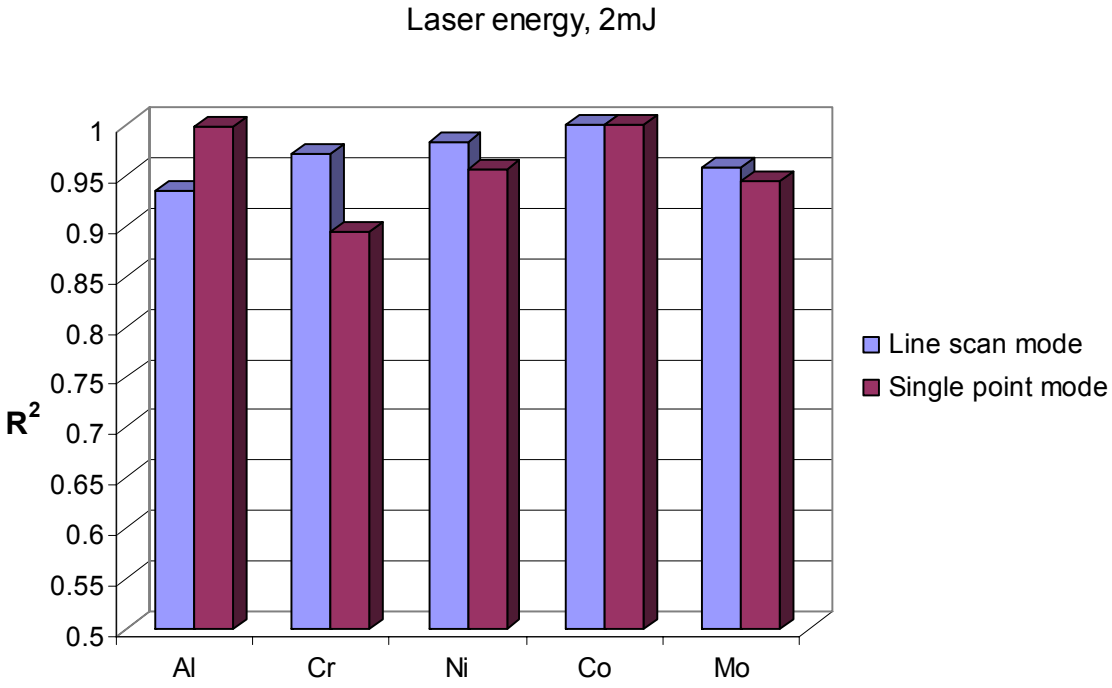

Fig. 5.2.6. Correlation coefficient (R^2) of the calibration curve measured in "single point" mode and "line scan" mode by LA-ICP-MS at 2 mJ energy of laser beam.

5.2.1.2. Quantification semiquantitatively and by solution-based calibration

Measurements by “single point” mode were performed for the NiCrAlY-based coatings on high-temperature alloy before and after oxidation in air during 5000 hours at a temperature of 980 °C. The bond coat is between surface and 200 µm and the base alloy is at a depth of 200 to 500 µm. The concentration was semi-quantitatively calculated using an internal standard element. Fig. 5.2.7. show Y and Zr concentration distribution as a function of thickness from 0 to 528 µm in a cross section of NiCrAlY-based coatings on high-temperature alloy.

(a)

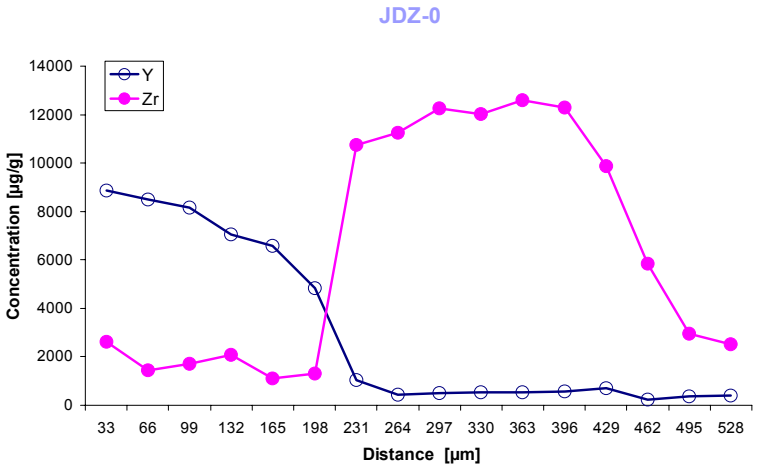

(b)

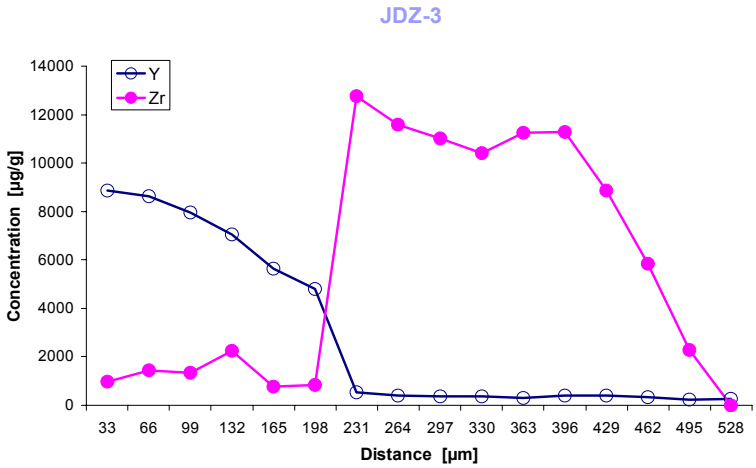

Fig. 5.2.7. Distribution of Y and Zr in the sample before oxidation (a) and after oxidation (b) in air measured by LA-ICP-MS.

LODs for Y and Zr were determined at 56 μg/g. No interdiffusion of elements (Y, Zr) between the coating and the substrate material was observed.

Quantification of elements which are not certified in standard reference materials is only possible by solution-based calibration using an ultrasonic nebulizer (USN) as described in[87]. Measured Ti concentration varied between 3.2-3.5%, which is in agreement with the known concentration of Ti (3.2%) in the base material of the sample before oxidation in air.

Fig.5.2.8 contains the distribution of Ti in the sample after 1000 hours oxidation. Mo was used as the internal standard element.

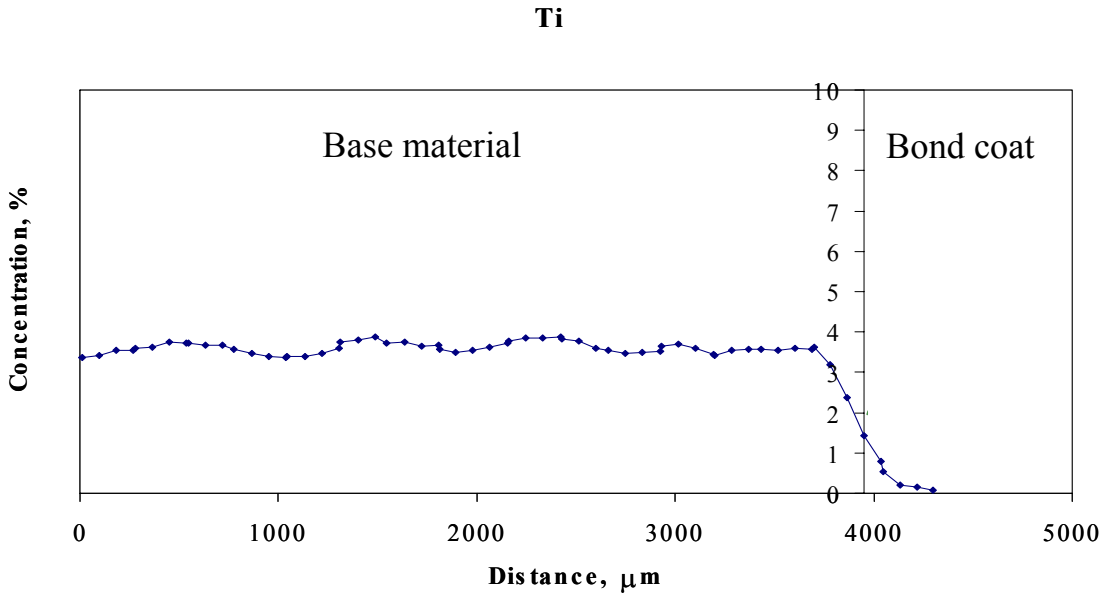

Fig. 5.2.8. Ti distribution in the sample after 1000 hours of oxidation quantified via solution-based calibration using Mo as internal standard.

5.2.1.3. Lateral element distribution of NiCrAlY-based coatings on high temperature alloy

The LA-based method was evaluated by comparison of LA-ICP-MS data with energy dispersive X-rays (EDX) measurements. Measurements by "single point" mode were performed for the NiCrAlY-based coatings on high-temperature alloys after oxidation in air at a temperature of 980 °C (1000 hours only) and those results were compared with EDX measurements for a selected number of elements. Good agreement between LA-ICP-MS and EDX techniques was found and is shown in Fig.5.2.9.

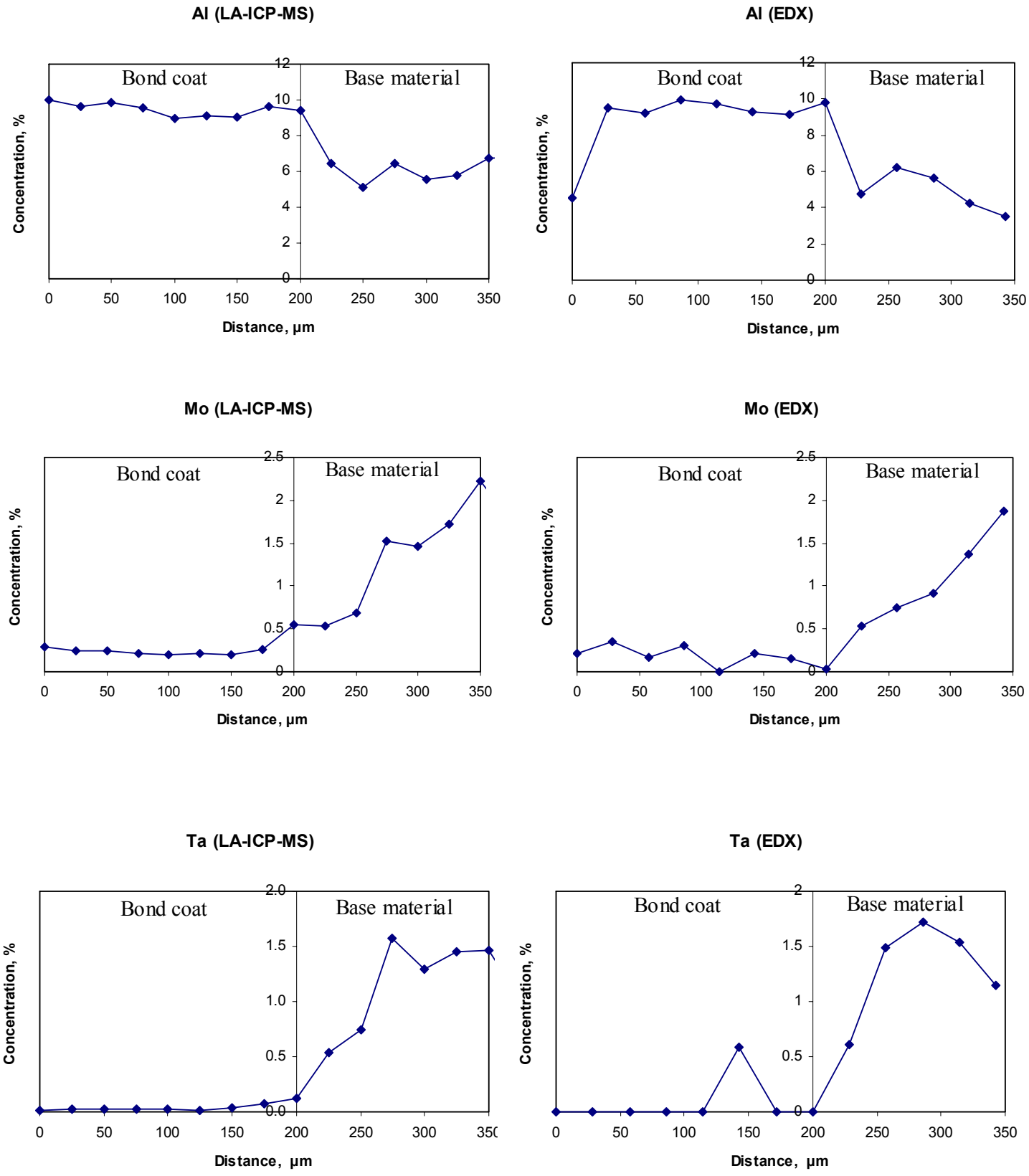

Fig. 5.2.9. Comparison of the quantitative distribution of Al (a), Mo (b), Ta (c) determined by LA-ICP-MS and EDX in a sample after 1000 h oxidation in air at 980 ºC.

The results of the lateral Al, Co, Cr, Mo, W, Ta distribution in NiCrAlY-based coatings on high-temperature alloy after oxidation in air at a temperature of 980 °C for 300, 1000, 5000 and 15000 hours are presented in Fig. 5.2.10. LA-ICP-MS measurements were performed under optimized conditions in "line scan" mode. In Fig.5.2.10, the concentrations of alloy elements are shown as a function of distance from 0 to 500 µm in a cross section of NiCrAlY-based coatings on high-temperature alloy. Based on the results shown in Fig. 5.2.10, an interdiffusion of elements (Al, Co, Mo, W, Ta) between coating and substrate material was determined.

(a)

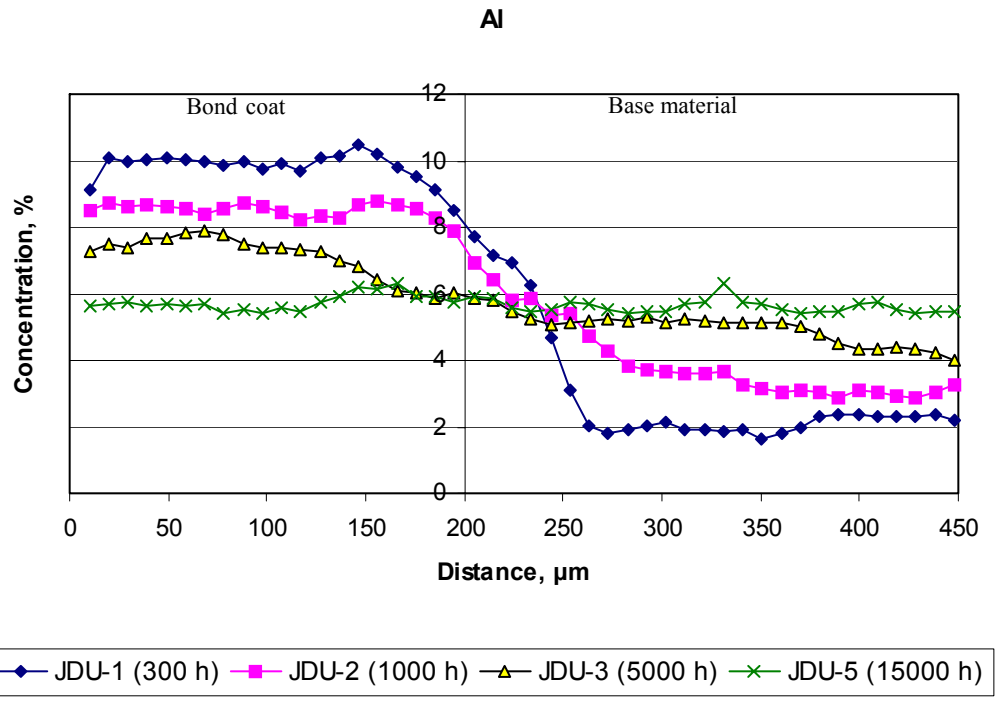

Fig. 5.2.10. Distribution of Al (a) in the sample after different oxidation times measured by LA-ICP-MS.

(b)

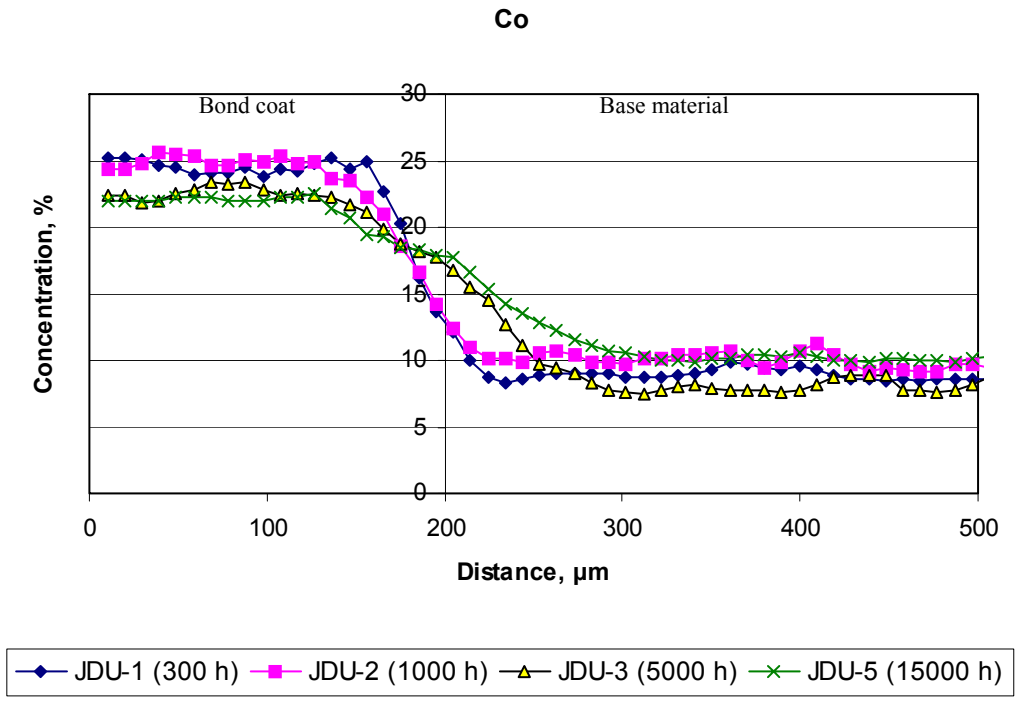

(c)

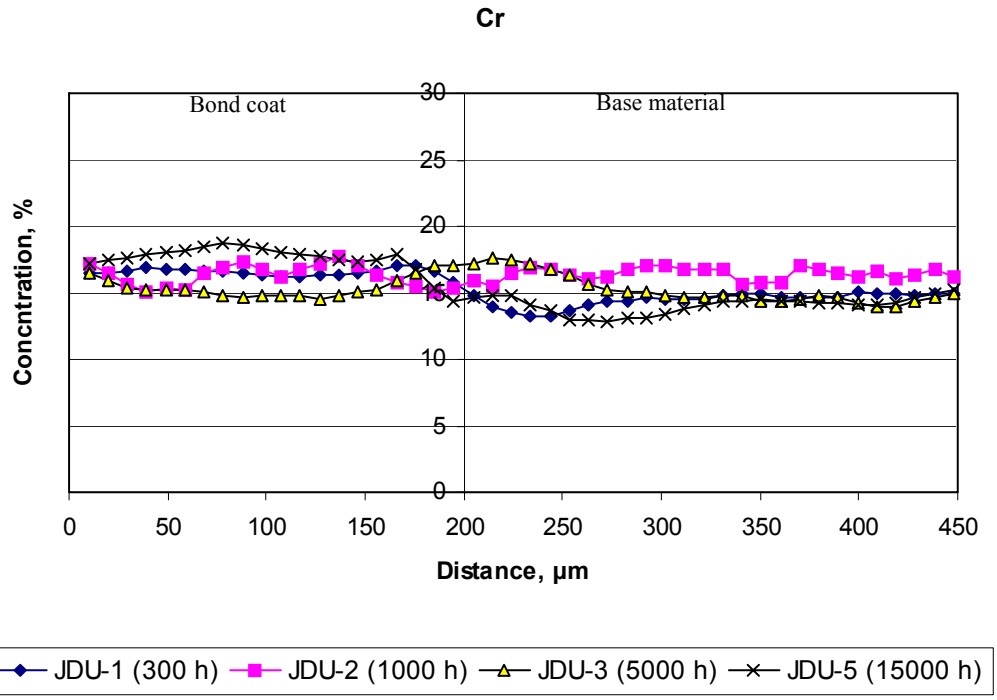

Fig. 5.2.10. Distribution of Co (b) and Cr (c) in the sample after different oxidation times measured by LA-ICP-MS.

(d)

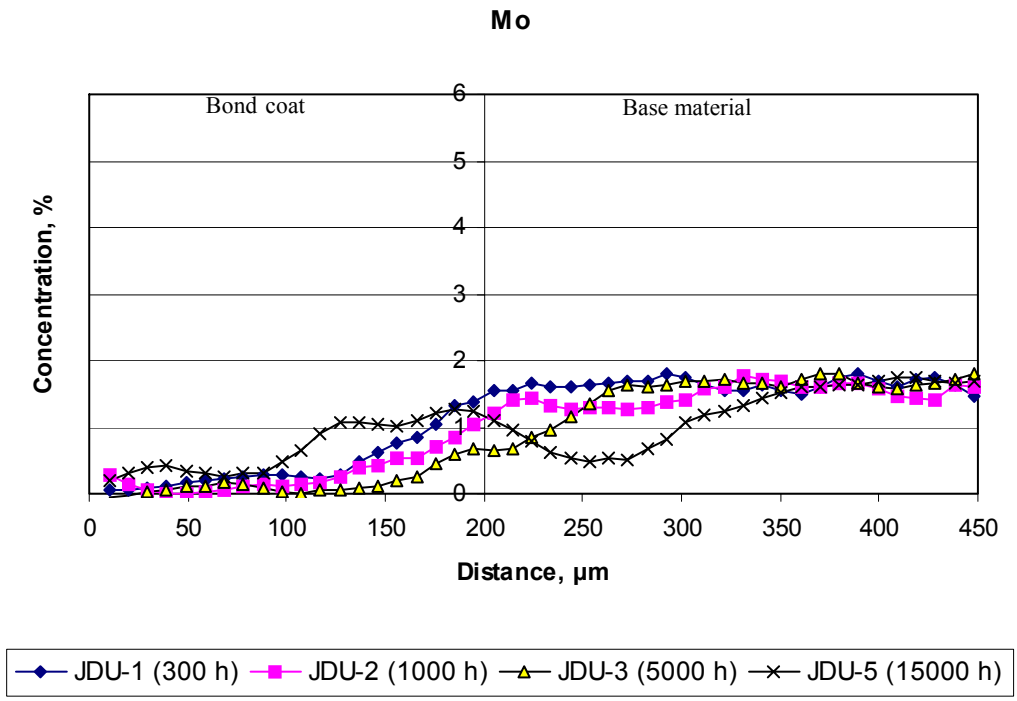

(e)

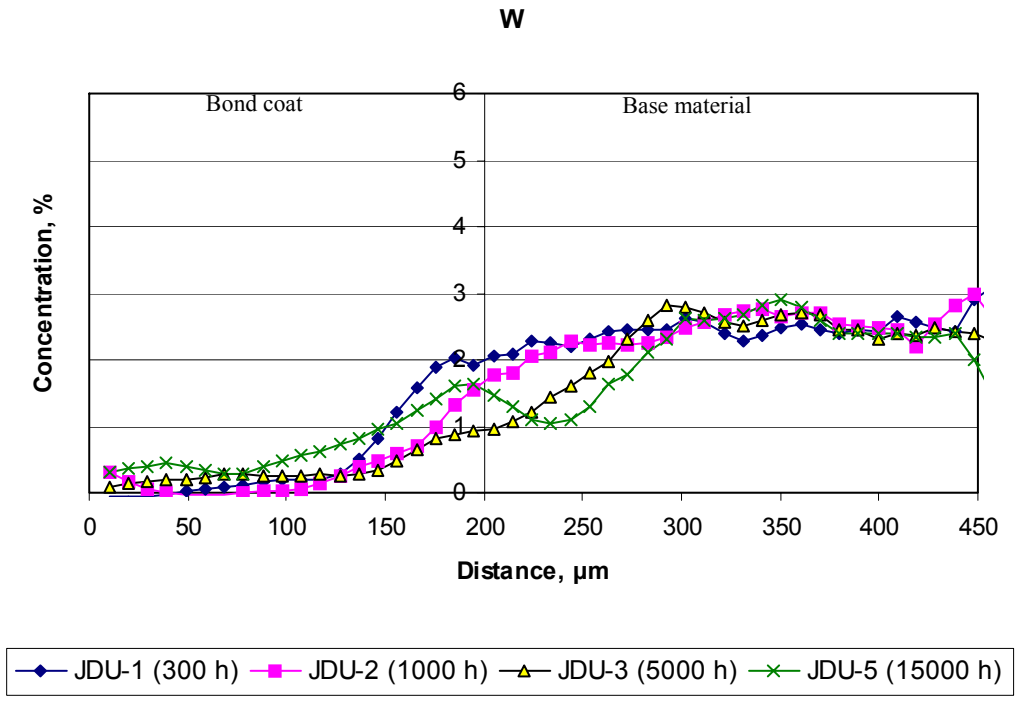

Fig. 5.2.10. Distribution of of Mo (d) and W (e) in the sample after different oxidation times measured by LA-ICP-MS.

(f)

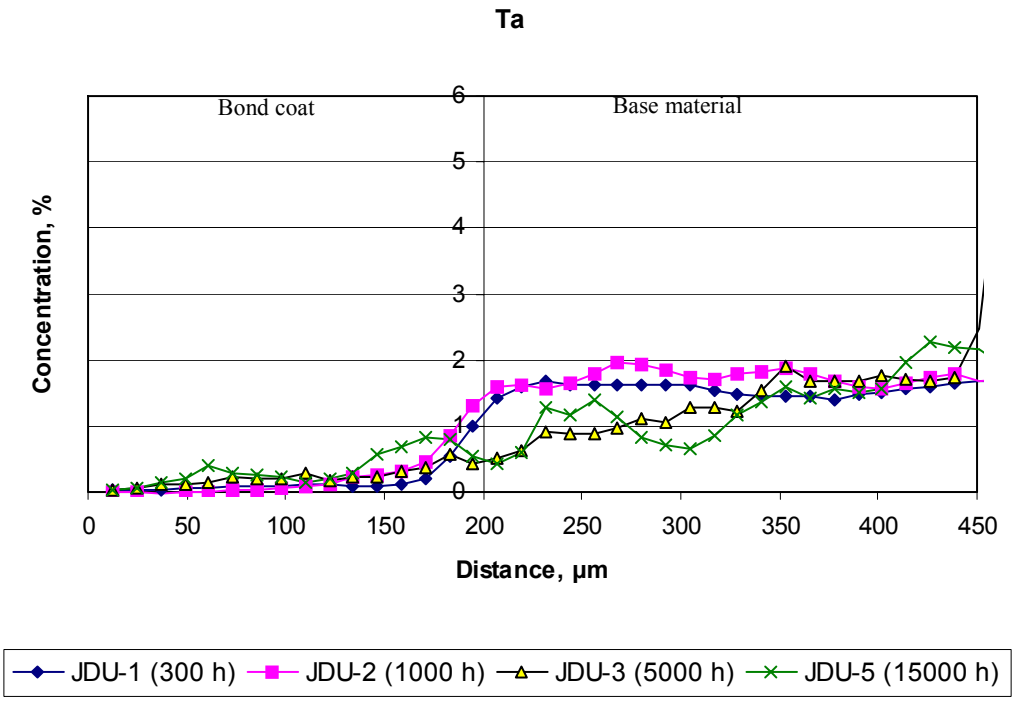

Fig. 5.2.10. Distribution of Ta (f) in the sample after different oxidation times measured by LA-ICP-MS.

Such interdiffusion affects the coating life mainly because of the following processes: aluminium loss due to diffusion from coating into the base metal and diffusion of substrate alloying elements into the coating layer, thereby altering the mechanical properties and/or oxidation performance.
Furthermore, images of element distribution in a cross section of NiCrAlY-based coatings on high-temperature alloy were acquired.
In order to obtain a two-dimensional imaging of the element distribution, the regions of interest (see Fig. 5.2.11a and Fig. 5.2.12a) was systematically screened (line by line). In Fig. 5.2.11b and Fig. 5.2.12b the ion intensity profiles of chromium measured in NiCrAlY-based coatings on high-temperature alloy before oxidation and after oxidation are shown.

(a)

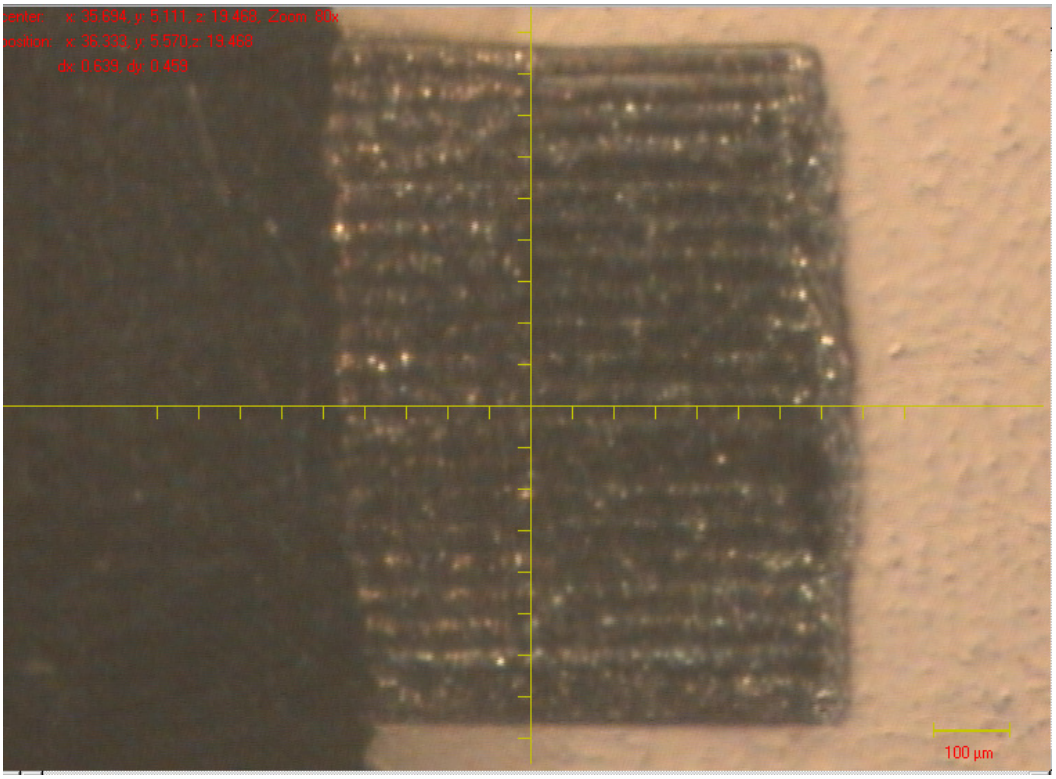

(b)

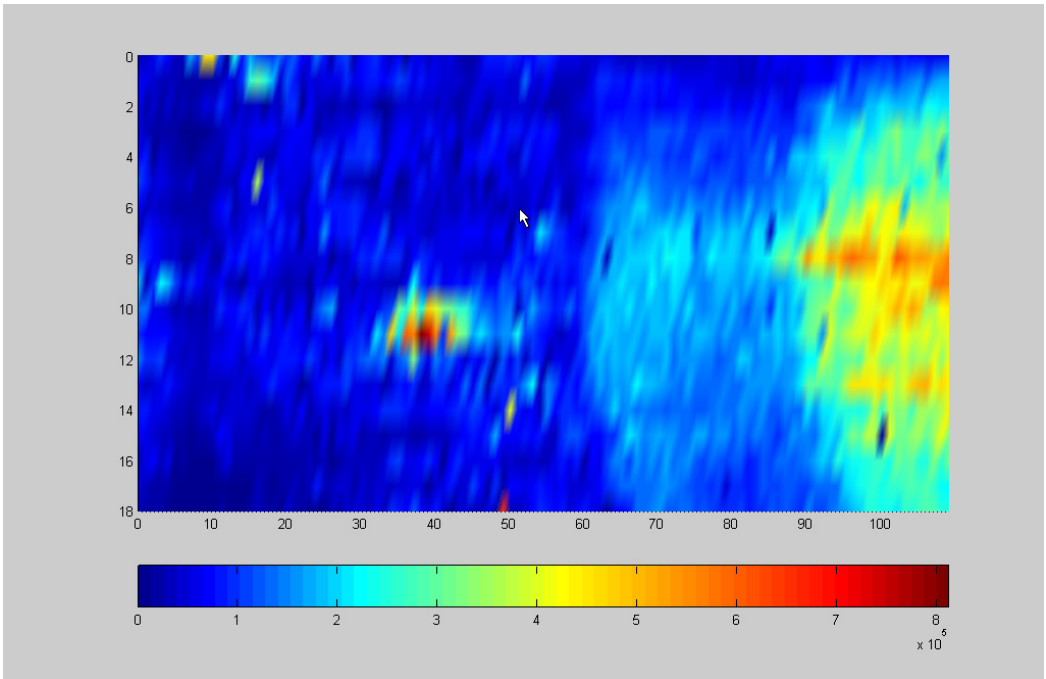

Fig. 5.2.11. Ablation area of the cross section of NiCrAlY-based coatings on high-temperature alloy before oxidation (a)and 2D image of ion intensity profiles of chromium measured by LA-ICP-MS (b).

(a)

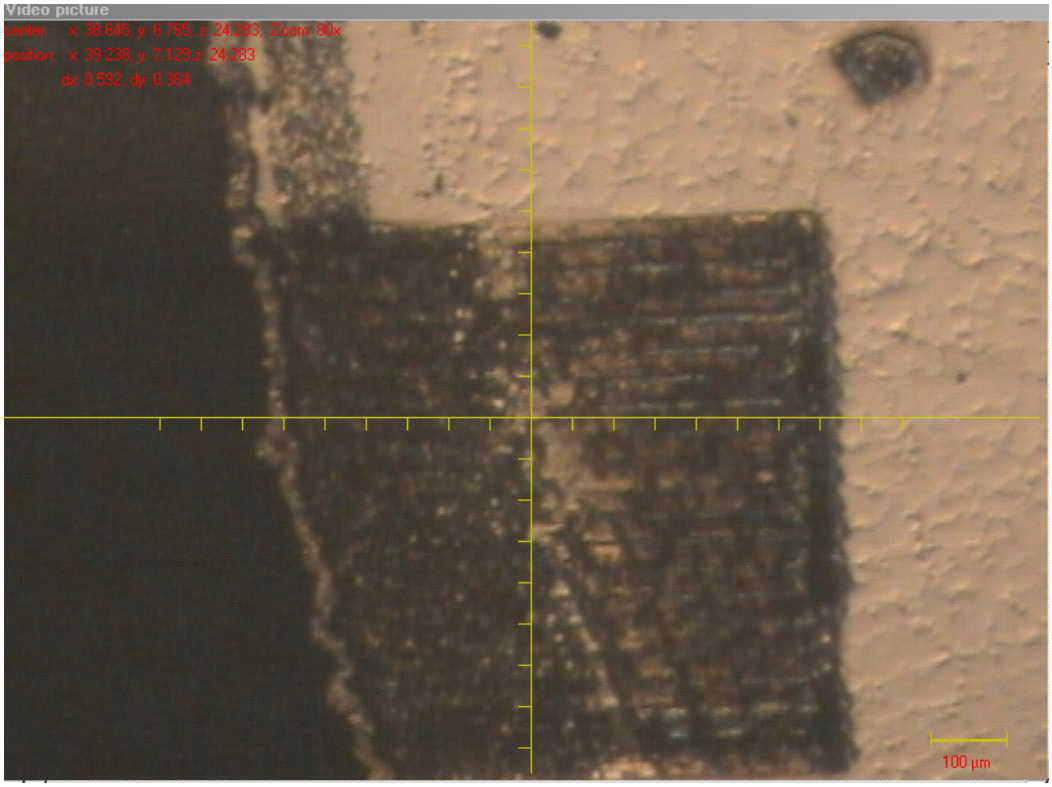

(b)

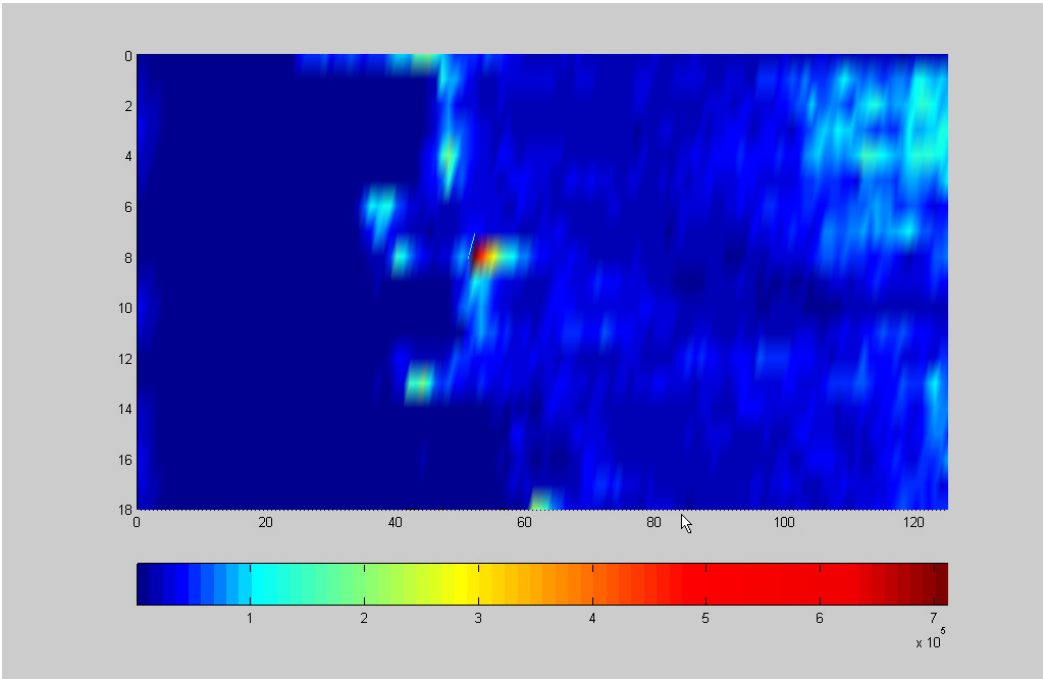

Fig. 5.2.12. Ablation area of the cross section of NiCrAlY-based coatings on high-temperature alloy after oxidation (5000 h) (a) and 2D image of ion intensity profiles of chromium measured by LA-ICP-MS (b).

Fig. 5.2.11 shows that there is more Cr in the base material than in the bond coat before oxidation. After oxidation, the content of Cr in the bond coat and in base material is changed (Fig. 5.2.12). Based on these results, the diffusion of substrate alloying element Cr into the coating layer can be supported by this study. The figures show also that some inhomogeneous distributions can be visualized for the elements of interest.

6. Conclusion

Within this PhD thesis several methods were developed and validated which can find applicationare suitable for environmental sample and material science and should be applicable for monitoring of particular radionuclides and the analysis of the chemical composition of construction materials in the frame of ESS project. The study demonstrated that ICP-MS is a powerful analytical technique for ultrasensitive determination of ^{129}I, ^{90}Sr and lanthanides in both artificial and environmental samples such as water and soil. In particular ICP-MS with collision cell allows measuring extremely low isotope ratios of iodine. Thus, LODs were improved by approximately two orders of magnitude in comparison to previously used techniques based on ICP-SFMS. Furthermore it was demonstrated that isotope ratios of $^{129}I/^{127}I$ as low as 10^{-7} can be measured with an accuracy and precision suitable for distinguishing sample origins. An advanced sample introduction technique delivering iodine via the gas phase and demonstrates detection limits of 30 pg g^{-1} for ^{129}I significantly simplifies the sample preparation procedure and reduce time and costs for the analysis.

ICP-MS with collision cell, in particular in combination with cool plasma conditions, reduces the influence of isobaric interferences on m/z = 90 and is therefore well-suited for ^{90}Sr analysis in water samples. However, the applied ICP-CC-QMS in this work is limited for the measurement of ^{90}Sr due to the tailing of $^{88}Sr^{+}$ and in particular Daly detector noise, which is a critical factor for the determination of typically ultra-low concentrations of ^{90}Sr. It was determined that a concentration of natural strontium in the sample above 25 ng ml^{-1}, which is very often case (e.g. digested bone samples), other techniques need to be applied (for instance MC-ICP-MS can be used which possesses significantly better abundance sensitivity and lower instrument background).

Hyphenation of capillary electrophoresis with ICP-MS was shown to resolve atomic ions of all lanthanides and polyatomic interferences. The elimination of polyatomic and isobaric ICP-MS interferences was accomplished without compromising the sensitivity by the use of a high resolution mode as available on ICP-SFMS. Therefore, this combination is suitable for the determination of samples with unknown nuclide abundances such as irradiated target of ESS.

Combination of laser ablation with ICP-MS allowed direct micro and local uranium isotope ratio measurements at the ultratrace concentrations on the surface of biological samples. In particular, the application of a cooled laser ablation chamber improves the precision and accuracy of

uranium isotopic ratios measurements in comparison to the non-cooled laser ablation chamber by up to one order of magnitude. In order to reduce the quantification problem, a mono gas on-line solution-based calibration was built based on the insertion of a microflow nebulizer DS-5 directly into the laser ablation chamber[191]. The low solution uptake rate of 7 µl min^{-1} for DS-5 reduces the amount of isotope-enriched tracer solution needed for on-line isotope dilution in LA-ICP-MS. Furthermore, the low solution uptake rate allows a better adjustment of small amounts of ablated material and nebulized solution. At present, LA-ICP-MS with cooled laser ablation chamber is successfully applied for micro local analysis of element distribution in thin section of tissue samples (e.g. brain, liver *etc.*)[218, 219]. Furthermore, this procedure allows quantitative element mappings and imaging as requested in materials science.

A micro local method to determine the lateral element distribution on NiCrAlY-based alloy and coating after oxidation in air was tested and validated. Calibration procedures involving external calibration, quantification by relative sensitivity coefficients (RSCs) and solution-based calibration were investigated. Increasing loss of aluminium due to diffusion from coating into the high-temperature base alloy was successfully proven. Diffusion of several substrate alloying elements (e.g. Co, Ta, Mo, W) into the coating after annealing was found, which could be one reason for the alteration of mechanical properties (high-temperature stability) or oxidation performance. The accuracy of the analytical results between 4 – 22 % demonstrates that this method can be applied as a fast screening technique. The analytical method was validated by comparison of the LA-ICP-MS results with data acquired by EDX. Both techniques provide similar results and allow the interpretation of the process.

In conclusion, the methods developed and validated on different applications validate that ICP-MS and LA-ICP-MS are very broad applicable techniques which are paramount for future application in the frame of ESS project. The access to concentrations and isotope ratios in liquids and solids will significantly contribute the general understanding of the composition of irradiated materials and will play a major role in providing *State of the Art* safety standards.

7. References

[1] J. A. Day, J. A. Caruso, J. S. Becker, H.-J. Dietze, *J. Anal. At. Spectrom.* **2000**, *15*, 1343.
[2] S. F. Boulyga, J. S. Becker, *Fresenius J. Anal. Chem.* **2001**, *370*, 612.
[3] S. F. Boulyga, J. L. Matusevich, V. P. Mironov, V. P. Kudrjashov, L. Halicz, I. Segal, J. A. McLean, A. Montaser, J. S. Becker, *J. Anal. At. Spectrom.* **2002**, *17*, 958.
[4] A. E. Eroglu, C. W. McLeod, K. S. Leonard, D. M. Cubbin, *J. Anal. At. Spectrom.* **1998**, *13*, 857.
[5] R. Meji, H. Winkel, *Fuel Processing Technology.* **2004**, *85*, 641.
[6] W. J. Quadakkers, in *7th Polish Corrosion Conference, KOROZJA*, Kraków, Poland, **2002**.
[7] J. Fabryka-Martin, H. Bentley, D. Elmore, P. L. Airey, *Geochim. Cosmochim. Acta.* **1989**, *49*, 337.
[8] F. A. Tikhomirov, A. I. Shcheglov, *Scien. Total Environ.* **1994**, *157*, 45.
[9] M. Edlund, H. Visser, P. Heitland, *J. Anal. At. Spectrom.* **2002**, *17*, 232.
[10] E. I. Tolstykh, E. A. Shishkina, M. O. Degteva, D. V. Ivanov, V. A. Shved, S. N. Bayankin, L. R. Anspaugh, B. A. Napier, A. Wieser, P. Jacob, *Health Phys.* **2003**, *85(4)*, 409.
[11] D. Desideri, M. A. Meli, C. Roselli, C. Testa, S. F. Boulyga, J. S. Becker, *Anal. Bioanal. Chem.* **2002**, *376(6)*, 1091.
[12] V. N. Egorov, G. Y. Kolomeitsev, P. P. Poluektov, N. A. Chirin, *At. En.* **2002**, *93(4)*, 827.
[13] A. Entwistle, A. G. Flowers, J. C. Greenwood, A. Mellor, G. Negeldinger, *Geoch. Expl. Env. A.* **2005**, *5*, 11.
[14] N. Spry, S. Parry, S. Jerome, *Appl. Radiat. Isotopes.* **2000**, *53*, 163.
[15] S. F. Boulyga, D. Desideri, M. A. Meli, C. Testa, J. S. Becker, *Int. J. Mass. Spectrom.* **2003**, *226*, 329.
[16] E. L. Callis, R. M. Abernathey, *Int. J. Mass Spectrom.* **1991**, *103*, 93.
[17] I. T. Platzner, *Modern Isotope Ratio Mass Spectrometry*, John Wiley, Chichester, **1997**.
[18] J. Rucklidge, *Analyst.* **1995**, *120*, 1283.
[19] M. Nunnemann, N. Erdmann, H.-U. Hasse, G. Huber, J. V. Kratz, P. Kunz, A. Mansel, G. Passler, O. Stetzer, N. Trautmann, A. Waldek, *J. Alloys Comp.* **1998**, *271*, 45.
[20] D. Elmore, H. E. Gove, R. Ferraro, L. R. Kilius, H. W. Lee, K. H. Chang, R. P. Beukens, A. E. Litherland, C. J. Russo, K. H. Purser, M. T. Murrell, R. C. Finkel, *Nature* **1980**, *286*, 138.
[21] S. Szidat, A. Schmidt, J. Handl, D. Jakob, R. Michel, H.-A. Synal, C. Schnabel, M. Suter, J. M. Lopez-Gutierrez, *Kerntechnik.* **2000**, *65*, 160.
[22] J. M. Lopez-Gutierrez, M. Garcia-Leon, C. Schnabel, M. Suter, H. A. Synal, S. Szidat, R. Garcia-Tenorio, *Sci. Total Environ.* **2004**, *323*, 195.
[23] A. Schmidt, C. Schnabel, J. Handl, D. Jakob, R. Michel, H.-A. Synal, J.M. Lopez, M. Suter, *Sci. Total Environm.* **1998**, *223*, 131.
[24] A. Alvarez, N. Navarro, *Appl. Radiat. Isotopes* **1996**, *47*, 869.
[25] M. Paul, D. Berkovits, L. D. Cecil, H. Feldstein, A. Hershkowitz, Y. Kashiv, S. Vogt, *Nucl. Instrum. Method. Phys. Res. B.* **1997**, *123*, 394.
[26] Z. Grahek, N. Zecevic, S. Lulic, *Anal. Chim. Acta.* **1999**, *399*, 237.
[27] K. Wendt, J. V. Kratz, J. Lantzsch, P. Muller, W. Northershauser, A. Seibert, N. Trautmann, W. Waldek, K.Zimmer, *Kerntechnik.* **1997**, *62*.
[28] K. Wendt, G. K. Bhomwick, B. A. Busha, G. Herrmann, J. V. Kratz, J. Lantzsch, P.

Muller, W. Nortershauser, E. W. Otten, R. Schwalbach, U.-A. Seibert, N. Trautmann, *Radiochim. Acta.* **1997**, *79*, 183.
[29] N. Trautmann, G. Passler, K. Wendt, *Anal. and Bioanal. Chem.* **2004**, *378*, 348.
[30] K. Wendt, N. Trautmann, *Int. J. Mass. Spectrom.* **2005**, *242*, 161.
[31] G. Radinger, K. G. Heumann, *Anal. Chem.*, *70*, 2221.
[32] G. Radinger, K. G. Heumann, *Environ. Sci. Technol.* **2000**, *34*, 3932.
[33] W. Kerl, J. S. Becker, H. J. Dietze, W. Dannecker, *J. Anal. Atom. Spectrom.* **1996**, *11 (9)*, 723.
[34] K. G. Heumann, *Anal. and Bioanal. Chem.* **2004**, *378*, 318.
[35] M. V. Zoriy, in *Ph.D.thesis*, Prague, **2005**, p. 117.
[36] S. Becker, M. Burow, M. Zoriy, C. Pickhardt, P. Ostapczhuk, R. Hille, *Atom. Spectr.* **2004**, *25*, 197.
[37] G. Radlinger, K. Heumann, *Anal. Chem.* **1998**, *70*, 2221.
[38] F. Vanhaecke, K. Heumann, *Anal. and Bioanal. Chem.* **2004**, *378*, 227.
[39] M. Agarande, S. Benzoubir, A. M. Neiva-Marques, P. Bouisset, *J. Environ. Radioact.* **2004**, *72*, 169.
[40] M. E. Ketterer, K. M. Hafer, C. L. Link, C. S. Royden, W. Hartsock, *J. Environ. Radioact.* **2003**, *67(3)*, 191.
[41] V. N. Epov, V. Taylor, D. Lariviere, R. D. Evans, R. J. Cornett, *J. Radioanal. Nucl. Chem.* **2003**, *258(3)*, 473.
[42] B. Kuczewski, C. M. Marquardt, A. Seibert, H. Geckeis, J. V. Kratz, N. Trautmann, *Anal. Chem.* **2003**, *75(24)*, 6769.
[43] I. Günther-Leopold, B. Wernli, Z. Kopajtic, D. Günther, *Anal. Bioanal. Chem.* **2004**, *378(2)*, 241.
[44] E. M. Krupp, F. X. Donard, *Int. J. Mass Spectrom.* **2005**, *242*, 233.
[45] M. D. Seltzer, *Appl. Spectrosc.* **2003**, *57*, 1173.
[46] S. F. Boulyga, M. Tibi, K. G. Heumann, *Anal. Bioanal. Chem.* **2004**, *378(2)*, 342.
[47] M. Tibi, K. G. Heumann, *Fresenius J. Anal. Chem.* **2001**, *370*, 521.
[48] S. F. Boulyga, K. G. Heumann, *J. Anal. At. Spectrom.* **2004**, *19*, 1501.
[49] T. Punshon, B. P. Jackson, P. M. Bertsch, J. Burger, *J. Environ. Monit.* **2004**, *6*, 153–159.
[50] J. S. Becker, *J. Anal. At. Spectrom.* **2002**, *17*, 1172.
[51] J. S. Becker, H.-J. Dietze, *Int. J. Mass Spectrom.* **2000**, *197*, 1.
[52] H. Nickel, W. J. Quadakkers, L. Singheiser, *Anal. Bioanal. Chem.* **2002**, *374*, 581.
[53] W. J. Quadakkers, H. Viefhaus, *Guidelines for Methods of Testing and Research in High Temperature Corrosion*, London, **1995**.
[54] R. Bungener, W. Pamler, U. Gosele, *Mater. Sci. Semicond. Process* **2003**, *6*, 43.
[55] S. Tsukui, K. C. Goretta, J. L. Routbort, A. Sin, *Physica C.* **2002**, *378*, 701.
[56] A. Sewing, M. Lakatos, D. Scharnweber, S. Roessler, R. Born, M. Dard, H. Worch, *Bioceramics.* **2004**, *254*, 419.
[57] M. Kilo, M. A. Taylor, C. Argirusis, G. Borchardt, B. Lesage, S. Weber, S. Scherrer, H. Scherrer, M. Schroeder, M. Martin, *J. Appl. Phys.* **2003**, *94(12)*, 7547.
[58] H. Haneda, *J. Ceram. Soc. Jpn.* **2003**, *111(7)*, 439.
[59] C. White, W. L. Wu, Y. X. Pu, M. Rafailovih, J. Sokolov, *Polym. Eng. Sci.* **2003**, *43(6)*, 1241.
[60] L. Lnantz, M. G. Pecht, *IEEE Trans. Compon. Packaging Technol.* **2003**, *26(1)*, 199.
[61] L. Y. Matzui, L. L. Vovchenko, L. M. Kapitanchuk, N. I. Zakharenko, N. G. Babich, *Inorg. Mater.* **2003**, *39(11)*, 1147.
[62] O. Dogan, M. Ertugrul, U. Cevik, E. Bacaksiz, E. Tirasoglu, A. I. Kobya, H. Erdogan, *X-Ray Spectrom.* **2003**, *32(5)*, 363.

[63] I. V. Gravetchi, M. Taschuk, G. V. Rieger, Y. Y. Tsui, R. Fedosejevs, *Appl. Optics.* **2003**, *42(30)*, 6138.
[64] M. P. Mateo, L. M. Cabalin, J. J. Laserna, *Appl. Spectrosc.* **2003**, *57(12)*, 1461.
[65] K. Loebe, A. Uhl, H. Lucht, *Appl. Optics.* **2003**, *42(30)*, 6166.
[66] A. I. Saprykin, J. S. Becker, U. Crone, H.-J. Dietze, *Fresenius J. Anal. Chem.* **1997**, *358*, 145.
[67] V. Hoffman, R. Kurt, K. Kammer, R. Thielsch, T. Wirth, U. Beck, *Applied Spectroscopy.* **1999**, *53*, 987.
[68] S. Itoh, H. Yamaguchi, T. Hobo, T. Kobayashi, T. T. Hagane, *J. Iron Steel Inst. Jpn.* **2002**, *88(9)*, 575.
[69] S. Barison, D. Barreca, G. A. Battiston, S. Daolio, M. Fabrizio, R. Gerbasi, E. Tondello, *Rapid Commun. Mass Spectrom.* **2003**, *17*, 996.
[70] J. S. Becker, *Spectrochimica Acta Part B-Atom. Spectr.* **2002**, *57*, 1805.
[71] J. B. Murphy, J. Fernandez-Suarez, T. E. Jeffries, R. A. Strachan, *J. Geol. Soc.* **2004**, *161*, 243.
[72] T. Prohaska, C. Latkoczy, G. Schultheis, M. Teschler-Nicola, G. Stingeder, *J. Anal. At. Spectrom.* **2002**, *17*, 887.
[73] M. Zoriy, M. Kayser, A. Izmer, C. Pickhardt, J. S. Becker, *Int. J. Mass Spectrom.* **2005**, *242*, 297.
[74] J. S. Becker, M. Zoriy, C. Pickhardt, N. Palomero-Gallagher, K. Zilles, *Anal. Chem.* **2005**, *77*, 3208.
[75] J. S. Becker, C. Pickhardt, *Laborpraxis.* **2004**, *Dezember*, 20.
[76] J. W. Westheide, J. S. Becker, R. Jäger, H.-J. Dietze, *J. Anal. At. Spectrom.* **1996**, *11*, 661.
[77] M. Bi, A. M. Ruiz, I. Gornushkin, B. W. Smith, J. D. Winefordner, *Applied Surface Science.* **2000**, *158*, 197.
[78] A. V. Karasev, H. Suito, *ISIJ Int.* **2004**, *44(2)*, 356.
[79] A. M. Ghazi, S. Shuttleworth, R. Simmons, S. J. Paul, D. H. Pashley, *J. Anal. At. Spectrom.* **2002**, *17(7)*, 682.
[80] C. Latkoczy, Y. Muller, P.Schmutz, D. Günther, *Appl. Surf. Science.* **2005**, *252 (1)*, 127.
[81] C. Pickhardt, I. J. Brenner, J. S. Becker, H.-J. Dietze, *Fresenius J. Anal. Chem.* **2000**, *368*, 79.
[82] P. J. Sylvester, S. M. Eggins, *Geostandards Newsletter.* **1997**, *21/2*, 215.
[83] K. P. Jochum, B. Stoll, K. Herwig, M. Amini, W. Abouchami, A. W. Hofmann, *Int. J. Mass Spectrom.* **2005**, *242*, 281.
[84] C. A. Heinrich, *Geochim. Cosmochim. Acta* **2003**, *67[18]*, 3473.
[85] D. Günther, B. Hattendorf, *Tr. Anal. Chem.* **2005**, *24[3]*, 255.
[86] D. Günther, H. Cousin, B. Magyar, I. Leopold, *J. Anal. At. Spectrom.* **1997**, *12*, 165.
[87] C. Pickhardt, J. S. Becker, H.-J. Dietze, *Fresenius J. Anal. Chem.* **2000**, *368*, 173.
[88] L. Halicz, D. Günther, *J. Anal. At. Spectrom.* **2004**, *19*, 1539.
[89] J. S. Becker, C. Pickhardt, W. Pompe, *Int. J. Mass Spectrom.* **2004**, *237*, 13.
[90] A. Montaser, *Inductively Coupled Plasma Mass Spectrometry*, Wiley-VCH, New York, **1998**.
[91] A.Montaser, *Inductively Coupled Plasma Mass Spectrometry*, Wiley-VCH, New York, **1998**.
[92] J. E. Meinhard, *ICP Inf. Newlet.* **1978**, *3*, 425.
[93] R. N. Kniseley, H. Amenson, C. C. Butler, V. A. Fassel, *Appl. Spec.* **1974**, *28*, 285.
[94] H. E. Taylor, *Inductively Coupled Plasma Mass-Spectrometry, Practices and Techniques*, Academic Press, New York, **2001**.
[95] A. Montaser, *Inductively Coupled Plasma Mass Spectrometry*, VCH Publishers, New

York, **1992**.
[96] M. Thompson, *A Hand-book of Inductively Coupled Plasma Spectrometry*, Blockier London, U.K., **1983**.
[97] J. A. McLean, J. S. Becker, S. F. Boulyga, H.-J. Dietze, A. Montaser, *Int. J. Mass. Spectrom.* **2001**, *208((1-3))*, 193.
[98] D. Schaumloffel, J. R. Encinar, R. Lobinski, *Anal. Chem.* **2003**, *75*, 6837.
[99] I. B. Brenner, A. Zander, M. Plantz, J. Zhu, *J. Anal. At. Spectrom.* **1997**, *12*, 273.
[100] A. L. Gray, *Analyst.* **1985**, *106*, 1255.
[101] D. Günther, A. V. Quadt, R. Wirz, *Microchim Acta.* **2001**, *136(3-4)*, 101.
[102] M. Resano, E. Garcia-Ruiz, L. Moens, F. Vanhaecke, *J. Anal. At. Spectrom.* **2005**, *20(2)*, 81.
[103] A. Martin-Esteban, B. Slowikowski, K. H. Grobecker, *Talanta.* **2004**, *63(3)*, 667.
[104] S. Q. Li, B. Hu, Z. C. Jiang, R. Chen, *Anal. Bioanal. Chem.* **2004**, *379(7-8)*, 1076.
[105] S.-J. Jiang, R. S. Houk, *Anal. Chem.* **1986**, *58*, 1739.
[106] D. M. Coleman, J. P. Walters, *Spectrochim. Acta.* **1976**, *31B*, 547.
[107] J. G. Williams, A. L. Gray, P. Norman, L. Ebdon, *J. Anal. At. Spectrom.* **1987**, *2*, 469.
[108] D. Günther, S. E. Jackson, H. P. Longerich, *Spectrochim. Acta Part B.* **1999**, *54*, 381.
[109] J. S. Becker, H.-J. Dietze, *Fresenius J. Anal. Chem.* **1999**, *364*, 482.
[110] F. Vanhaecke, S. Saverwyns, G. D. Wannemacker, L. Moens, R. Dams, *Anal. Chim. Acta.* **2000**, *419*, 55.
[111] A. Newman, *Anal. Chem.* **1996**, *68*, 46A.
[112] I. Feldmann, W. Tittes, N. Jakubowski, D. Stuewer, *J. Anal. At. Spectrom.* **1994**, *9*, 1007.
[113] K. E. Jarvis, A. L. Gray, S. R. Houk, *Handbook of Inductively Coupled Plasma Mass Spectrometry*, Blackie Academic and Professional, London, **1997**.
[114] www.thermo.com.
[115] J. S. Becker, *Int. J. Mass Spectrom.* **2005**, *242*, 183.
[116] J. T. Watson, *Introduction to Mass Spectrometry*, Raven Press, New York, **1985**.
[117] P. H. Dawnson, N. R. Whetten, *Adv. Electron. Electron Phys.* **1969**, *27*, 59.
[118] J. N. Bilton, N. Kyriakidis, E. S. Waight, *Organic Mass Spect.* **1978**, *13[8]*, 489.
[119] W. V. Ligon, J. L. Webb, *Int. J. Mass. Spectrom.* **1976**, *22[3-4]*, 359.
[120] U. Herzig, P. Krenmayr, *Organic Mass Spect.* **1979**, *14[2]*, 75.
[121] M. V. Straaten, *Analytical glow discharge mass spectrometry: physical aspects and applications*, University of Antwerpen, Belgium, **1993**.
[122] www.science.duq.edu.
[123] www.gvinstruments.co.uk.
[124] J. S. Becker, H.-J. Dietze, *Isotopenpraxis.* **1983**, *19*, 105.
[125] J. T. Rowan, R. S. Houk, *Appl.Spectrosc.* **1989**, *43[6]*, 976.
[126] R. F. Bonner, R. E. March, J. Durup, *Int. J. Mass Spectrom. Ion Phys.* **1976**, *22*, 17.
[127] D. J. Douglas, J. B. French, *J. Am. Soc. Mass. Spectrom.* **1992**, *3*, 398.
[128] D. J. Douglas, *J. Am. Soc. Mass Spectrom.* **1998**, *9*, 101.
[129] P. Turner, T. Merren, J. Speakman, C. Haines, *Plasma Source Mass Spectrometry: Development and Applications*, Royal Society of Chemistry, Cambridge, **1997**.
[130] J. S. Becker, H. J. Dietze, *Fresenius J. Anal. Chem.* **1997**, *359[4-5]*, 338.
[131] G. C. Eiden, C. J. Barinaga, D. W. Koppenaal, *J. Anal. At. Spectrom.* **1996**, *11*, 317.
[132] V. I. Baranov, S. D. Tanner, *J. Anal. At. Spectrom.* **1999**, *14*, 1133.
[133] S. D. Tanner, V. I. Baranov, *J. Am. Soc. Mass Spectrom.* **1999**, *10*, 1083.
[134] S. F. Boulyga, J. S. Becker, *Fresenius J. Anal. Chem.* **2001**, *370*, 618.
[135] www.perkinelmer.com.
[136] www.home.agilent.com.

[137] S. D. Tanner, V. I. Baranov, *Atom. Spectrosc.* **1999**, *20*, 45.
[138] S. F. Boulyga, J. S. Becker, *J. Anal. Atom. Spectrom.* **2002**, *17*, 1202.
[139] D. R. Bandura, V. I. Baranov, S. D. Tanner, *Journal of the American Society for Mass Spectrometry.* **2002**, *13*, 1176.
[140] S. F. Boulyga, K. G. Heumann, *Int. J. Mass. Spectrom.* **2005**, *242*, 291.
[141] A. L. Gray, *Analyst (Cambridge, UK)* **1985**, *110*, 551.
[142] R. E. Russo, *Appl.Spectrosc.* **1995**, *49[9]*, A 14.
[143] M. A. Shannon, *Anal. Chem.* **1995**, *67[24]*, 4522.
[144] X. Mao, *Appl.Surf.Sci.* **1996**, *30*, p.126.
[145] W. T. Chan, A. P. K. Leung, X. L. Mao, R. E. Russo, *Appl.Surf.Sci.* **1998**, *129*, 269.
[146] O. V. Borisov, X. L. Mao, R. E. Russo, *Spectrochim.Acta B.* **2000**, *55[11]*, 1693.
[147] J. Gonzalez, *J. Anal. At. Spectrom.* **2002**, *17[9]*, 1108.
[148] F. Poitrasson, X. L. Mao, S. S. Mao, R. Freydier, R. E. Russo, *Anal. Chem.* **2003**, *75*, 6184.
[149] C. Liu, *Anal. Chem.* **2004**, *76[2]*, 379.
[150] S. M. Eggins, L. P. Kinsley, J. M. Shelley, *Appl. Surf. Sci.* **1998**, *129*, 278.
[151] D. Bleiner, H. Altorfer, *J. Anal. At. Spectrom.* **2005**, *20[8]*, 754.
[152] D. Bleiner, *J. Anal. At. Spectrom.* **2005**, *20[12]*, 1337.
[153] D. Bleiner, D. Günther, *J. Anal. At. Spectrom.* **2001**, *16[5]*, 449.
[154] J. Koch, I. Feldmann, N. Jakubowski, K. Niemax, *Spectrochim. Acta B.* **2002**, *57[5]*, 975.
[155] B. J. Fryer, S. E. Jackson, H. P. Longerich, *Can. Mineral.* **1995**, *33*, 303.
[156] H. P. Longerich, D. Günther, S. E. Jackson, *Fresenius J. Anal. Chem.* **1996**, *355*, 538.
[157] P. M. Outridge, W. Doherty, D. C. Gregoire, *Spectroch. Acta B.* **1997**, *52*, 2093.
[158] I. Horn, M. Guillong, D. Günther, *Appl. Surf. Sci.* **2001**, *182*, 91.
[159] M. Guillong, I. Horn, D. Günther, *J. Anal. At. Spectrom.* **2003**, *18*, 1224.
[160] J. S. Becker, D. Tenzler, *Fresenius J. Anal. Chem.* **2001**, *370*, 637.
[161] H. R. Kuhn, D. Günther, *Anal. Chem.* **2003**, *75*, 747.
[162] J. Koch, A. Bohlen, R. Hergenroder, K. Niemax, *J. Anal. At. Spectrom.* **2004**, *19*, 267.
[163] H.-J. Dietze, J. S. Becker, A.Vertes, R. Gijbels, F. Adams, in *Book*, New York, **1993**, pp. 453.
[164] I. Horn, R. L. Rudnik, W.-F. McDonough, *Chem. Geol.* **2000**, *164*, 281.
[165] M. Gastel, J. S. Becker, H.-J. Dietze, *Spectroch. Acta B.* **1997**, *52*, 2051.
[166] D. Günther, *J. Anal. At. Spectrom.* **1997**, *12*, 939.
[167] R. E. Russo, X. L. Mao, C.Liu, J.Gonzalez, *J. Anal. At. Spectrom.* **2004**, *19*, 1084.
[168] S. E. Jackson, H. P. Longerich, G. R. Dunning, B. J. Freyer, *Can. Mineral.* **1992**, *30*, 1049.
[169] G. A. Jenner, S. E. Jackson, S. F. Foley, T. H. Green, B.J. Fryer, H. P. Longerich, *EOS Trans.* **1993**, *74*, 344.
[170] R. R. Loucks, in *Annual Report*, Australian National University, Canberra, **1995**.
[171] F. Bea, P. Montero, A. Stroh, J. Baasner, *Chem. Geol.* **1996**, *133*, 145.
[172] D. Figg, M. S. Kahr, *Appl. Spectrosc.* **1997**, *51*, 1185.
[173] C. Leloup, P. Marty, D. Dallava, M. Perdereau, *J. Anal. Atom.Spectrom.* **1997**, *12*, 945.
[174] T. E. Jeffries, S. E. Jackson, H. P. Longerich, *J. Anal. Atom.Spectrom.* **1998**, *13*, 935.
[175] R. E. Russo, X. L. Mao, J. J. Gonzalez, S. S. Mao, *J. Anal. Atom.Spectrom.* **2002**, *17*, 1072.
[176] P. Telouk, E. F. Rose-Koga, F. Albarede, *Geostand. Newsl.* **2003**, *27*, 5.
[177] I. Horn, D. Günther, M. Guillong, *Spectrochim. Acta, Part B.* **2003**, *58* 1837.
[178] J. S. Fritz, D. T. Gjerde, *Ion chtomatography*, Weinheim: Wiley-VCH, **2000**.
[179] J. Landers, *Handbook Of Capillary Electrophoresis*, CRC Press, Washington, **1996**.

[180] A. Rizzi, *Electrophoresis.* **2001**, *22[15]*, 3079.
[181] A. V. Izmer, S. F. Boulyga, J. S. Becker, *J. Anal. At. Spectrom.* **2003**, *18*, 1339.
[182] P. Mason, K. Kaspers, M. Bergen, *J. Anal. At. Spectrom.* **1999**, *14*, 1067.
[183] J. Feldmann, A. Kindness, P. Ek, *J. Anal. At. Spectrom.* **2002**, *17*, 813.
[184] C. Latkoczy, D. Günther, *J. Anal. At. Spectrom.* **2002**, *17[10]*, 1264.
[185] A. Stroh, *Atom. Spectr.* **1992**, *13[3]*, 89.
[186] J. S. Fedorowich, J. P. Richards, J. C. Jain, R. Kerrich, J. Fan, *Chem. Geology* **1993**, *106[3-4]*, 229.
[187] L. Moens, F. Vanhaecke, J. Riondato, R. Dams, *J. Anal. At. Spectrom.* **1995**, *10[9]*, 569.
[188] F. Vanhaecke, M. VanHolderbeke, L. Moens, R. Dams, *J. Anal. At. Spectrom.* **1996**, *11[8]*, 543.
[189] G. A. Pedersen, E. H. Larsen, *Fresenius J. Anal. Chem.* **1997**, *358[5]*, 591.
[190] Q. L. Xie, R. Kerrich, *J. Anal. At. Spectrom.*, *17[1]*, 69.
[191] C. Pickhardt, A. V. Izmer, M. V. Zoriy, D. Shaumlöffel, J. S. Becker, *Int. J. Mass. Spectrom.* **2006**, *248*, 136.
[192] H.-J. Dietze, *Berichte des Zentralinstitut fuer Isotopen und Strahlenforschung der Akademie der Wissenschaften der DDR* **1979**, *Vol. 27*, 101.
[193] M. V. Zoriy, L. Halicz, M. E. Ketterer, P. Ostapczuk, J. S. Becker, *J. Anal. At. Spectrom.* **2004**.
[194] O. T. Farmer, C. J. Barinaga, D. W. Koppenaal, *J. Radioanal. Nucl. Chem.* **1998**, *234 (1-2)*, 153.
[195] G. C. Eiden, C. J. Barinaga, D. W. Koppenaal, *Rapid Comm. Mass Spectrom.* **1997**, *11*, 37.
[196] S. D.Tanner, V. I. Baranov, *J. Am. Soc. Mass Spectrom.* **1999**, *10*, 1083.
[197] A. V. Izmer, S. F. Boulyga, M. V. Zoriy, S. Becker, *J. Anal. At. Spectrom.* **2004**, *19*, 1278.
[198] www.nist.gov.
[199] S. F. Boulyga, J. S. Becker, J. L. Matusevitch, H.-J. Dietze, *Int. J. Mass. Spectrom.* **2000**, *203*, 143.
[200] M. V. Prasad, D. S. Narayana, R. K. Jeevanram, *J. Radioanal. Nucl. Chem.* **1995**, *197*, 281.
[201] J. S. Becker, H. J. Dietze, *J. Anal. At. Spectrom.* **1998**, *13*, 1057.
[202] S. B. Clark, *J. Radioanal. Nucl. Chem.* **1995**, *194*, 297.
[203] J. T. Chuang, J. G. Lo, *J. Radioanal. Nucl. Chem.* **1995**, 307.
[204] M. J. Keith-Roach, S. Sturup, D. H. Oughton, H. Dahlgaard, *Analyst.* **2002**, *127*, 70.
[205] N. Jakubowski, L. Moens, F. Vanhaecke, *Spectrochim. Acta Part B.* **1998**, *53*, 1739.
[206] M. Hamester, D. Wiederin, J. Wills, W. Kerl, C. B. Douthitt, *Anal. Bioanal. Chem.* **1999**, *364*, 495.
[207] S. D. Tanner, V. I. Baranov, D. R. Bandura, *Spectrochim. Acta Part B.* **2002**, *57*, 1361.
[208] A. P. Vonderheide, J. Meija, M. Montes-Bayon, J. A. Caruso, *J. Anal. At. Spectrom.* **2003**, *18*, 1097.
[209] J. S. Becker, H.-J. Dietze, *J. Anal. At. Spectrom.* **1999**, *14*, 1493.
[210] K. E. Murphy, S. E. Long, M. S. Rearick, O. S. Ertas, *J. Anal. At. Spectrom.* **2002**, *17*, 469.
[211] A. P. Vonderheide, M. V. Zoriy, A. V. Izmer, C. Pickhardt, J. A. Caruso, P. Ostapczuk, R. Hille, J. S. Becker, *J. Anal. At. Spectrom.* **2003**, *19*, 675.
[212] P. D. Taylor, P. D. Bievre, A. J. Walder, A. Entwistle, *J. Anal. At. Spectrom.* **1995**, *10*, 395.
[213] M. E. Ketterer, J. A. Jordan, S. C. Szechenyi, D. D. Hudson, R. R. Layman, *J. Anal. At.*

Spectrom. **2000**, *15*, 1569.
[214] S. F. Boulyga, C. Pickhardt, J. S. Becker, *At. Spectr.* **2004**, *25*, 53.
[215] C. Pickhardt, J. S. Becker, *Fresenius J. Anal. Chem.* **2001**, *370(5)*, 534.
[216] H. Reinhardt, M. Kriews, D. T. Miller, O. Schrems, C. Luedke, E. Hoffmann, J. Skole, *Fresenius J. Anal. Chem.* **2001**, *370(5)*, 629.
[217] H. Reinhardt, M. Kriews, H. Miller, C. Ludke, E. Hoffmann, J. Skole, *Anal. Bioanal. Chem.* **2003**, *375(8)*, 1265.
[218] J. S. Becker, M. Zoriy, M. Dehnhardt, C. Pickhardt, K. Zilles, *J. Anal. At. Spectrom.* **2005**, *20*, 912.
[219] J. S. Becker, M. Zoriy, J. S. Becker, C. Pickhardt, E. Damoc, G. Juhacz, Palkovits, M. Przybylski, *Anal. Chem.* **2005**, *242*, 5851.